INTEGRATED SENSOR ARRAY FOR ON-LINE MONITORING MICRO BIOREACTORS

The described research has been carried out at the BIOS Lab-on-a-Chip group of the MESA+ Institute for Nanotechnology of the University of Twente, Enschede, The Netherlands. The research was financially supported by the Dutch Science Foundation (NWO) through the ACTS program IBOS (Integration of Biosynthesis and organic synthesis), DSM Anti-Infectives, Organon and Applikon.

Samenstelling promotiecommissie:

voorzitter:

prof. dr. W.H.M. Zijm

secretaris:

prof. dr. ir. A.J. Mouthaan

promotor:

prof. dr. ir. A. van den Berg

assistent promotor:

prof. dr. J.G.E. Gardeniers

leden:

prof. dr. P. Renaud

prof. dr. ir. P.H. Veltink

prof. dr. I. Vermes

dr. H.J. Noorman

prof. dr. ir. J.J. Heijnen

Title: Integrated sensor array for on-line monitoring micro bio reactors
Author: Erik Krommenhoek
ISBN: 978-90-365-2593-0
Printing: PrintPartners Ipskamp

INTEGRATED SENSOR ARRAY FOR ON-LINE MONITORING MICRO BIOREACTORS

PROEFSCHRIFT

ter verkrijging van
de graad van doctor aan de Universiteit Twente,
op gezag van rector magnificus,
Prof. Dr. W.H.M. Zijm,
volgens het besluit van het College voor Promoties
in het openbaar te verdedigen
op donderdag 29 november 2007 om 13.15 uur

door

Erik Eduard Krommenhoek
geboren op 29 juli 1979
te Apeldoorn

Dit proefschrift is goedgekeurd door:

promotor: prof. dr. ir. Albert van den Berg
co-promotor: prof. dr. Han Gardeniers

Contents

Chapter 1: Scope and outline of this thesis 5
1.1 Introduction 5
1.2 Yeasts in biotechnology 6
1.3 Research goal 9
1.4 Outline of this thesis 10
References 11

Chapter 2: Exploration of miniaturized fermentation monitoring techniques 13
2.1 Introduction 13
2.2 Biosensor fundamentals 14
2.2.1 Optical sensors 15
2.2.2 Electrochemical sensors 17
2.3 Fermentation monitoring 21
2.3.1 pH 22
2.3.2 Dissolved oxygen 25
2.3.3 Biomass 28
2.3.4 Temperature 28
2.4 Experimental 29
2.4.1 pH 29
2.4.2 Dissolved oxygen 32
2.4.3 Biomass 34
2.4.4 Temperature 34
2.5 Measurement results 34
2.5.1 pH 35
2.5.2 Dissolved oxygen 38
2.5.3 Biomass 41
2.6 Discussion & conclusions 42
References 44

Chapter 3: Monitoring of yeast cell concentration using a micromachined impedance sensor 51
3.1 Introduction 51
3.2 Theory 52
3.3 Experimental 55
3.3.1 Device fabrication 55
3.3.2 Measurement procedures 56
3.4 Measurement results 57
3.5 Conclusion 61
References 62

Chapter 4: Integrated electrochemical sensor array for on-line monitoring of yeast fermentations 65
4.1 Introduction 65
4.2 Theory 67
4.2.1 Biomass 67
4.2.2 Dissolved oxygen 70
4.2.3 pH 72
4.2.4 Temperature 73
4.3 Experimental 74
4.3.1 Sensor design 74
4.3.2 Device fabrication 75
4.3.3 Measurement setup 76
4.4 Results 77
4.4.1 Biomass measurement results 77
4.4.2 Dissolved oxygen measurement results 78
4.4.3 pH measurement results 79
4.4.4 Temperature measurement results 80
4.5 Conclusions 80
References 81

Chapter 5: Lab-scale fermentation tests of micro chip with integrated electrochemical sensors for pH, temperature, dissolved oxygen and viable biomass concentration 85
5.1 Introduction 85
5.1.1 pH 87
5.1.2 Dissolved oxygen concentration 88
5.1.3 Biomass concentration 88
5.1.4 Temperature 89
5.1.5 Sensor integration 89
5.2 Materials and methods 90
5.2.1 Design and fabrication of the multi-sensor chip 90
5.2.2 Readout of the sensor chip 91
5.2.3 Batch and continuous cultivation 91
5.3 Results and discussion 93
5.3.1 Sensor chip 93
5.3.2 Dissolved oxygen measurements 94
5.3.3 pH measurements 97
5.3.4 Biomass concentration measurements 98
5.3.5 Temperature measurements 101
5.4 Conclusions 102
References 103

Chapter 6: Fermentation monitoring in a batch micro bioreactor array 107
6.1 Introduction.....108
6.2 Microreactor design 109
6.2.1 Reference electrode configuration 109
6.2.2 Mixing method 110
6.2.3 Complete micro bioreactor array design 112
6.3 Experimental 113
6.3.1 Device fabrication.....113
6.3.2 Measurements 115
6.4 Results 117
6.4.1 Salt bridge characterization 117
6.4.2 Cell cultivation 119
6.5 Discussion & conclusions.....126
References.....128

Chapter 7: Microfluidics for pH control and fed-batch functionality.....131
7.1 Introduction.....131
7.2 Theory.....134
7.2.1 Microvalve fabrication 135
7.2.2 Microvalve actuation.....136
7.3 Experimental 137
7.3.1 Microvalve fabrication 137
7.3.2 Microvalve actuation.....140
7.3.3 Microvalve characterization.....143
7.4 Measurement results 144
7.4.1 Electromagnetic actuation 144
7.4.2 Braille display actuation 146
7.4.3 Pneumatic actuation 149
7.5 Discussion & conclusion 150
References.....151

Chapter 8: Conclusions and recommendations 155
8.1 Conclusions.....155
8.2 Recommendations 161

Samenvatting.....163

List of publications.....165

Dankwoord.....169

Chapter 1: Scope and outline of this thesis

In the first chapter of this thesis, a brief introduction to the scope of the research project is presented. The research goal, i.e. the development of a micro bioreactor array suitable for high-throughput screening of micro-organisms, is presented. The chapter ends with an overview of the chapters in this thesis.

1.1 Introduction

The BIOS, lab-on-a-chip group of the University of Twente has a long standing tradition in developing chemical sensors since its former chair holder, prof. Bergveld, invented the Ion-Selective Field Effect Transistor (ISFET) sensor more than 35 years ago (Bergveld 1970). Besides various FET-based sensors, such as the ChemFET (van den Berg 1988), and ImmunoFET (Schasfoort 1989), also chemical sensors based on new materials were developed recently, like a hydrogel based CO_2 sensor (Herber 2005). As new technologies emerged and miniaturization of devices and structures became more and more applicable, in the last decade the focus of this group was more on the integration of different functionalities into so-called lab-on-a-chips, such as the μdialysis system (Böhm 2000) and the Amina-Chip (Timmer 2004). More recently, lab-on-a-chip systems developed within the BIOS group found application in biological fields such as single-cell electroporation (Valero 2006) or apoptosis detection (Wolbers 2007). The development of a total analysis system suitable for inorganic ion analysis at the point of care (Vrouwe 2005) recently resulted in the foundation of the spin-off company Medimate.

This thesis presents the development and testing of an integrated system suitable for the parallel fermentation and on-line screening of micro-organisms. Since the project is focused on screening yeast cells, a short introduction on yeast cells and their application in biotechnology will be given in section 1.2. Section 1.3 gives the goal of the current research and section 1.4 includes an outline of this thesis.

1.2 Yeasts in biotechnology

Yeasts are single small cells of 5-10 μm in size and usually spherical to egg-shaped (Prescott et al. 1990). Yeasts typically multiply as single cells by budding, although a few species of yeast are known to reproduce in an alternative manner (Shuler and Kargi 2002). Yeasts have found broad application in biotechnology, because of their useful metabolic products, such as antibiotics, flavors and organic acids. New products can be obtained by genetic modification of the cells (Archer et al. 2006).

Batch fermentation procedures, where cells are cultured in a vessel with an initial charge of medium that is not altered by further nutrient addition or removal, are simple and widely used in laboratories and industrially (Shuler and Kargi 2002). After inoculation of a sterile nutrient solution with microorganisms and cultivation under physiological

conditions, the four typical phases of growth as depicted in figure 6-1 can be observed (Crueger and Crueger 1990).

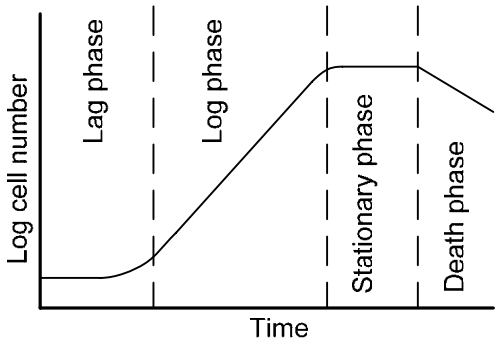

Figure 1: typical growth curve

During the *lag phase*, which typically takes several hours for yeast cultures, the microorganisms adapt to their new environment and there is no increase in the number of cells. When the cells have adapted to their new environment, growth of biomass can be described as a doubling of biomass per unit time, hence the term *log phase*. The lag phase and the log phase will be referred to as the *batch phase* in the following sections. At the end of the batch phase, the substrate is metabolized and growth slows down or completely stops, although the composition of the cells may change. This phase is referred to as the *stationary phase*. In the *death phase*, the energy reserves of the cells are exhausted and cells die at an exponential rate.

An enhancement of the batch fermentation process described above is the fed-batch fermentation process. In this case, substrate is added in increments as the fermentation progresses thereby allowing for maintaining the glucose concentration at a certain level (Nielsen 2006). This is desirable because product formation is often subject to catabolic repression by high concentrations of glucose, other carbohydrates or nitrogen compounds (Crueger and Crueger 1990). Another advantage of fed-batch cultivation is that the process allows for very high cell densities and thereby high final titers.

Consistent yeast quality and product yield require accurate control of the conditions under which the cultivation process is performed. Critical process parameters such as temperature, aeration and pH are usually under closed-loop control. Feed rates frequently are controlled according to preset schedules (Verachtert and de Mot 1990). Moreover, the exact course of the cultivation process and the resulting product yield strongly depend on the performance of the microbial strain used to run the process.

Therefore, in order to optimize growth kinetics and product yield, screening for the best performing microbial strains and optimization of process conditions are required. In conventional methods, this is done by first culturing the micro-organisms in Petri dishes or microtiter plates. Only the best performing strains of cells are selected for fermentation under industrially relevant conditions in a lab-scale fermentor with working volumes typically varying from 0.5 to several liters. The monitoring and control features of these fermentors allow for optimization of growth media composition and culture conditions. The process can then be scaled up from laboratory, through pilot plant to manufacturing scale (Doig et al. 2006). A typical lab-scale fermentor is depicted in figure 1-2.

Figure 1-2: A typical lab-scale fermentor

Running fermentations on this scale is very cost- and labor-intensive. Therefore, there is a growing interest in the further miniaturization and parallelization of bioreactors with full functionality (Lee et al. 2006). Microbioreactor technology therefore aims at combining the small working volume and the high-throughput possibilities of microtiter plates with the monitoring and control features of lab-scale bioreactors (Kumar et al. 2004; Lye et al. 2003). Two complementary approaches can be distinguished. The first is trying to understand in a more sophisticated manner the quantitative process features of shaken bioreactors (hydrodynamics and mass transfer) as well as the performance of bioprocesses in shaken bioreactors by introducing sensors for the parallel online measurement of dissolved oxygen (DO) and pH. The second approach is trying to miniaturize the industrial cultivation technology by scale-down of more or less complete stirred-tank reactors with

gas supply, control of relevant state variables and fed-batch operation capability (Weuster-Botz et al. 2005).

The work described in this thesis tries to combine the best of both worlds by scaling bioreactors with high monitoring and control capabilities down to the microtiter plate format.

1.3 Research goal

The "Fed-batch on a Chip" project is a joint project from the BIOS, lab-on-a-chip group at the University of Twente and the Department of Biotechnology at Delft University of Technology. The "Fed-batch on a Chip" project aims to miniaturize and parallelize micro bioreactors with high monitoring and control functionality. A schematic representation such a system is depicted in figure 1-3.

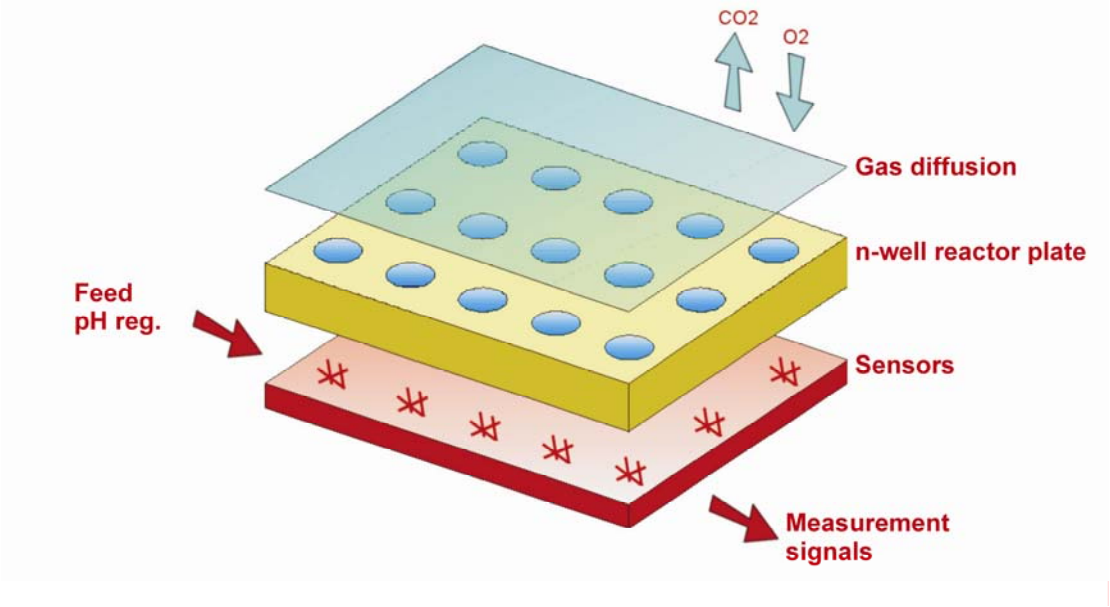

Figure 1-3: Schematic representation of micro bioreactor array

The arrangement of the cultivation chambers is preferably compatible with a microtiter plate format. Microtiter plates form a common standard in many biotechnological applications and benefit from small working volumes, a high degree of parallelization and the already available robotics, shakers and liquid handling equipment (Duetz et al. 2000; Warringer and Blomberg 2003). Inside the reactor chambers, adequate mixing and in-situ product removal should be ensured. The cell culture should be interfaced by a gas phase, as to accommodate in-diffusion of oxygen (to feed the cells) and out-diffusion of carbon

dioxide (produced by the cells). Integrated sensors are required for on-line monitoring of relevant fermentation parameters. As to accommodate pH control or fed-batch functionality, continuous control of the glucose feed and pH regulating flows is required.

The work covered in this thesis focuses on the development of a sensor platform suitable for on-line monitoring of the most relevant fermentation parameters and microfluidics enabling pH control and fed-batch functionality.

1.4 Outline of this thesis

A general introduction, explaining the scope and the goal of the project, has been given in this chapter.

Chapters 2 to 6 describe the development and testing of integrated sensors suitable for on-line monitoring of the most relevant fermentation parameters.

In chapter 2, these fermentation parameters are designated and an overview of different techniques for monitoring these parameters is given. The chapter also includes a comparison between these techniques and feasibility tests on specific techniques. The resulting approach towards the development of the sensor system is explained at the end of the chapter.

Chapter 3 shows the results of more in-depth feasibility tests on impedance spectroscopy as a technique for on-line monitoring of viable cell concentrations. A three electrode configuration allowing for more accurate measurements is presented.

Chapter 4 describes the design, fabrication and in-vitro calibrations of an electrochemical sensor array suitable for on-line monitoring of pH, dissolved oxygen concentrations, biomass concentrations and temperature.

Chapter 5 shows in-situ tests of the developed sensor array. These measurements were done under the conditions of both dynamic batch cultivations as well as prolonged continuous yeast cultivations performed in a lab-scale bioreactor. The measurement results were compared to those obtained using conventional measurement techniques.

The design and fabrication of a micro bioreactor array suitable for the batch cultivation and on-line monitoring of micro-organisms is presented in chapter 6. Measurement results obtained during the batch growth of *candida utilis* cells are shown and discussed.

Chapter 7 deals with the development of microfluidics enabling to expand the system with pH control and fed-batch functionality. The chapter gives an overview of different techniques for fabrication and actuation of PDMS microvalves and consequently shows the design and characterization of microvalves that were developed for the aforementioned purpose.

In chapter 8 of this thesis, a summary of the conclusions is given. Subsequently, recommendations are given for future research and improvements on the presented cell screening system.

References

Archer DB, MacKenzie DA, Jeenes DJ. 2006. Basic Biotechnology. Ratledge C, Kristiansen B, editors. Cambridge Cambridge University Press. 470-471 p.

Bergveld P. 1970. Development of an Ion-Sensitive Solid-State Device for Neurophysiological Measurements. IEEE Transactions on Biomedical Engineering BME-17(1):70-71.

Böhm S. 2000. The comprehensive integration of microdialysis membranes and silicon sensors [PhD]. Enschede: University of Twente.

Crueger W, Crueger A. 1990. Biotechnology: a textbook of industrial microbiology. Haessly C, translator. Brock TD, editor. Sunderland: Sinauer Associates, Inc. 64-73 p.

Doig SD, Baganz F, Lye GJ. 2006. Basic Biotechnology. Ratledge C, Kristiansen B, editors. Cambridge Cambridge University Press. 470-471 p.

Duetz WA, Rüedi L, Hermann R, O'Connor K, Büchs J, Witholt B. 2000. Methods for intense aeration, growth, storage, and replication of bacterial strains in microtiter plates. Applied and Environmental Microbiology 66:2641-2646.

Herber S. 2005. Development of a hydrogel-based carbon dioxide sensor [PhD]. Enschede: University of Twente.

Kumar S, Wittmann C, Heinzle E. 2004. Minibioreactors. Biotechnology Letters 26(1):1-10.

Lee HLT, Boccazzi P, Ram RJ, Sinskey AJ. 2006. Microbioreactor arrays with integrated mixers and fluid injectors for high-throughput experimentation with pH and dissolved oxygen control. Lab on a Chip 6(9):1229-1235.

Lye GJ, Ayazi-Shamlou P, Baganz F, Dalby PA, Woodley JM. 2003. Accelerated design of bioconversion processes using automated microscale processing techniques. Trends in Biotechnology 21(1):29-37.

Nielsen J. 2006. Basic Biotechnology. Ratledge C, Kristiansen B, editors. Cambridge Cambridge University Press. 470-471 p.

Prescott LM, Harley JP, Klein DA. 1990. Microbiology. Dubuque: Wm. C. Brown Publishers. 501 p.

Schasfoort RBM. 1989. A new approach to ImmunoFET operation [PhD]. Enschede: University of Twente.

Shuler ML, Kargi F. 2002. Bioprocess engineering - basic concepts. Guerrierri P, editor. Upper Saddle River: Prentice Hall PTR. 156-175 p.

Timmer BH. 2004. AMINA-chip [PhD]. Enschede: University of Twente.

Valero A. 2006. Single cell electroporation on chip [PhD]. Enschede: University of Twente.

van den Berg A. 1988. Ion Sensors based on ISFETs with Synthetic Ionophores [PhD]. Enschede: University of Twente.

Verachtert H, de Mot R. 1990. Yeast: Biotechnology and Biocatalysis. McGregor WC, editor. New York: Marcel Dekker, Inc. 122-123 p.

Vrouwe EX. 2005. Quantitative microchip capillary electrophoresis for inorganic ion analysis at the point of care [PhD]. Enschede: University of Twente.

Warringer J, Blomberg A. 2003. Automated screening in environmental arrays allows analysis of quantitative phenotypic profiles in Saccharomyces cerevisiae. Yeast 20(1):53-67.

Weuster-Botz D, Puskeiler R, Kusterer A, Kaufmann K, John GT, Arnold M. 2005. Methods and milliliter scale devices for high-throughput bioprocess design. Bioprocess and Biosystems Engineering 28(2):109-119.

Wolbers F. 2007. Apoptosis chip for drug screening [PhD]. Enschede: University of Twente.

Chapter 2: Exploration of miniaturized fermentation monitoring techniques

In this chapter, the specifications of the measurement system under development are presented. Some biosensor fundamentals as well as their feasibility to the current application will be discussed. The feasibility of several electrochemical measurement techniques is investigated in more detail. Results will be shown and discussed for feasibility studies on ISFETs for pH sensing, ^{E}MOSFETs and amperometry for monitoring dissolved oxygen concentrations and impedance spectroscopy for monitoring viable biomass concentrations.

2.1 Introduction

Adequate on-line monitoring techniques are essential for successful control and evaluation of microreactor processes. Since the microreactor platform under study aims at the control and monitoring of yeast growth processes, the most relevant parameters to monitor are pH, biomass, dissolved oxygen concentration and temperature (Vojinovic 2006). Parameter ranges relevant to typical batch yeast fermentation processes are listed in table 2-1 (Hensing et al. 1995).

Table 2-1: parameter ranges typical for batch yeast fermentation processes

pH	pH 3 – pH 8
Biomass	0 - 15 g dry weight (DW)/l
Dissolved oxygen	0 - 15 mg/l
temperature	25 – 40 °C

Since yeast fermentations typically last up to several days and need to be carried out under sterile conditions, long-term stability and sterilizability are major concerns.

In section 2.2 some of the most relevant principles in biosensor theory will be explained. Section 2.3 deals with the investigation and discussion of the applicability of specific sensors in more detail. In section 2.4 feasibility tests, of which the results are shown in section 2.5, are described. The results are discussed and conclusions are made in section 2.6.

2.2 Biosensor fundamentals

A biosensor is a device for the detection of an analyte and combines a biological component with a physicochemical detector component (McNaught and Wilkinson 1997). Many different types of microscale biosensors have been developed for monitoring fermentation parameters as can be deduced from numerous books and review articles that have been published on the subject (Brett and Brett 1983; Hall 1990; Wolfbeis 2006). They can basically be subdivided into 2 categories, however; optical and electrochemical sensors. Basic principles relevant to the detection of the four aforementioned parameters are discussed below for both categories of sensors.

2.2.1 Optical sensors

Microscale optical transducers use optical fibers to transport the signal from the biological material to the detection system. Optical transducers avoid such problems as electrical interference, junction potentials and the need for a reference electrode. On the other hand, interference from ambient light, sample turbidity, air bubbles or other sample components should be avoided. Many different types of fiber-optic sensors have been developed, as indicated by the large number of review articles that have been published on the subject (Bosch et al. 2007; Cooper 2006; Epstein and Walt 2003; Leung et al. 2007; Marazuela and Moreno-Bondi 2002; Yotter et al. 2004).

A few basic principles relevant to detection of the parameters listed in table 2-1 are briefly described below.

Absorbance

The simplest optical detection systems use absorbance measurements to determine changes in concentration of species that absorb a given wavelength of light. The light is brought to the sample through an optical fiber and the amount of light absorbed by the system is detected through the same, or a second optical fiber (Wingard and Ferrance 1991). Spectroscopy, i.e. wavelength scanning of absorbance, gives information about the chemical composition of the sample (Mignani and Mencaglia 2002).

Fluorescence

Fluorescence is a special type of photoluminescence where the molecular absorption of a photon triggers the emission of another photon with a longer wavelength. Although there are few analytes that may naturally be detected in this manner, this method is usually used with artificially labeled compounds. For the direct measurement of bound fluorescent-labeled analyte, labeled analyte must be added to the analyte of interest prior to each measurement. These sensors are therefore not suitable for in situ measurements. If the labeled analyte is entrapped within the sensor, measuring the amount of unbound labeled analyte will give the concentration of analyte of interest in the sample (Wingard and Ferrance 1991).

Fluorescence quenching

In case of fluorescence quenching, the fluorescence of a compound bound within the biosensor is affected by the presence of a specific analyte. Usually, the fluorophore is immobilized in a polymer matrix at the tip of the fiber. There are various models describing

the relationship between the measured fluorescence signal and the amount of analyte quenching the fluorescence intensity signal. One of the most popular models is the two-site model (James Demas).

Fluorescence quenching techniques are usually considered more sensitive, selective and compatible with laser excitation sources compared to absorbance techniques (Bambot et al. 1994). There are major drawbacks concerning long-term stability, however, since the measured signal directly depends on specific properties of the applied indicator, which usually is an organic material. It is well known that these materials are not stable for arbitrary time. The concentration is changed by thermal decomposition, photochemical or biological degradation or leaching from the sensor element.

Fluorescence lifetime

In case of fluorescence lifetime measurements, use is made of a phenomenon called fluorescence resonance energy transfer (FRET) (Bambot et al. 1994). FRET is a distance-dependent nonradiant energy transfer arising from dipole-dipole interactions between a donor and an acceptor. The dye immobilized at the tip of the fiber is a mixture consisting of a donor, selected for excitation with inexpensive sources, and an acceptor with an absorbance dependent on the analyte of interest that spectrally overlaps the donor fluorescence. FRET from the donor to the acceptor will quench the fluorescence and alter the fluorescence lifetime.

In this type of sensors, the fluorescence lifetime is usually determined using phase fluorometry (Lippitsch and Draxler 1993). In this technique, the exciting light is modulated sinusoidally with a high frequency. The modulation then also shows up in the emitted light, but, because of the finite lifetime of the excited state, the phase between the two modulations is shifted and the modulation depth is reduced. These quantities therefore form good measures for the fluorescence lifetime.

Fluorescence lifetime techniques have several advantages over fluorescence quenching techniques, such as being free of such interferences as drifts of the optoelectronic system or optical properties of the sample solution (Borisov et al. 2006). However, also this technique suffers from problems with material stability, such as aging effects or photochemical stability (Oige et al. 2005) and it has been stated that there are cases where lifetime measurements by phase fluorometry are not suitable for analytical applications (Hendrick and van der Donckt 1999).

2.2.2 Electrochemical sensors

Many different types of microscale electrochemical sensors for the detection of a wide variety of chemical compounds have been reported to date as can be concluded from numerous review articles that have been published on this subject (Bakker 2004; Bakker and Qin 2006; Bakker and Telting-Diaz 2002; Pejcic and De Marco 2006). Nevertheless, many electrochemical sensor systems rely on a limited number of electrochemical techniques. The operation principles most relevant to detection of the parameters listed in table 2-1 are briefly described below

Potentiometry

Potentiometric sensors rely on the measurement of the potential of an electrochemical cell. All electrochemical cells are considered as the combination of two half-cells, each of them represented by a half-reaction written as a reduction

$$Ox + ne^{-} \rightarrow Red \qquad (2\text{-}1)$$

The Nernst equation gives a quantitative relation between the potential of the half-cell, E, and the concentration of an electroactive species;

$$E = E^{0} + \frac{RT}{nF} \ln \frac{[Ox]}{[Red]} \qquad (2\text{-}2)$$

where E^{0} is the standard potential of the half-reaction, R is the gas constant, T is the absolute temperature, n is the number of electrodes involved in the electrode reaction, $[Ox]$ is the concentration of reducing agent and $[Red]$ is the concentration of oxidizing agent.

Potentiometric electrodes are used in many different types and configurations. They can be categorized upon the type of indicating electrode being implemented. In “first class” electrode systems, the primary electrode reaction contains the ion or species being measured itself. In “second class” electrode systems, the electrode is in direct contact with a slightly soluble salt of the electroactive species, such that the potentiometric response is indicative of the concentration of the inactive anion species. A typical example is the silver-silver chloride electrode system, where the potential response is directly related to the chloride ion activity, though it is not the electroactive species. “Third class” electrodes are

really a special case of second class electrodes. Here the metal is in contact with a slightly soluble salt of the metal which is then used to monitor the activity of an electroinactive metal ion in equilibrium with a more soluble salt which includes the same anion as the electrode-salt system (Sawyer and Roberts 1974).

Another special category of electrodes used in potentiometric cells, is the ion-selective electrode (ISE). With an ISE, the membrane potential, which itself comprises the junction potential between two electrolytic phases, of an ion selective membrane is measured. If the activity of the species of interest is held constant in one phase, the measured output responds in a Nernst-like fashion to the ion's activity in the other phase (Bard and Faulkner 2001).

In case of an Ion-Selective Field Effect Transistor (ISFET), the chemically sensitive film is deposited directly on the insulating material of a FET device. The surface charge of this film now leads to an ion-selective contribution to the threshold voltage of the FET device. The ISFET potentially has a better signal-to-noise ratio compared to a conventional ISE, since the on-chip sensing and control construction eliminates wire connections between high-impedance components (Hall 1990).

Amperometry

Potentiometric measurements are usually carried out in the equilibrium situation when there is no net charge transfer. This situation may be described by the Nernst equation. In amperometry, the electrode potential is forced to adhere to a known program. If the electrode potential is altered from the equilibrium potential, then equilibrium can only be re-established by adjustment of the concentrations of oxidant and reductant. This will require charge transfer and thus a net current flow (Hall 1990). Chemically, the current is the flow of electrons needed to support the active electrochemical processes at rates consistent with the potential. The Faradaic component of the electrical current is proportional to the flux according to (Bard and Faulkner 2001):

$$i(t) = nFAD\left[\frac{\delta c_0(x,t)}{\delta x}\right]_{x=0} \qquad (2\text{-}3)$$

where n is the number of electrons being transferred, A is the electrode area, F is the Faraday constant, D is the diffusion constant of the reduced species, c_0 is the concentration of the redox active species in the bulk of the electrolyte, t is time and x is the distance from the, usually planar, electrode.

For unstirred aqueous solutions, mass transfer of the electroactive species to the electrode surface occurs only by diffusion. The derivative of the concentration profile $c_0(x,t)$ can be evaluated from Fick's second law of diffusion:

$$\frac{\delta c_0(x,t)}{\delta t} = D\frac{\delta^2 c_0(x,t)}{\delta x^2} \tag{2-4}$$

under the assumptions that the solution is homogeneous before the experiment starts and that regions distant from the electrode are unperturbed by the experiment. Furthermore, it is assumed that the concentration of reactant at the electrode surface is zero during the experiment.

Substitution in (2-3) yields:

$$i(t) = nFAc_0\sqrt{\frac{D}{t\pi}} \tag{2-5}$$

which is known as the Cottrell equation.

In Clark type amperometric sensors (Clark 1956), the cathode and anode are placed in an internal cavity filled with electrolyte and shielded from the test liquid by means of a membrane. The oxygen gradient towards the cathode is now confined in a region unaffected by convection. Therefore, the sensor obeys Cottrell. Moreover, the membrane might be perm-selective thereby enhancing the selectivity of the sensor. The performance of Clark-type sensors

Impedimetry

In impedimetry, an electrochemical cell consisting of two electrodes is perturbed with an alternating signal of small magnitude and the way in which the system follows the perturbation at steady state is followed. In electrochemical impedance spectroscopy (EIS), the electrochemical cell impedance is measured as a function of the ac source. For two equally large facing electrodes, the cell constant κ is written as:

$$\kappa = \frac{l}{A} \tag{2-6}$$

where l is the distance between the electrodes and A is the electrode area. A simple electrical equivalent circuit of such a conductivity cell and a typical impedance curve are shown in figure 2-1.

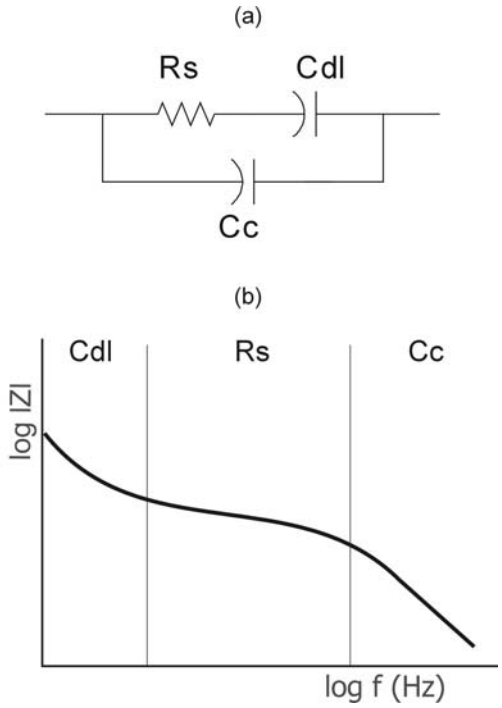

Figure 2-1: (a) Typical impedance model of a conductivity sensor, consisting of solution resistance R_s, combined double layer capacitance C_{dl} and electrochemical cell capacitance C_c (b) corresponding impedance spectrum

C_{dl} is the double layer capacitance that is attributed to the electrical double layers that build up at the electrode-electrolyte interfaces. The value of the electrolyte resistance R_s and the electrochemical cell capacitance C_c depend on the sensor dimensions and the conductivity σ and permittivity ε_r of the electrolyte, respectively, according to:

$$R_s = \frac{\kappa}{\sigma} \tag{2-7}$$

$$C_c = \frac{\varepsilon_0 \varepsilon_r}{\kappa} \tag{2-8}$$

where ε_0 is the permittivity of free space. For planar electrode configurations, the cell constant can be determined using conformal mapping of the electrodes(Olthuis et al. 1995).

2.3 Fermentation monitoring

As previously stated, the aforementioned optical and electrochemical techniques are relevant to the on-line detection of fermentor parameters listed in table 2-1. Autoclavable sensors for in situ detection of pH, dissolved oxygen concentration and temperature are commercially available and widely used in industrial bioreactors. pH measurements are performed with potentiometric ion-selective glass electrodes, Clark-type amperometric electrodes are used for dissolved oxygen measurements and platinum thermistors are used for temperature determination. Together with at-line manual optical density or offline dry cell weight measurements, they commonly form the means of bioreactor process monitoring (Vojinovic 2006). Macroscale impedimetric probes allowing for on-line measurement of viable biomass concentrations using impedance spectroscopy have been commercialized by Aber Instruments (Carvell et al. 1998).

In the past, several types of microscale sensors suitable for the on-line monitoring of parameters relevant to fermentation processes have been developed. Some of them have become commercially available. Examples are fiber-optical sensors based on luminescence lifetime for determination of pH or dissolved oxygen, microscale optical density sensors and pH-ISFETs.

Several groups working on the development of miniaturized bioreactors rely on the application of commercially available fiber-optic sensors (Kostov et al. 2001; Lee et al. 2006; Zanzotto et al. 2006). These groups used commercially available fiber-optic pH and dissolved oxygen sensors based on luminescence lifetime. In these systems, optical density serves as a measure for the biomass concentration and temperature is controlled externally. Maharbiz et al. (Maharbiz et al. 2004) combined commercially available ISFETs together with microfabricated thermistors and optical density sensors in microreactor arrays.

Optical sensors versus electrochemical sensors

In the previous sections, biosensors suitable for monitoring fermentation parameters listed in table 2-1 were subdivided into optical and electrochemical sensors. Since the system

under study requires integrated small scale sensors, a technology has the highest potential for the specified application is a crucial step in the development of the system under study.

For the monitoring of yeast fermentations, which are usually carried out at pH 5, the low sensitivity of fiber-optical sensors in low pH regimes becomes a major concern. When the further miniaturization and parallelization of the biological assays becomes an issue, microfabricated electrochemical sensors become an attractive alternative to fiber-optic sensors since sensors of different types can easily be integrated in a single substrate (Arquint et al. 1994; Van Steenkiste et al. 1997) and the devices become very cheap when fabricated at high volumes. Integrated electrochemical sensors that obey the requirements of the aimed system are not commercially available. Therefore, the potential of several electrochemical concepts for such a system requires further investigation.

The following sections will discuss and investigate the feasibility of microscale electrochemical means for measurement of pH, dissolved oxygen, biomass and temperature.

2.3.1 pH

The pH-ISFET forms the most frequently used microscale electrochemical method for pH measurements. In case of a pH ISFET, hydrogen ions in the solution can associate with or dissociate from the oxide groups at the gate oxide of the field effect transistor. The surface charge of the gate oxide thus depends on the concentration of hydrogen ions in the solution, making the threshold voltage of the device a good measure for the solution pH (Bergveld 1970; Bergveld 2003).

ISFETs are widely used and have become commercially available. Especially for long-term monitoring applications, however, there is one major drawback that needs to be dealt with: they exhibit transient behavior, generally referred to as drift. This drift behavior is usually characterized by an exponential threshold voltage shift in the first few hours of operation, which is followed by a slower, linear voltage shift. Drift is shown to be linear with pH (Bousse et al. 1983; Chou and Wang 2002) and exponentially with temperature (Chung et al. 2006a). To date, the exact cause of ISFET drift has remained unknown. Several groups did try counteracting the effect, however. If pH changes are expected to happen fast compared to the signal changes due to ISFET drift, drift can easily be filtered out using a high-pass filter (Jamasb 2004). Other groups compensated for ISFET drift using empiric models (Chung et al. 2006b).

Some of the factors that might influence the drift behavior are listed below.

Slow pH response

Slow pH response is generally related to the 'buried sites' underneath the oxide surface (Woias et al. 1998). It is assumed that these groups react with hydrogen ions in the electrolyte, just like the surface groups do according to the site-binding model. A schematic representation of this effect is depicted in figure 2-2

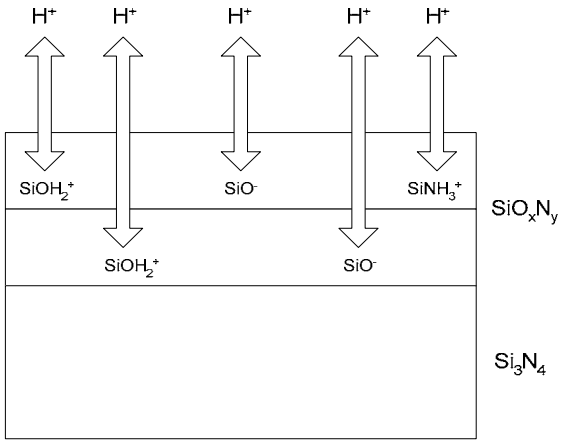

Figure 2-2: Slow pH response of "buried sites"

The delay in protonization and de-protonization of the buried sites might lead to certain memory effects, due to which the measured slow response depends on the electrolyte the ISFET was placed in before. According to the slow pH response model, the transient behavior of ISFETs can be described with:

$$S(t) = S_0 \Delta pH \left(1 - \sum_{i=1}^{n} \varepsilon_i e^{-\left(\frac{t}{\tau_i}\right)} \right) + \frac{\Delta S}{\Delta t} t$$

where long-term drift rate and the normalized amplitudes and time constants of the exponential terms have to be found experimentally. Other research states that the long-term drift rate is not constant, but is also described by an exponential term (Jamasb et al. 1998b).

It is generally believed that during the first few hours of operation, the slow pH response dominates the transient behavior of ISFETs. Once the slow pH response has reached its end value, the transient ISFET behavior will be dominated by long-term drift effects.

Charge carriers drifting through the oxide layer

From MOSFET theory, it is known that traps and charges inside or near the substrate/oxide interfaces lead to drift currents resulting from temporal threshold shifts (Masson et al. 2002). An overview of these traps and charges is depicted in figure 2-3

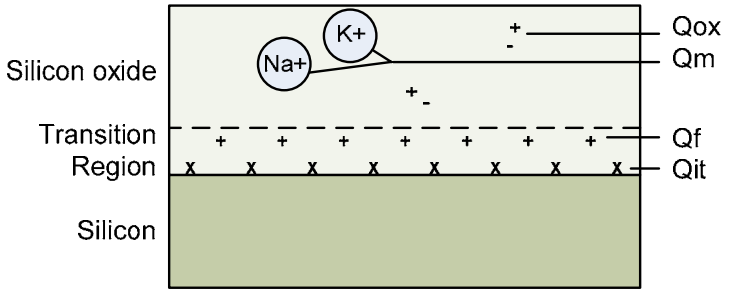

Figure 2-3: Traps and charges inside or near the oxide layer

Fixed charge *Qf* is due to incompletely oxidized silicon atoms and does not change during normal device operation. Interface trapped charge, *Qit*, is likely due to incompletely oxidized silicon atoms with unsatisfied or dangling bonds located in the oxide, but very close to the interface. *Qf* is positive and fixed, while *Qit* may be positive, neutral, or negative and may change during normal device operation because of the capture of holes or electrons. *Qm* is the mobile oxide charge that may be located anywhere in the oxide. *Qox* or oxide trapped charge, located anywhere in the oxide, is due to broken Si-O bonds in the bulk of the oxide.

All these charges inside or near the gate oxide are believed to be able to drift through the oxide layer, thereby increasing the overall oxide layer capacitance and thus decreasing the threshold voltage (Campbell 1995).

Hydratation of the oxide surface

When immersed into a certain liquid, the top layer of the gate oxide will get hydrated. This chemical modification of the oxide layer surface changes the overall oxide layer capacitance. The thickness of the modified surface layer increases exponentially in time following:

$$x_{SL}(t) = x_{SL}(\infty)\left(1 - e^{-\left(\frac{t}{\tau}\right)^{\beta}}\right) \qquad (2\text{-}9)$$

where the time constants and the final thickness are obtained from experimental data. Hydratation rate is strongly dependent on the type of gate oxide used, but even for very hard oxides like Ta_2O_5, chemical modification of the first few atomic layers as a result of exposure to electrolyte is highly conceivable (Jamasb et al. 1998a). The exponential increase in modified surface layer thickness leads to exponential transient threshold voltage.

2.3.2 Dissolved oxygen

In industrial bioreactors, the dissolved oxygen concentration is commonly measured using an amperometric Clark type electrode. An obvious approach towards a microscale oxygen sensor thus is to miniaturize the Clark cell. Several types of miniature Clark-type oxygen electrodes have been proposed (Koudelka 1986; Suzuki et al. 2001; Wu et al. 2005). Due to the complex structure of the sensor, the fabrication process remains rather complex and the robustness of the sensor fabricated device is questionable.

Ultra Micro Electrodes

Another way to reduce flow dependence of the current detection is by applying an "ultra micro electrode" (UME) array, where the term UME generally denotes a circular electrode with a radius r below 2.5 μm. Compared to Clark cells, arrays of ultra micro electrodes can relatively easily be manufactured and integrated with other miniaturized electrochemical sensors. In case of an UME, the equilibrium oxygen concentration profile builds up within a few milliseconds and the contribution of diffusion to the total mass transfer of oxygen becomes so high, that it is hardly influenced by convection (Brett and Brett 1983). For an array of disc ultra micro electrodes, the Cottrell equation therefore converts into:

$$I = mnFAD\frac{c_0}{r} \qquad (2\text{-}10)$$

where m is the number of electrodes that constitute the array.

^{E}MOSFET

Potentiometric sensors hardly consume oxygen and generally have a better signal-to-noise ratio at low concentrations compared to amperometric sensors. Despite these advantages, the potentiometric detection of oxygen has not been given much interest in the past. Only a few potentiometric types of oxygen sensors have been reported (Hendrikse et al. 1999; Lehmann et al. 2001; Martinez-Manez et al. 2004). The ^{E}MOSFET is a field effect transistor where the gate oxide is covered by a thin film of iridium oxide. A schematic representation of the device can be found in figure 2-4 (Hendrikse et al. 1998).

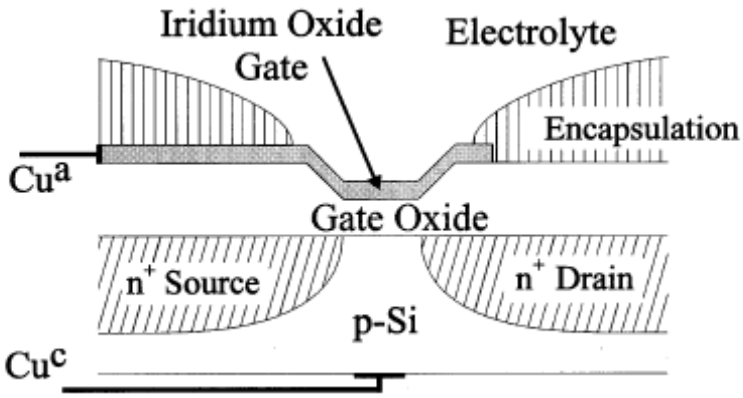

Figure 2-4: Schematic representation of an ^{E}MOSFET

To understand its functionality, assume oxygen is reduced at an electrode surface according to:

$$O_2 + 4e + 4H^+ \leftrightarrow 2H_2O \qquad (2\text{-}11)$$

The equilibrium electrode potential, E_{eq}, can then be calculated using:

$$E_{eq} = E^0 + \frac{kT}{4q}\ln(a_{O2}) + \frac{kT}{q}\ln a_{H+} \qquad (2\text{-}12)$$

where E^0 is the standard electrode potential, $kT/q = 0.059\,V$ and a_{O2} and a_{H+} are the activities of dissolved oxygen molecules and protons respectively. This means that the oxygen concentration can be determined by measuring the equilibrium electrode potential at zero current. It may, however, take a very long time before equilibrium is reached as the oxygen reduction reaction consists of a large number of intermediate steps. Moreover,

small concentrations of impurities are likely to lead to large errors in the equilibrium electrode potential, as the slower intermediate steps have very small exchange currents.

We can speed up the reactions taking place at the electrode surface by applying a small reduction current. In case of an iridium oxide electrode, most of the current will at first be used to reduce the iridium oxide according to:

$$IrO_2 + e \leftrightarrow IrO(OH) + H^+ \tag{2-13}$$

From (1), it can be shown that the corresponding electrode potential depends on the ratio Ir^{III} over Ir^{IV}, following:

$$E = E^0 + \frac{kT}{q}\ln\left(\frac{\gamma_{Ox}^M[Ox]}{\gamma_{\mathrm{Re}}^M[\mathrm{Re}]}\right) + \frac{kT}{q}\ln a_{H+}^S \tag{2-14}$$

where $\gamma_{Ox}^M[Ox]$ and $\gamma_{\mathrm{Re}}^M[\mathrm{Re}]$ are the activity coefficients of the oxidized and reduced species respectively and give the ratio $\mathrm{Ir^{III}}$ over $\mathrm{Ir^{IV}}$. a_{H+}^S is the hydrogen activity in the solution. Equation (2-14) states that the electrode potential will fall due to iridium oxide reduction after the current is applied. The electrode potential will finally become low enough for the reduction of oxygen to occur, according to equation (2-13). Based on equation (2-12), it can be found that the equilibrium threshold voltage as a function of the oxygen activity can be written as:

$$V_{T,eq} = E^0 + C + \frac{kT}{4q}\ln(a_{O2}) \tag{2-15}$$

where C is a device dependent constant. From this formula, the sensitivity of V_T to the oxygen activity can be found to equal:

$$\frac{dV_T}{d\ln(a_{O2})} = \frac{kT}{4q} + \frac{\delta kT}{q}\frac{1-\alpha}{\alpha} \tag{2-16}$$

where δ is the proportion of the Cu|M|S-overpotential that falls across the Cu|M-interface and is usually very close to unity and α is the dimensionless transfer coefficient of the reaction. In most cases, α is assumed to equal 0.5 (Bard and Faulkner 2001), which

would correspond to a sensitivity towards the dissolved oxygen concentration of 80 mV per decade. However, empiric data shows transfer coefficient numbers ranging from 0.1 to 0.9 (Olthuis 2005). ^{E}MOSFET sensitivity obtained in previous work indeed suggests that its value is close to 0.1.

2.3.3 Biomass

Impedance spectroscopy, i.e. wavelength scanning of impedance, can be used as a means for cell concentration measurements. For living cells present in an AC electrical field, interfacial polarization of the cell membrane occurs. If the signal frequency exceeds a so-called characteristic frequency, dielectric dispersion occurs (Schwan 1957). Therefore, the conductivity of the cell suspension increases and the permittivity of the suspension decreases for frequencies above the characteristic frequency. The impedance change is a measure for the viable cell concentration (Asami and Yonezawa 1995). The characteristic frequency typically equals a few MHz for intact yeast cells (Hauttmann and Muller 2001). More details about the method will be presented in the next chapters.

2.3.4 Temperature

A very common method for temperature monitoring is by means of a thermistor (Ruben 1935), which comprises the measurement of the resistance of a metallic structure. The resistance of the metallic structure increases with increasing temperature, as the movement of free charge in the metal is increasingly hindered by thermal vibrations. For platinum, the relation between electrical resistance and temperature is nearly linear over a wide temperature range (Gong et al. 2006). The temperature coefficient of resistance (TCR) of platinum equals $3.9 \times 10^{-3} / °C$ (Cobbold 1974).

A platinum thermistor can easily be integrated with the aforementioned types of sensors by photostructuring a platinum thin-film resistor on the common substrate. Platinum thin films are known to show a lower TCR compared to pure platinum (Mailly et al. 2001). Application of a tantalum adhesion layer is known to further reduce the TCR, compared to the case of pure platinum (Tiggelaar et al. 2005).

2.4 Experimental

As to determine whether application of sensor concepts discussed above is feasible for real-time monitoring of yeast fermentations, feasibility studies were carried out with ISFETs, platinum macro electrodes and ^{E}MOSFETs.

2.4.1 pH

For studying the feasibility of ISFETs for our approach, Ta_2O_5 ISFETs fabricated on two different wafers were investigated. Both types of ISFETs were fabricated using the same fabrication process, but the tantalum deposited to form the gate oxide was deposited using two different deposition machines. The sputter machine used to deposit tantalum on the first wafer was used for different types of metal, whereas the evaporation machine used to deposit tantalum oxide on the second wafer was dedicated to the deposition of tantalum oxide only. It is therefore presumed that the gate oxide of the second type of ISFETs (*type 2*) is more pure and less contaminated than the oxide of the first type of ISFETs (*type 1*).

Sensitivity of Ta_2O_5 ISFETs bondwired to a printed circuit board (PCB) and packaged using Hysol® in the pH range relevant to yeast fermentations was characterized in a reservoir which was controlled at 30 °C. The reservoir was not transparent, as to prevent light interference. The solution in the reservoir was stirred by means of a mechanical stirrer. The ISFET was connected to a home built ISFET amplifier together with a glass Ag/AgCl reference electrode (REF 201, Radiometer Analytical). Actual pH was measured using a glass pH electrode (PHM83, Radiometer Analytical) and could be controlled by titrating acid or base solutions using a titrator (T200, Schott). The output signals of the ISFET amplifier and the pH meter were logged to the computer using home written LabVIEW software.

For our application, it is expected that the applicability of ISFETs is mainly limited by its drift behavior. Although ISFET drift has been intensively studied in the past, the exact cause of this undesirable phenomenon is still not completely understood. As to determine how the drift phenomenon could be dealt with, more study in the drift characteristics and possible causes is required. Drift behavior at different pH values can be determined using the measurement configuration described above in combination with different pH buffer solutions (Radiometer Analytical).

It was also investigated whether long-term ISFET drift is enhanced by the presence of an electrical field across the gate oxide. This was done using the measurement

configuration described above. In this case, however, the ISFET is coupled to the ISFET amplifier according to a pre-set duty cycle.

Further insight in gate oxide properties that might influence ISFET drift can be gained from capacitance-voltage measurements (Pulfrey and Tarr 1989) on MOSFETs fabricated on the same wafer as the ISFETs under study. In particular, the amount of mobile charge inside the gate oxide can be estimated from these measurements. In case of capacitance-voltage measurements, the gate-bulk capacitance C_{MOS} is monitored as a function of the applied gate-bulk voltage V_{GB}. A typical measurement curve for n-type field effect transistors is schematically drawn in figure 2-5:

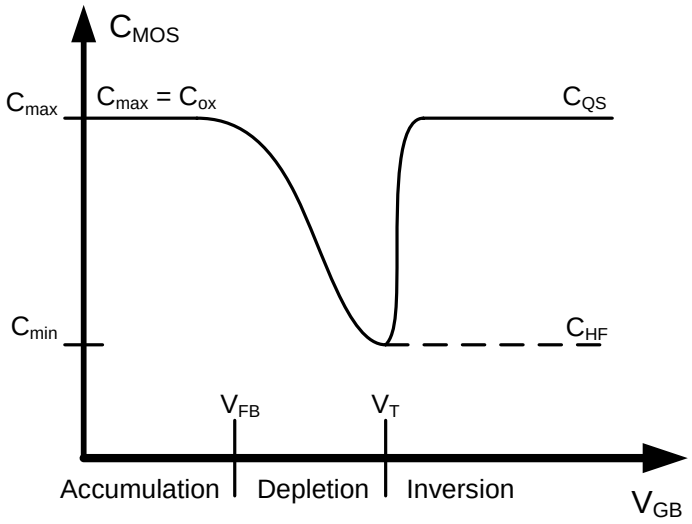

Figure 2-5: Typical capacitance-voltage measurement

As can be seen in this figure, three regimes separated by the threshold- and the flatband voltage, V_T and V_{FB}, respectively, can be distinguished. In accumulation, the applied voltage attracts majority carriers to the oxide-semiconductor interface. Gate capacitance is maximal in accumulation, i.e.:

$$C_{MOS,accumulation} = C_{\max} = C_{ox} = \frac{\varepsilon_{ox}}{t_{ox}} \qquad (2\text{-}17)$$

with ε_{ox} and t_{ox} being the permittivity and the thickness of the gate oxide, respectively. In depletion, the gate-bulk voltage is insufficient to attract minority carriers to the semiconductor surface, but sufficiently high to push away the majority carriers at the interface. Therefore, a depletion layer is formed. This depletion layer can be characterized

by a capacitance in series with the oxide capacitance, thereby decreasing the overall gate-bulk capacitance C_{MOS}. In inversion, minority carriers are attracted to the interface and a negatively charged inversion layer is created. The capacitance in this quasistatic situation, C_{QS}, equals C_{max}. At high signal frequencies, however, the generation of minority carriers in the depletion layer can not follow the signal frequency, leading to a lower gate oxide capacitance.

An estimate of the amount of mobile charge in the oxide layer can be made by performing a bias temperature stress test (Bhat et al. 1997). First, the capacitance-voltage characteristics at room temperature are measured. Then, a relatively high bias voltage is applied to the gate while the device is being heated up to several hundreds °C. The mobility of ions contaminating the gate oxide is increased and the ions are attracted to the semiconductor/oxide interface, thereby altering V_T and V_{FB} with voltage ΔV. The concentration of mobile charge per unit area contributing to this threshold voltage shift, Q_m, can now be estimated according to:

$$Q_m \cong -\frac{\Delta V}{C_{ox}} \tag{2-18}$$

Capacitance-voltage measurements were done using a potentiostat (PAR2263, Princeton Applied Research), which was to superimpose a 100 mV rms AC signal with a frequency of 10 kHz on a DC voltage sweep. Measurements were carried out in a Faraday cage to reduce environmental noise and data quality was set to 5. C_{MOS} was estimated to be in the pF range, where parasitic capacitance arising from wiring and the input impedance of the measurement device might influence the measurements considerably. Therefore, first this parasitic capacitance was determined by performing a capacitance-voltage measurement with no device connected to the potentiostat. Then the capacitance-voltage characteristics of the MOSFETs under study were measured. Bias temperature stress was applied by applying $V_{GB} = 10V$ using a DC voltage supply (E030-1, Delta Elektronika) and gradually heating up the device to 200 °C for 20 minutes using a hotplate (RET Basic, IKA Werke). Initial tests showed that at higher temperatures the bondwires to the ISFET broke down. After letting the devices cool down to room temperature, a second capacitance-voltage measurement was performed.

2.4.2 Dissolved oxygen

In order to find a suitable dissolved oxygen sensor for our application, the feasibility of both amperometry and ^{E}MOSFETs is investigated.

Amperometry

An UME array is an attractive candidate to serve as dissolved oxygen sensor because of its simple structure and because it relies on a very well established measurement technique, i.e. amperometry. It is expected that the feasibility of amperometry mainly depends on its selectivity towards oxygen since selectivity can only be attained by choosing a proper electrode polarization voltage with respect to a well-defined reference electrode potential, if no additional measures to enhance selectivity are taken.

In order to determine whether electrode polarization can be chosen such that selectivity is assured in a certain solution, cyclic voltammetry experiments with Pt macro electrodes were carried out in a 0.1M KNO_3 solution where no interfering redox reactions are expected to take place and in a supernatant solution taken from a running fermentor. In cyclic voltammetry, the potential applied to the working electrode is varied linearly with time along a triangular waveform while the resulting current is continuously monitored. In these experiments, a Princeton 263A galvanostat/potentiostat was used, in combination with an Ag/AgCl reference electrode (REF201, Radiometer Analytical) and two platinum macro electrodes with 1 cm^2 area serving as working electrode (WE) and counter electrode (CE).

Once the proper electrode polarization voltage has been determined, the amperometric cell is calibrated in both a 0.1M KNO_3 solution and in a supernatant solution. Calibrations were done at room temperature. Solutions were stirred using a magnetic stirrer bar and the dissolved oxygen concentration was varied by bubbling nitrogen and air through the solution. The actual dissolved oxygen concentration is monitored using a Clark cell (810, Orion). The maximum dissolved oxygen concentration can be determined from Henry's law (Fogg and Gerrard 1991):

$$p = K'c \qquad (2\text{-}19)$$

with p being the partial pressure of the gas, K' being the Henry constant at the system temperature and c being the molar concentration of the gas in the liquid phase. If we

assume a system pressure of 101300 Pa, an oxygen concentration in air of 20.95% and fill in $K' = 74.68 \cdot 10^6 \frac{Pa}{mol/l}$, we obtain that:

$$c = \frac{p}{K}' = \frac{0.2095 \cdot 101300}{74.68 \cdot 10^6} = 0.284\ mmol/l = 9.09\ mg/l \qquad (2\text{-}20)$$

^{E}MOSFET

For studying the feasibility of ^{E}MOSFETs, several devices with an iridium oxide gate were available from stock. A typical measurement setup that can be used to do oxygen measurements with an ^{E}MOSFET is depicted in figure 2-6.

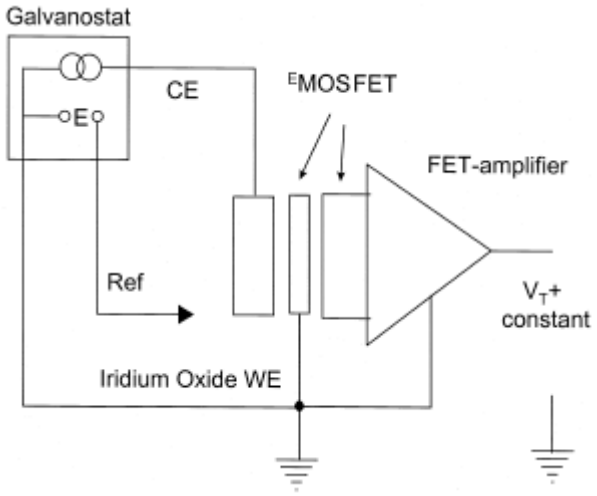

Figure 2-6: ^{E}MOSFET measurement setup

The device is connected to an ISFET-amplifier which monitors the potential difference between the platinum contacting the iridium oxide gate and the source/bulk contact under constant drain-source voltage and constant drain current conditions. Additionally, a small reduction current is needed to speed up the reaction between the iridium oxide and the dissolved oxygen. This current (100 nA) is applied by connecting the device to a potentiostat (263A, Princeton Applied Research) together with a platinum macro electrode with an area of 1 cm^2 and a Ag/AgCl reference electrode (REF201, Radiometer Analytical). As in the amperometry experiments, the dissolved oxygen concentration is simultaneously monitored using a Clark cell (810, Orion) and varied by bubbling nitrogen and air through the solution which was contained in a dark reservoir and mixed by means of a magnetic stirrer.

2.4.3 Biomass

For studying the feasibility of impedance spectroscopy, a planar conductivity sensor microfabricated on an oxidized silicon substrate was readily available from stock. The sensor consists of two planar 2200×100 µm platinum electrodes with a spacing of 60 µm. Yeast cell suspensions of different concentration were made by suspending weighed amounts of pressed *Saccharomyces cerevisiae* yeast cells in a mineral medium (Verduyn et al. 1992). The pH of the buffer solution was adjusted to 5.0 using concentrated sodium hydroxide .

The conductivity sensor described above was immersed in the yeast cell suspensions and connected to an impedance analyzer (HP4194A, Hewlett Packard). The capacitance between the electrodes was measured as a function of the applied signal frequency in the range of 10 kHz – 10 MHz as to investigate whether the capacitance variation with signal frequency shows dependence on the cell concentration. These measurements were performed in a Faraday cage as to reduce interference of environmental electromagnetic fields. Additional feasibility studies on this method will be presented in the next chapters.

2.4.4 Temperature

Platinum thin-film resistors have very frequently been applied for temperature measurements. The feasibility of this method was therefore not thoroughly investigated. Temperature measurements performed with a newly developed sensor array containing integrated sensors suitable for on-line monitoring of temperature, pH, dissolved oxygen concentrations and biomass concentrations will be presented in chapter 4.

2.5 Measurement results

In this section, the measurement results obtained from the experiments described in section 2.4 are shown. Section 2.5.1 shows the results of feasibility studies performed with ISFETs, while in section 2.5.2 the results of experiments on amperometry and ^{E}MOSFETs are shown.

2.5.1 pH

First, the sensitivity of *type 2* Ta_2O_5 ISFETs was determined in the range pH 4 – pH 8 using the measurement setup described above. Figure 2-7a shows both the measured pH and the output signal of the ISFET amplifier in time. Figure 2-7b shows the output of the ISFET amplifier with respect to the measured pH.

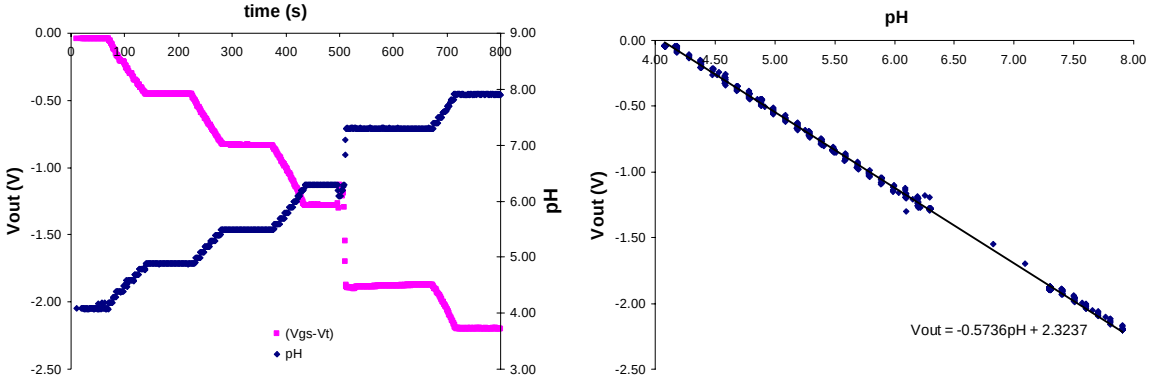

Figure 2-7: ISFET signal as a function of (a) time and (b) pH

The measurement results show the ISFET signal linearly varies with pH with a close to Nernstian sensitivity of -57.4 mV/pH.

The same setup used for determination of the sensitivity was used for long-term drift measurements at different solution pH values. Therefore, the slope of the transient response curve was determined after at least 2 hours of immersion in a certain liquid. A *type 2* ISFET was connected to the ISFET amplifier according to a pre-set duty cycle having a period of 1 minute while being immersed in a pH 7 buffer solution. After 2 hours, the resulting drift rate was determined and plotted as a function of the duty cycle. The result is depicted in figure 2-8.

From these results, it can be concluded that ISFET drift is enhanced by the presence of electrical fields and therefore not caused by hydratation of the oxide surface only.

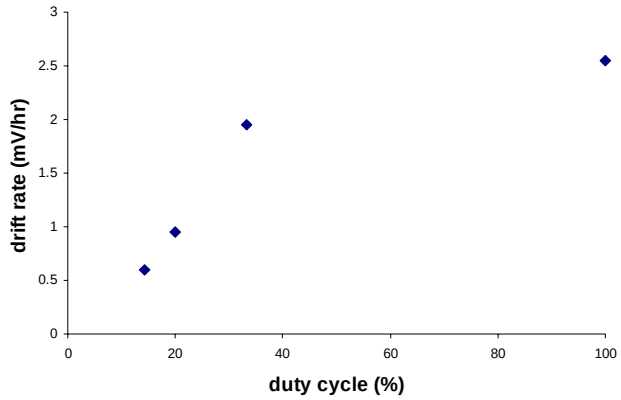

Figure 2-8: drift rate versus duty cycle

Drift measurements at different solution pH values were performed in duplo with 3 *type 2* ISFETs as to investigate reproducibility amongst ISFETs taken from the same wafer. For comparison to *type 1* ISFETs, also their drift behavior was characterized in duplo in a pH 4 buffer solution. The observed drift rates are plotted as a function of solution pH in figure 2-9.

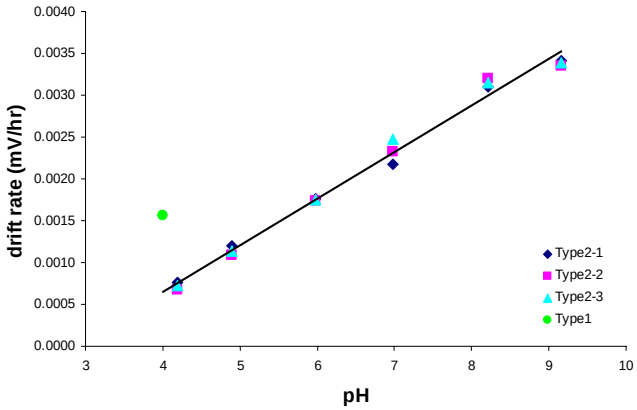

Figure 2-9: ISFET drift rate as a function of pH

From this figure, it can be concluded that in line with reports on tin oxide gate ISFETs in literature (Chou and Wang 2002), a linear relation between the drift rate and solution pH was obtained. Moreover, the drift characteristics of different ISFETs fabricated on the same wafer are very comparable.

From figure 2-8, it can be noted that long-term drift rate as obtained for *type 1* ISFETs is significantly higher. It can be expected this is due to contaminations in the oxide layer, which can be further investigated with both drift measurements and capacitance-

voltage measurements on MOSFETs fabricated on the same wafers of the used ISFETs. Drift measurements on *type 1* and *type 2* MOSFETs are depicted in figure 2-10.

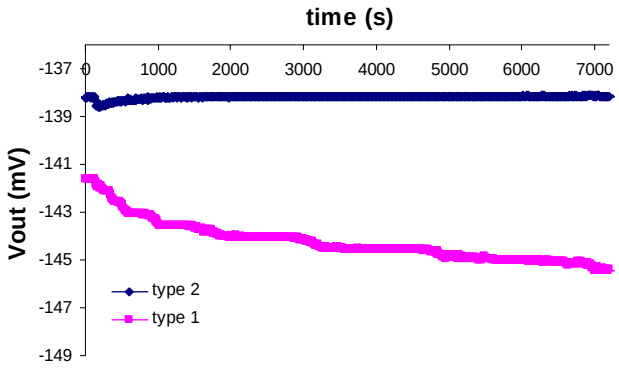

Figure 2-10: MOSFET drift for type 1 and type 2 devices

From the curves in figure 2-10, it can be seen that drift of *type 2* MOSFETs is negligible. This suggests that drift of *type 2* ISFETs is due to oxide-electrolyte interactions. Drift rate as obtained for a *type 1* MOSFET, however, is considerably higher, i.e. ~1mV/hr. It is conceivable that this drift is due to contaminations in the oxide layer. This can be studied in more detail by capacitance-voltage measurements on *type 1* and *type 2*

In order to do capacitance-voltage measurements on *type 1* and *type 2* MOSFETs, first the input capacitance of the potentiostat and the wiring were measured. This parasitic capacitance equals ~32 pF and was very dependent on wiring characteristics and positioning. The capacitance voltage characteristics before and after application of bias temperature stress (btst) for both types of MOSFETs are depicted in figures 2-11a and b, respectively.

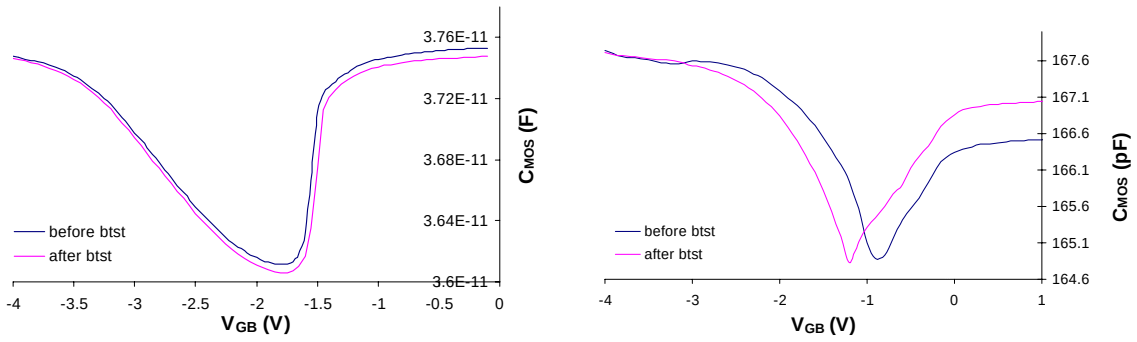

Figure 2-11: Capacitance voltage measurements for (a) type 1 and (b) type 2 MOSFETs

One can clearly distinguish between the accumulation, depletion and inversion regions for both types of MOSFETs. The oxide capacitance measured in accumulation is 5.6 pF for the *type 1* device and 132.5 pF for the *type 2* device. This is somewhat lower than the expected values of 4.6 pF and 173.6 pF respectively (see appendix 1), which probably has to do with simplifications made in the theoretical model, uncertainties due to parasitic impedances and limited control of process parameters.

Moreover, it can be seen that the capacitance-voltage curve for the *type 1* device did not shift significantly after applying bias temperature stress, indicating the gate oxide contamination is too low to be measured accurately using this method. The curve for the *type 2* device did shift. Since the threshold voltage was shifted approximately 0.35 V, it can be calculated that the mobile charge concentration responsible for this shift equals:

$$Q_m \cong -\frac{\Delta V}{C_{ox}} \cong \frac{0.35}{165 \cdot 10^{-12}} \cong 2.59 \cdot 10^9 \ m^{-2}$$

Since the bias temperature stress test was done under relatively mild conditions, the actual mobile charge concentration is presumably higher.

2.5.2 Dissolved oxygen

The next subsections will consecutively show the results of the feasibility tests performed with amperometry and ^{E}MOSFETs, respectively.

Amperometry

With the amperometric configuration described in section 2.4, cyclic voltammograms were obtained in a 0.1M KNO_3 buffer solution and in a supernatant solution taken from a running yeast fermentation. The result is depicted in figures 2-12a and 2-12b, respectively.

In figure 2-11a, the current plateau due to the reduction of oxygen is clearly visible for voltages ranging from approx. -0.4 V vs. NHE to -1 V vs. NHE. For lower voltages, electrolysis occurs and the current magnitude dramatically increases. After reversal of the voltage sweep, a positive current peak is detected due to re-oxidization of reduced species.

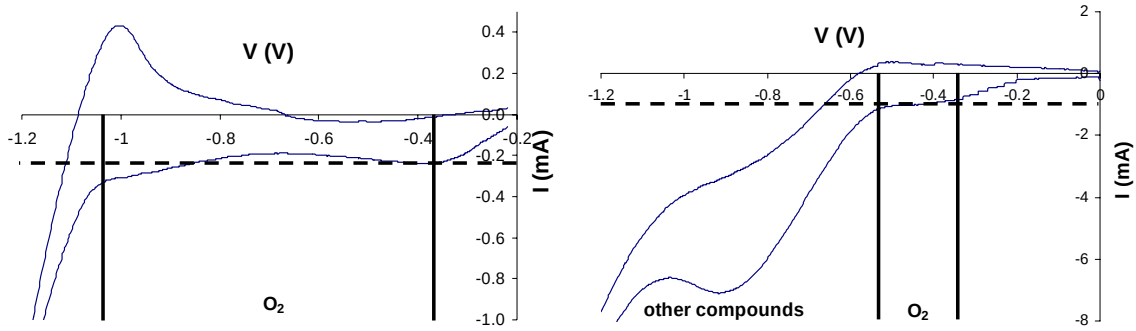

Figure 2-12: Cyclic voltammogram obtained in (a) 0.1M KNO_3 and (b) supernatant

The current plateau due to oxygen reduction can also be observed in figure 2-11b. For a voltage below -0.6V vs. NHE, however, reduction of other species starts taking place and the current magnitude increases even further for lower voltage values due to electrolysis. Concludingly, it can be noted that in order to be selective to oxygen using amperometric electrodes not covered by a membrane, an electrode polarization near the beginning of the plateau for oxygen reduction (~ -0.4 V vs. NHE) should be used.

Now that the proper electrode polarization voltage has been determined, the amperometric cell can be calibrated with respect to the actual dissolved oxygen concentration determined using a Clark cell. The results obtained in 0.1 M KNO_3 and supernatant are depicted in figures 2-13a and 2-13b, respectively.

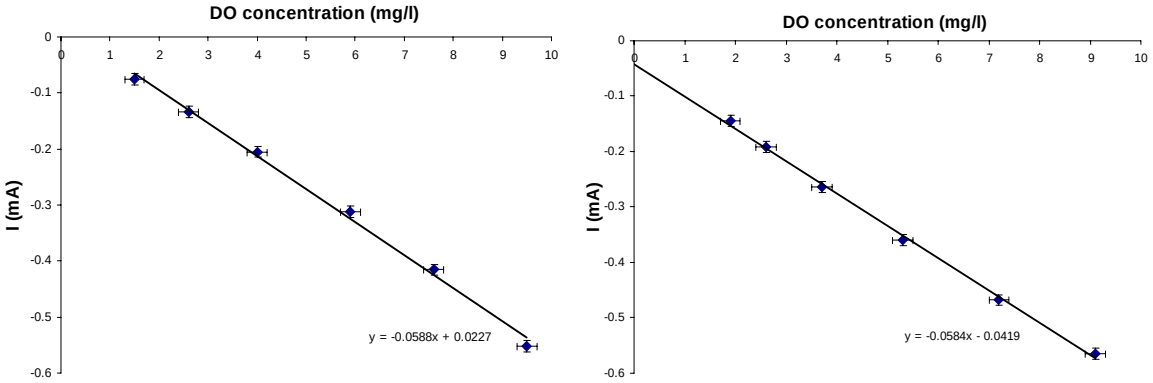

Figure 2-13: Current versus the dissolved oxygen concentration in (a) 0.1M KNO_3 and (b) supernatant

The error margins plotted indicate noise magnitude on both the oxygen measurement as on the current measurement. The calibration curves as obtained in 0.1M KNO_3 and supernatant look very similar and the extrapolated current at zero concentration is very low in both cases. This indicates that the cell is indeed selective towards oxygen.

^{E}MOSFET

^{E}MOSFET threshold voltage at different dissolved oxygen concentrations was measured using the experimental setup described in section 2.4.2. A stable value was reached within 30 seconds. Figure 2-14 a and b show the measurement results at different dissolved oxygen concentrations as obtained in pH 4 and pH 10 buffer solutions, respectively.

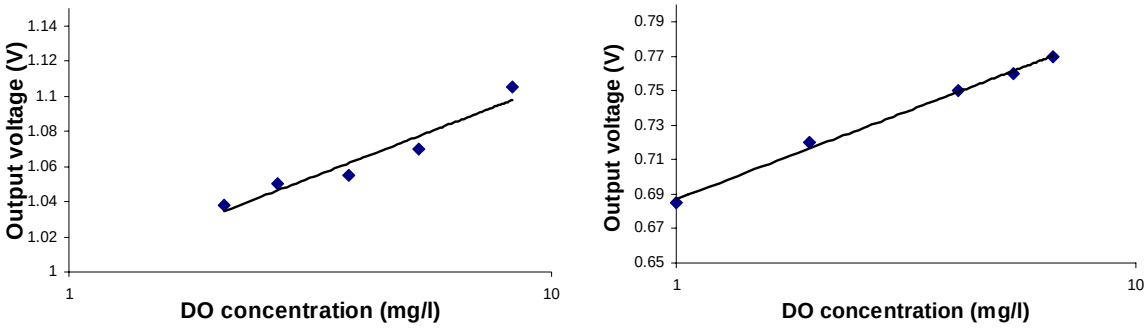

Figure 2-14: ^{E}MOSFET response in (a) pH 4 and (b) pH 10 buffer solutions

In both cases, a clear logarithmic response to the dissolved oxygen concentration and a sensitivity of ~110 mV/decade was obtained. In line with literature, these results confirm the transfer coefficient is independent of the dissolved oxygen concentration and solution pH.

The reproducibility of the sensor response was determined by calibrating two ^{E}MOSFETs fabricated on the same wafer in triplo (with several hours in between each measurement) in pH 7 buffer solutions. The results are depicted in figure 2-15.

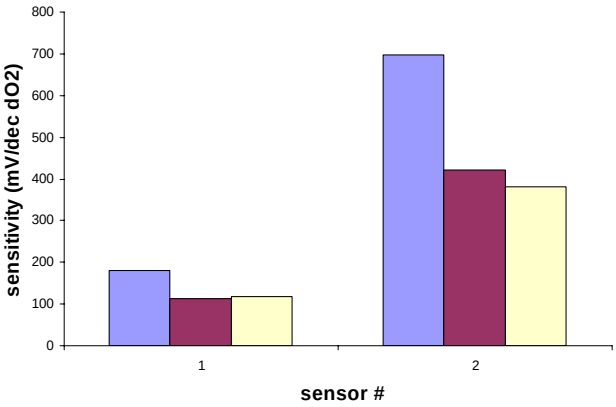

Figure 2-15: ^{E}MOSFET sensitivity in pH 7 buffer solution

From this figure, it can be observed that ^{E}MOSFET sensitivity and thus the value of the dimensionless transfer coefficient α was not reproducible for two devices fabricated on

the same wafer. Since α strongly depends on the properties of the iridium oxide surface, it can be assumed that the obtained spread in ^{E}MOSFET sensitivity originates from effects influencing the iridium oxide surface, such as fouling or hydratation.

2.5.3 Biomass

As described above, impedance spectra were obtained in the frequency range of 10 kHz – 10 MHz for yeast cell suspensions of various concentrations. The electrochemical cell capacitance was determined under the assumption that the impedance of the electrochemical cell can be modeled using the simple electrical equivalent circuit depicted in figure 2-1a. The capacitance values thus obtained for 10 spectral points around 70 kHz was compared to the values obtained for 10 spectral measurement points around 1.5 MHz. The difference between the low-frequency and high-frequency capacitance values was plotted as a function of the cell concentration in figure 2-16. The measurements were done in triplo; the error bars represent the standard deviation between the measurements.

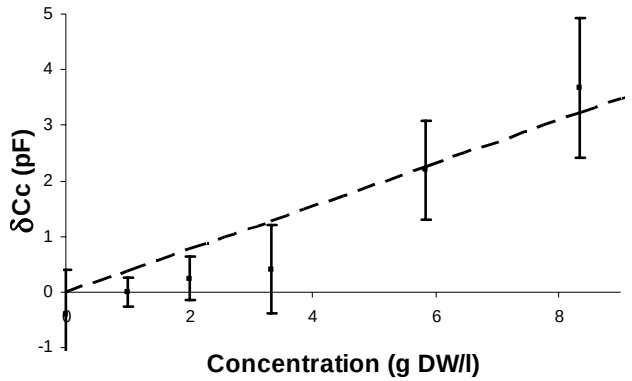

Figure 2-16: Difference between low-frequency and high-frequency capacitance values as a function of the yeast cell concentration

According to the results in figure 2-16, the observed capacitance difference increases significantly with increasing cell concentration. The increase is nearly linear. Deviations are assumed to be due to the process of making the cell suspensions, which involves weighing of the cell mass and adding a measured amount of medium. The error margins observed are considerable, because the capacitance changes are very small and therefore easily influenced by noise and minor variations in the parasitic impedance of the wiring and the measurement device.

2.6 Discussion & conclusions

The applicability of ISFETs for long-term measurements was investigated by studying characteristics of ISFET drift. It was observed that drift rate of *type 2* ISFETs shows a strong correlation with solution pH, which suggests drift behavior is influenced by effect at the oxide-liquid interface. Both drift measurements as temperature stress tests on *type 2* MOSFETs revealed no contaminations in the gate oxide layer of *type 2* devices, although bias temperature stress was applied under relatively mild conditions. On the other hand, both drift measurements ad bias temperature stress tests did show that the gate oxide of *type1* ISFETs is more severely contaminated. This probably explains why the drift rate for *type 1* ISFETs was observed to be higher.

If the ISFET is connected to the ISFET amplifier according to a <100% duty cycle, the observed drift rate is reduced considerably. This indicates that the cause of ISFET drift is electrical field enhanced. On the other hand, low duty cycles limit the measurement resolution and might lead to noise since after connecting an ISFET to the ISFET amplifier, some time is needed before a stable output signal is observed.

Drift characterization of *type 2* ISFETs furthermore shows that the long-term drift response of ISFETs fabricated on the same wafer is very comparable. This suggests that if the drift response of an ISFET placed in a constant pH environment is subtracted from the drift response of an ISFET in an environment where small changes with respect to this constant pH value need to be monitored, the influence of ISFET drift can be reduced to at most a few tenths of millivolts. This is acceptable for the targeted application.

For monitoring the dissolved oxygen concentration, two different techniques were investigated. ^{E}MOSFETs showed a good sensitivity towards the dissolved oxygen concentration. Corresponding transfer coefficient values were in accordance with previous studies on ^{E}MOSFETs. Sensitivity was shown to be independent of solution pH. However, ^{E}MOSFET sensitivity was not reproducible for different devices fabricated on the same wafer and tends to decrease considerably in a time span of several hours. This might indicate the device is very sensitive to fouling or other effects taking place at the iridium oxide interface.

Amperometry is a well established technique to monitor dissolved oxygen. Drawbacks related to amperometric cells consisting of macro electrodes, such as high oxygen consumption and flow dependence, can be circumvented by applying ultra micro electrodes (see also chapter 3). Main limitation in application of amperometry not solved by using ultra micro electrodes is whether sensitivity towards oxygen can be achieved in yeast culture. Therefore, cyclic voltammograms obtained in a supernatant solution were

compared to those obtained in 0.1 M KNO_3 solution where no interfering redox reactions were expected. From these voltammetry experiments, it was concluded that at an electrode polarization close to the beginning of the current plateau corresponding to the reduction of oxygen (i.e. ~-0.4V vs. NHE), selectivity towards oxygen is assured in supernatant. Calibrations in supernatant indeed showed a linear relation towards the dissolved oxygen concentration with low offset.

Concluding, the ^{E}MOSFET shows high, but irreproducible sensitivity towards dissolved oxygen, whereas high and selective sensitivity towards dissolved oxygen was obtained using amperometry. Moreover, amperometry is a much more mature technique and amperometric ultra micro electrode arrays are less complex in structure and thus easier to fabricate. It was therefore concluded that amperometry is the preferred method to monitor dissolved oxygen.

A limitation in the applicability of ISFETs and amperometric oxygen sensors is that for both techniques, a reference electrode is needed. Especially for the ISFET, the voltage drop across this reference electrode needs to be very stable for a duration of up to several days, since the potential drops in series with the voltage signal to be measured. Therefore, solid-state reference electrodes are not suitable for our application (Polk et al. 2006). Several microfabricated liquid junction reference electrodes have been reported in literature (Bakker and Qin 2006; Suzuki et al. 1999; van den Berg et al. 1990), but these require complex fabrication processes and also again, long-term stability is not always obvious.

Generally speaking, commercially available aqueous reference electrodes, like the Ag/AgCl reference electrode, do possess good stability characteristics. However, their integration in micro bioreactors is expensive and difficult, even though reference electrodes with a tip size below 2 mm are on the market. Moreover, silver chloride solution leaking into the bioreactor might harm the cell culture. Therefore, it is proposed to place a single conventional glass reference electrode in a separate reservoir which is connected to the micro bio reactors using saltbridges. By filling the saltbridges with a conductive liquid not harmful to the cell culture, the amount of silver chloride solution leaking into the reactor can be greatly reduced. If the solution in the reservoir containing the reference electrode is buffered at a pH value corresponding to the value at which the fermentation is performed, the ISFET used for differentially subtracting out the effect of ISFET drift can be placed in this reservoir as well. A schematic representation of the proposed microreactor configuration is depicted in figure 2-17.

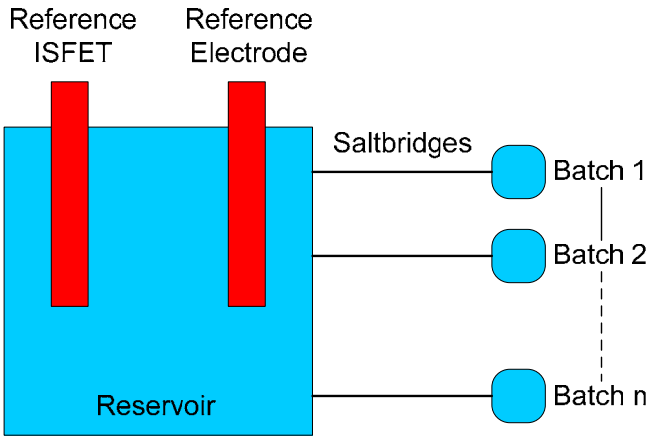

Figure 2-17: Proposed measurement setup

Impedance measurements show that impedance spectroscopy is a feasible method for biomass determination. The measured capacitance change, as obtained by comparing the capacitance between the electrodes at both high and low frequencies, increases linearly with the biomass concentration in a range of 0-10 g DW/l. Observed noise magnitude was considerable, since the capacitance changes measured were very small. Signal-to-noise performance can be enhanced by adjusting the geometry of the conductivity sensor in such a way that the capacitance between the electrodes is increased. An alternative is to measure the spectral variation in solution resistance instead of the variation in electrochemical cell capacitance.

The feasibility of impedance spectroscopy will be discussed in more detail in the next chapters.

References

Arquint P, Koudelka-Hep M, Van Der Schoot BH, Van Der Wal P, De Rooij NF. 1994. Micromachined analyzers on a silicon chip. Clinical Chemistry 40(9):1805-1809.

Asami K, Yonezawa T. 1995. Dielectric Analysis of Yeast-Cell Growth. Biochimica Et Biophysica Acta-General Subjects 1245(1):99-105.

Bakker E. 2004. Electrochemical sensors. Analytical Chemistry 76(12):3285-3298.

Bakker E, Qin Y. 2006. Electrochemical sensors. Analytical Chemistry 78(12):3965-3983.

Bakker E, Telting-Diaz M. 2002. Electrochemical sensors. Analytical Chemistry 74(12):2781-2800.

Bambot SB, Sipior J, Lakowicz JR, Rao G. 1994. Lifetime-Based Optical Sensing of Ph Using Resonance Energy-Transfer in Sol-Gel Films. Sensors and Actuators B-Chemical 22(3):181-188.

Bard AJ, Faulkner LR. 2001. Electrochemical Methods, Fundamentals and Applications: John Wiley & Sons, Inc.

Bergveld P. 1970. Development of an ion-sensitive solid-state device for neurophysiological measurements. IEEE Transactions on Biomedical Engineering 17:70-71.

Bergveld P. 2003. Thirty years of ISFETOLOGY - What happened in the past 30 years and what may happen in the next 30 years. Sensors and Actuators B-Chemical 88(1):1-20.

Bhat N, Cao M, Saraswat KC. 1997. Bias temperature instability in hydrogenated thin-film transistors. Ieee Transactions on Electron Devices 44(7):1102-1108.

Borisov SM, Vasylevska AS, Krause C, Wolfbeis OS. 2006. Composite luminescent material for dual sensing of oxygen and temperature. Advanced Functional Materials 16(12):1536-1542.

Bosch ME, Sanchez AJR, Rojas FS, Ojeda CB. 2007. Recent development in optical fiber biosensors. Sensors 7(6):797-859.

Bousse L, De Rooij NF, Bergveld P. 1983. The Influence of Counterion Adsorption on the Psi-0/Ph Characteristics of Insulator Surfaces. Surface Science 135(1-3):479-496.

Brett CMA, Brett AMO. 1983. Electrochemistry: Principles, Methods and Applications. New York: Oxford University Press. 81-90 p.

Campbell SA. 1995. The Science and Engineering of Microelectronics Fabrication. Oxford: Campbell.

Carvell JP, Harding CL, Oddi L. 1998. Laboratory yeast analyser for off-line measurement of viable yeast concentrations in brewing. Food Australia 50(8):389.

Chou JC, Wang YF. 2002. Preparation and study on the drift and hysteresis properties of the tin oxide gate ISFET by the sol-gel method. Sensors and Actuators B-Chemical 86(1):58-62.

Chung WY, Lin YT, Pijanowska DG, Yang CH, Wang MC, Krzyskow A, Torbicz W. 2006a. New ISFET interface circuit design with temperature compensation. Microelectronics Journal 37(10):1105-1114.

Chung WY, Yang CH, Pijanowska DG, Grabiec PB, Torbicz W. 2006b. ISFET performance enhancement by using the improved circuit techniques. Sensors and Actuators B-Chemical 113(1):555-562.

Clark LC. 1956. Monitor and control of blood and tissue oxygen tensions. Transactions - American Society for Artificial Internal Organs 2:41.

Cobbold RSC. 1974. Transducers for Biomedical Measurements. New York: John Wiley & Sons. 58-73 p.

Cooper MA. 2006. Optical biosensors: where next and how soon? Drug Discovery Today 11(23-24):1061-1067.

Epstein JR, Walt DR. 2003. Fluorescence-based fibre optic arrays: a universal platform for sensing. Chemical Society Reviews 32(4):203-214.

Fogg PGT, Gerrard W. 1991. Solubility of gases in liquids. New York: John Wiley & Sons, Inc. 24-25 p.

Gong JW, Chen QF, Lian MR, Liu NC, Daoust C. 2006. Temperature feedback control for improving the stability of a semiconductor-metal-oxide (SMO) gas sensor. Ieee Sensors Journal 6(1):139-145.

Hall EAH. 1990. Biosensors. Bryant JA, Kennedy JF, editors. Buckingham: Open University Press. 110 p.

Hauttmann S, Muller J. 2001. In-situ biomass characterisation by impedance spectroscopy using a full-bridge circuit. Bioprocess and Biosystems Engineering 24(3):137-141.

Hendrick F, Van Der Donckt E. 1999. Chemical optical sensing based on luminescence lifetime measurements: a caveat. Sensors and Actuators B-Chemical 61:218-221.

Hendrikse J, Olthuis W, Bergveld P. 1998. Characterization of the (MOSFET)-M-E, a novel one-electrode chemical transducer for redox measurements. Journal of Electroanalytical Chemistry 458(1-2):23-29.

Hendrikse J, Olthuis W, Bergveld P. 1999. The (MOSFET)-M-E as an oxygen sensor: constant current potentiometry. Sensors and Actuators B-Chemical 59(1):35-41.

Hessing CM, Panama KA, Asdonk LM, De Hulster E, Van Dijken JP, Pronk JT. 1995. Effects of Cultivation Conditions on the Production of Heterologous Alpha-Galactosidase by Kluyveromyces-Lactis. Applied Microbiology and Biotechnology 43(1):58-64.

Jamasb S. 2004. An analytical technique for counteracting drift in ion-selective field effect transistors (ISFETs). Ieee Sensors Journal 4(6):795-801.

Jamasb S, Collins S, Smith RL. 1998a. A physical model for drift in pH ISFETs. Sensors and Actuators B-Chemical 49(1-2):146-155.

Jamasb S, Collins SD, Smith RL. 1998b. A physical model for threshold voltage instability in Si3N4-gate H+-sensitive FET's (pH ISFET's). Ieee Transactions on Electron Devices 45(6):1239-1245.

Kostov Y, Harms P, Randers-Eichhorn L, Rao G. 2001. Low-cost microbioreactor for high-throughput bioprocessing. Biotechnology and Bioengineering 72(3):346-352.

Koudelka M. 1986. Performance-Characteristics of a Planar Clark-Type Oxygen Sensor. Sensors and Actuators 9(3):249-258.

Lee HLT, Boccazzi P, Ram RJ, Sinskey AJ. 2006. Microbioreactor arrays with integrated mixers and fluid injectors for high-throughput experimentation with pH and dissolved oxygen control. Lab on a Chip 6(9):1229-1235.

Lehmann M, Baumann W, Brischwein M, Gahle HJ, Freund I, Ehret R, Drechsler S, Palzer H, Kleintges M, Sieben U and others. 2001. Simultaneous measurement of cellular respiration and acidification with a single CMOS ISFET. Biosensors & Bioelectronics 16(3):195-203.

Leung A, Shankar PM, Mutharasan R. 2007. A review of fiber-optic biosensors. Sensors and Actuators B: Chemical 125(2):688-703.

Lippitsch ME, Draxler S. 1993. Luminescence Decay-Time-Based Optical Sensors - Principles and Problems. Sensors and Actuators B-Chemical 11(1-3):97-101.

Maharbiz MM, Holtz WJ, Howe RT, Keasling JD. 2004. Microbioreactor arrays with parametric control for high-throughput experimentation. Biotechnology and Bioengineering 85(4):376-381.

Mailly F, Giani A, Bonnot R, Temple-Boyer P, Pascal-Delannoy F, Foucaran A, Boyer A. 2001. Anemometer with hot platinum thin film. Sensors and Actuators a-Physical 94(1-2):32-38.

Marazuela MD, Moreno-Bondi MC. 2002. Fiber-optic biosensors - an overview. Analytical and Bioanalytical Chemistry 372(5-6):664-682.

Martinez-Manez R, Soto J, Lizondo-Sabater J, Garcia-Breijo E, Gil L, Ibanez J, Alcaina I, Alvarez S. 2004. New potentiomentric dissolved oxygen sensors in thick film technology. Sensors and Actuators B-Chemical 101(3):295-301.

Masson P, Autran JL, Munteanu D. 2002. DYNAMOS: a numerical MOSFET model including quantum-mechanical and near-interface trap transient effects. Solid-State Electronics 46(7):1051-1059.

McNaught AD, Wilkinson A. 1997. Compendium of Chemical Terminology. Oxford: Blackwell Science Ltd.

Mignani AG, Mencaglia AA. 2002. Direct and chemically-mediated absorption spectroscopy using optical fiber instrumentation. Sensors Journal, IEEE 2(1):52-57.

Oige K, Avarmaa T, Suisalu A, Jaaniso R. 2005. Effect of long-term aging on oxygen sensitivity of luminescent Pd-tetraphenylporphyrin/PMMA films. Sensors and Actuators B-Chemical 106(1):424-430.

Olthuis W. 2005. Chemical and physical FET-based sensors or variations on an equation. Sensors and Actuators B-Chemical 105(1):96-103.

Olthuis W, Streekstra W, Bergveld P. 1995. Theoretical and Experimental-Determination of Cell Constants of Planar-Interdigitated Electrolyte Conductivity Sensors. Sensors and Actuators B-Chemical 24(1-3):252-256.

Pejcic B, De Marco R. 2006. Impedance spectroscopy: Over 35 years of electrochemical sensor optimization. Electrochimica Acta 51(28):6217-6229.

Polk BJ, Stelzenmuller A, Mijares G, MacCrehan W, Gaitan M. 2006. Ag/AgCl microelectrodes with improved stability for microfluidics. Sensors and Actuators B-Chemical 114(1):239-247.

Pulfrey DL, Tarr NG. 1989. Introduction to microelectronic devices. London: Prentice Hall, Inc. 255-260 p.

Ruben S; 1935 19-11-1935. Electrical pyrometer resistance. USA patent US2021491.

Sawyer DT, Roberts J, J. L. 1974. Experimental Electrochemistry for Chemists. New York: John Wiley & Sons, Inc.

Schwan HP. 1957. Electrical properties of tissues and cell suspensions. Advances in Biological and Medical Physics 5:147.

Suzuki H, Hirakawa T, Sasaki S, Karube I. 1999. An integrated three-electrode system with a micromachined liquid-junction Ag/AgCl reference electrode. Analytica Chimica Acta 387(1):103-112.

Suzuki H, Hirakawa T, Watanabe I, Kikuchi Y. 2001. Determination of blood pO(2) using a micromachined Clark-type oxygen electrode. Analytica Chimica Acta 431(2):249-259.

Tiggelaar RM, Berenschot JW, de Boer JH, Sanders RGP, Gardeniers JGE, Oosterbroek RE, van den Berg A, Elwenspoek MC. 2005. Fabrication and characterization of high-temperature microreactors with thin film heater and sensor patterns in silicon nitride tubes. Lab on a Chip 5(3):326-336.

van den Berg A, Grisel A, van den Vlekkert HH, de Rooij NF. 1990. A Microvolume Open Liquid-Junction Reference Electrode for Ph-Isfets. Sensors and Actuators B-Chemical 1(1-6):425-432.

Van Steenkiste F, Baert K, Debruyker D, Spiering V, van der Schoot B, Arquint P, Born R, Schumann K. 1997. A microsensor array for biochemical sensing. Sensors and Actuators B: Chemical 44(1-3):409-412.

Verduyn C, Postma E, Scheffers WA, Van Dijken JP. 1992. Effect of Benzoic-Acid on Metabolic Fluxes in Yeasts - a Continuous-Culture Study on the Regulation of Respiration and Alcoholic Fermentation. Yeast 8(7):501-517.

Vojinovic V. 2006. Real-time bioprocess monitoring Part I: In situ sensors. Sensors and actuators. B, Chemical 114(2):1083-1091.

Wingard J, L. B., Ferrance JP. 1991. Biosensors with Fiberoptics. Hieftje GM, editor. Clifton, New Jersey: Humana Press. 16-18 p.

Woias P, Meixner L, Frostl P. 1998. Slow pH response effects of silicon nitride ISFET sensors. Sensors and Actuators B-Chemical 48(1-3):501-504.

Wolfbeis OS. 2006. Fiber-optic chemical sensors and biosensors. Analytical Chemistry 78(12):3859-3873.

Wu CC, Yasukawa T, Shiku H, Matsue T. 2005. Fabrication of miniature Clark oxygen sensor integrated with microstructure. Sensors and Actuators B-Chemical 110(2):342-349.

Yotter RA, Lee LA, Wilson DM. 2004. Sensor technologies for monitoring metabolic activity in single cells - Part I: Optical, methods. Ieee Sensors Journal 4(4):395-411.

Zanzotto A, Boccazzi P, Gorret N, Van Dyk TK, Sinskey AJ, Jensen KF. 2006. In situ measurement of bioluminescence and fluorescence in an integrated microbioreactor. Biotechnology and Bioengineering 93(1):40-47.

Chapter 3: Monitoring of yeast cell concentration using a micromachined impedance sensor

This chapter describes the design, modelling and experimental characterization of a micromachined impedance sensor for on-line monitoring of the viable yeast cell concentration (biomass) in a miniaturized cell assay. Measurements in Saccharomyces Cerevisiae cell culture show that characteristic frequency of the β–dispersion of S. cerevisiae cells is around 2.8 MHz. The permittivity of the cell suspension depends linearly on the biomass concentration within the range of 0 to 9 g/l/. In order to compensate the measurements for changes in the dielectric properties of the background electrolyte, the use of a three-electrode configuration in combination with a semi-permeable pHEMA membrane was explored. Measurements showed that the impedance of the hydrated pHEMA varies with only the background electrolyte conductivity, and not with the concentration of cells, indicating that pHEMA is suitable for this purpose. The optimal pHEMA membrane thickness was determined using finite element modelling.

3.1 Introduction

There is a growing interest in the miniaturization of cell cultivation systems, both for single-cell analysis (Gawad et al. 2004) and for fermentation studies (Maharbiz et al. 2004; Szita et al. 2005). For the latter, monitoring of biomass concentration with time is important for the assessment of the influence of fermentor conditions.

In this chapter, it is shown that dielectric spectroscopy is a convenient method for the on-line determination of biomass. In this method, the impedance of an electrochemical cell that contains the cell suspension is measured. The method is minimally invasive and selective for viable biomass only, as dead cells with leaky membranes do not affect the measurement (Markx and Kell 1995). It will be shown that changes in the background electrolyte conductivity can be compensated for by applying a three-electrode configuration in combination with a microporous poly(2-hydroxyethyl methacrylate) (pHEMA) membrane.

3.2 Theory

The design of the electrochemical cell requires only two metal electrodes with a defined spacing. Such a device can be fabricated using standard thin-film processes and is cheap, small, scalable, steam-sterilizable and suitable for integration with other microfabricated electrochemical devices. The electrical equivalent circuit of the electrochemical cell and a typical impedance curve are shown in figure 3-1.

The value of the electrolyte resistance R_s and the electrochemical cell capacitance C_c depend on the sensor dimensions and the conductivity σ and permittivity ε_r of the electrolyte, respectively, according to:

$$R_s = \frac{\kappa}{\sigma} \tag{3-1}$$

$$C_c = \varepsilon_0 \varepsilon_r \kappa \tag{3-2}$$

where ε_0 is the permittivity of free space and κ is the so-called cell constant describing the geometry of the electrode configuration. For planar electrode configurations, this cell constant can be determined using conformal mapping of the electrodes (Olthuis et al. 1995).

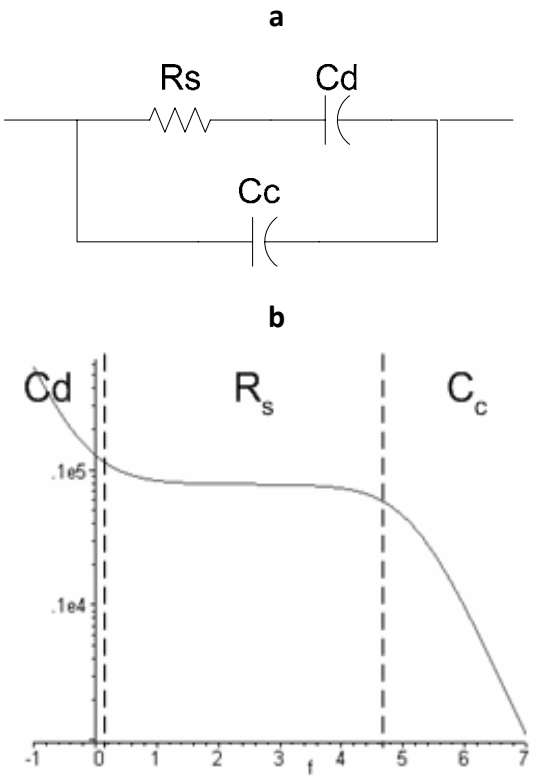

Figure 3-1: (a) Electrical equivalent circuit and (b) typical impedance curve. Cd is the electrode double layer capacitance.

The dielectric spectra of biological cells show three distinct dispersions in the frequency range of 1 Hz – 1 GHz, termed α-, β- and γ-dispersion (Asami 2002). β-dispersion originates from interfacial polarization, that is the accumulation of charges at the boundaries between the membrane and aqueous phases of different electrical properties. This polarization is frequency dependent and shows relaxation (Schwan 1957).

The dispersive frequency range is represented by a characteristic frequency, which depends strongly on the exact morphology of the cells and the electric properties of the cells and the background electrolyte (Hauttmann and Muller 2001). Previous studies showed characteristic frequencies in the order of a few MHz for viable Saccharomyces *cerevisiae* cells (Asami and Yonezawa 1995; Hauttmann and Muller 2001).

Theoretical descriptions of how β-dispersion affects the conductivity and permittivity of the cell suspension and how the cell concentration can be estimated from these data have been reported previously (Asami and Yonezawa 1995). In this work, the viable yeast cells are modeled as single-shell spherical cells. Our work relates this theory to experimental results obtained with a micromachined impedance sensor that was designed

for the on-line monitoring of biomass in a miniaturized yeast assay. The sensor is also suitable for use in larger (up to industrial scale) fermentation systems.

The main reason that dielectric spectroscopy is still not a widely used method for biomass monitoring, that the measured signals suffer from interference of the electric properties of the background electrolyte. The ionic concentration of the background electrolyte affects its conductivity. The measured permittivity is affected as well, as it determines the rate of electrode polarization. This effect is frequency dependent and cannot reliably be subtracted out, as the ionic content of the medium changes during the fermentation process (Siano 1997). Therefore, we have explored a method that compensates for changes in the electric properties of the background electrolyte by differential measurement using a three-electrode configuration (Varlan et al. 1996) in which the impedance measured between two closely spaced electrodes is made insensitive to biomass by covering it with a porous membrane that prevents cells to approach the electrodes. A schematical representation of such a three-electrode configuration is depicted in figure 3-2.

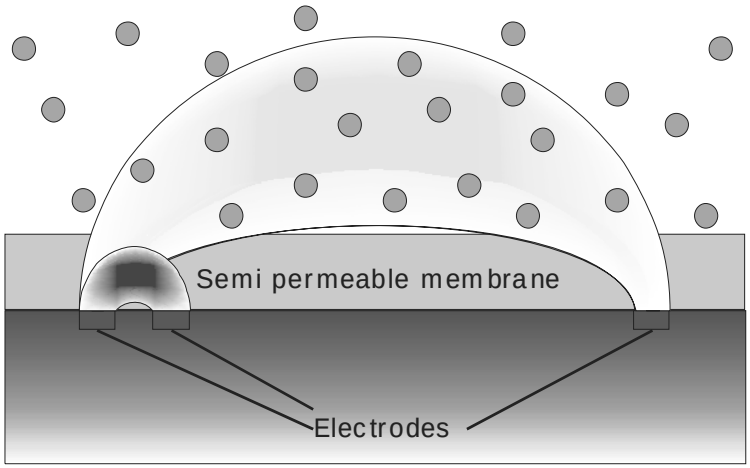

Figure 3-2 Schematical representation of the three-electrode configuration.

The electric properties of a microporous poly(2-hydroxyethyl methacrylate) (pHEMA) membrane were characterized for this purpose. The advantages of pHEMA as membrane material are that it can easily be photostructured using standard photolithographic processes and that it withstands standard sterilization by autoclaving.

3.3 Experimental

3.3.1 Device fabrication

Planar Ta/Pt electrodes were fabricated on an oxidized silicon substrate using a sputtering technique for metal deposition and lift-off photolithography. The processed electrode configuration consists of two 2200 μm × 100 μm electrodes, spaced by 60 μm. A photograph of the device is depicted in figure 3-3.

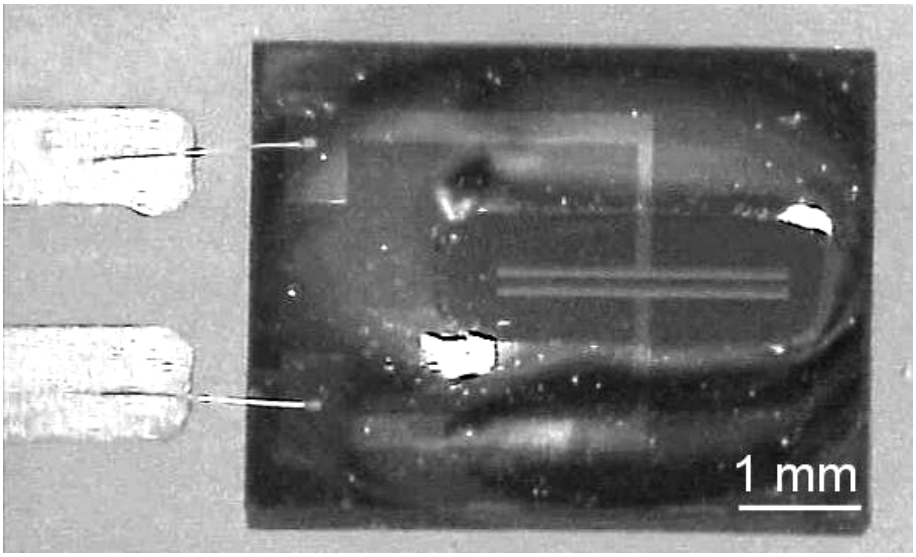

Figure 3-3: Photograph of fabricated planar electrode structure.

One pair of electrodes was covered by a pHEMA membrane. The HEMA mixture consists of 2.426ml HEMA, 0.092 ml cross linker (TEGDMA), 0.1538 gr. UV initiator (2, 2dimetoxy-2-phenylacetophenone, DMPAP) and 1.169 ml solvent (ethyleneglycol). The UV initiator is added at the end, in order to prevent the mixture from polymerizing too early.

The prepared solution is pipetted on the sensor surface, covered with a piece of Mylar® foil and subsequently exposed to 366 nm UV light for 2 minutes. The non-optimized membrane pHEMA thickness of 300 □m was high enough to assure that the electric field between the electrodes is concentrated within the hydrated pHEMA layer.

3.3.2 Measurement procedures

As stated above, the characteristic frequency for dielectric dispersion typically is around a few MHz for S. *Cerevisiae* cells. However, the exact frequency value depends on the morphology of the cells and the electrical properties of the medium. Therefore, the medium conductivity in a standard yeast suspension with a concentration of 7 g/l DW was determined from impedance measurements in the frequency range of 10 kHz – 40 MHz. These measurements were performed by connecting a pair of bare Ta/Pt electrodes as depicted in figure 3-1 to a Hewlett Packard HP 4194A gain-phase analyzer and fitting the impedance data on the simple electrical equivalent circuit depicted in figure 3-1a. The applied voltage was kept below 100 mV_{rms} in order to prevent redox reactions to take place.

The theoretical response of the change in electrochemical cell capacitance due to dielectric dispersion to varying cell concentrations was calculated, based on the single-shell model for characterizing the suspended cells, the impedance model shown in figure 3-1 (a), the conformal mapping technique and the actual suspension parameters.

Viable *Saccharomyces cerevisiae* cell concentration was also measured. To this end, the yeast cells were suspended in a mineral medium, containing 10 g/l ammonium sulphate, 6 g/l potassium phosphate monobasic and 1 g/l magnesium sulphate heptahydrate (Verduyn et al. 1992). The pH of the buffer solution was adjusted to 5.0 using concentrated sodium hydroxide.

Using the pHEMA-covered pair of electrodes, the electrolyte conductivity was measured in solutions containing known concentrations of sodium chloride. The measurements were compared to the theoretical electrolyte conductivity values, calculated using:

$$\sigma = \sum_i z_i c_i \lambda_i \qquad (3\text{-}3)$$

with σ being the electrolyte conductivity and z_i and c_i being the species valence and molar concentration of ion i, respectively. λ_i is a parameter that describes the concentration dependence of the conductivities at 25 ^{o}C (Bockris and Reddy 1970). The sensor response was also measured in cell suspensions of different biomass concentrations in order to verify whether the membrane is impermeable to yeast cells.

3.4 Measurement results

First, the frequency range in which dielectric dispersion occurs was determined. Therefore, the spectral conductivity increase was determined from impedance measurements performed with a pair of bare Ta/Pt electrodes in a 7 g/l DW yeast cell suspension. The observed conductivity increase, normalized on the conductivity measured around 10 kHz, is depicted in figure 3-4.

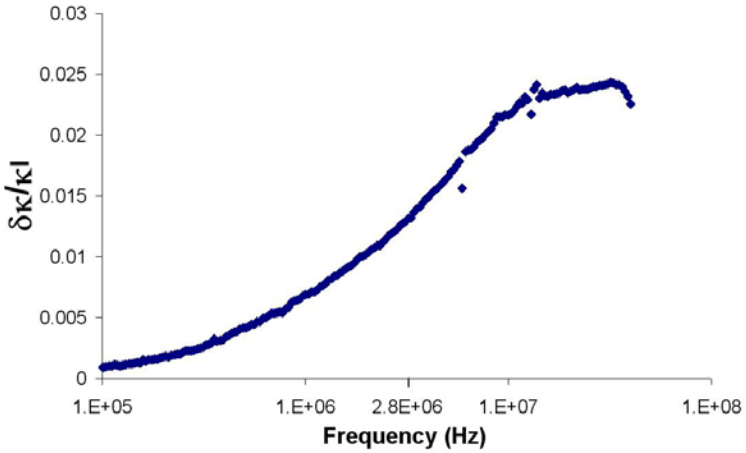

Figure 3-4: Change in electrolyte conductivity versus frequency

From the results in figure 3-4, the characteristic frequency describing the dispersion effect is observed to equal around 2.8 MHz; at lower frequencies dispersion magnitude decays to zero.

The electrochemical cell capacitance was determined from impedance measurements in two different frequency ranges; the low-frequency limit was determined in the range of 60-80 kHz and the dispersive value was determined in the range of 1-2 MHz. The measured difference between these values, δC_c is depicted in figure 3-5.

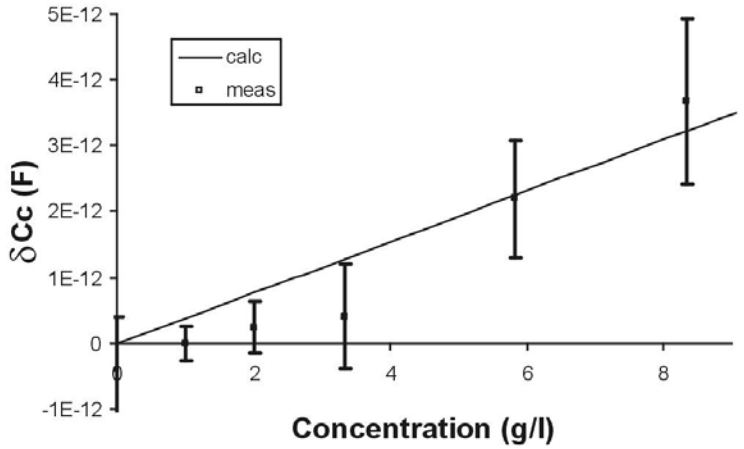

Figure 3-5: Theoretical and measured response in yeast suspensions of various concentrations.

The results in figure 3-5 show that a linear relation is observed between the electrochemical cell capacitance difference and the yeast cell concentration. The results match the calculations quite well for typical fermentor concentrations of yeast cells in a standard yeast buffer solution. The sensor performance depends to a large extent on the match between the sensor dimensions and the electric properties of the yeast suspension. The measurements show that a detection limit below 1 g/l can be achieved with the current configuration.

After placement in solution, the electrolyte resistance measured with the pHEMA covered electrode pair keeps decreasing for 40 minutes and then reaches a stable value. This can be seen in figure 3-6a. Once hydrated, the sensor responds to conductivity changes with a considerable delay as can be seen in figure 3-6b.

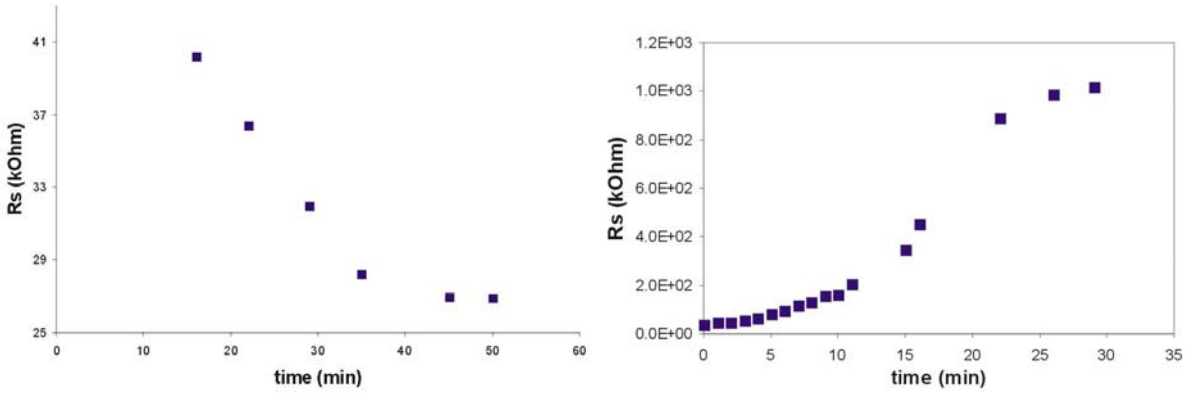

Figure 3-6: Electrolyte resistance versus time after (a) placing in solution (b) changing the ionic concentration from 100 mM to 2 mM.

It is assumed that the observed behaviour is due to hydration of the membrane and because ions slowly diffuse in this hydrated layer. In future configurations, the electrodes will be much more closely spaced and the membrane thickness required to assure that the electrical field between the electrodes is concentrated within the hydrated membrane layer will be much lower. This will decrease the time required for membrane hydration and uniform distribution of ions. The time can be reduced even further by adding solvent to the HEMA mixture during fabrication, resulting in an opener structure.

The results of electrolyte resistance measurements performed at different concentrations of a NaCl solution with both uncovered and pHEMA covered impedance sensors, are depicted in figures 3-7 a and b, respectively.

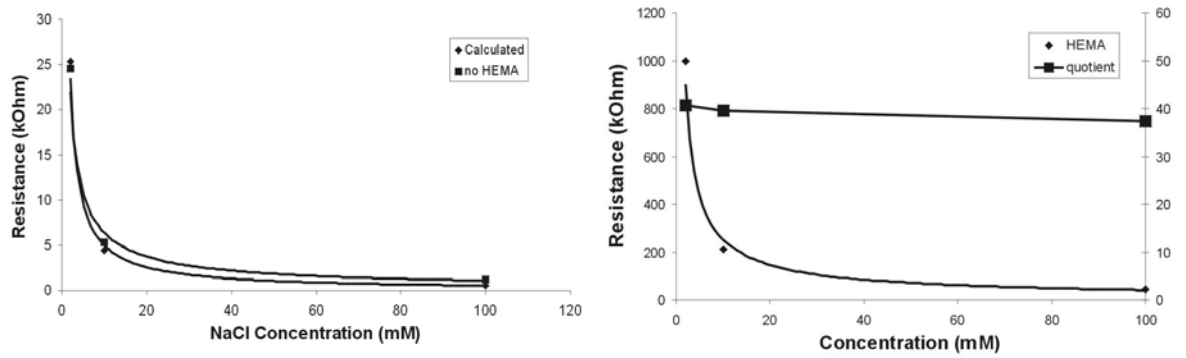

Figure 3-7: Theoretical electrolyte resistance and measurements with (a) a planar conductance sensor and (b) a planar conductance sensor covered with a pHEMA membrane. The quotient plotted in (b) shows the relation between the resistances measured with both sensors is constant.

Figure 3-7a shows that the solution resistance measured with a pair of uncovered electrodes matches the expected resistance values very well. Calculations were based on equations (3-1) through (3-3) and the conformal mapping method referred to above. The solution resistance measured with a pHEMA covered conductivity sensor in 1-100 mM NaCl solutions is higher than the theoretical and experimentally obtained response plotted in figure 3-7a. The factor characterizing the difference between the measurements in figures 3-7a and b is constant with the ion concentration.

Therefore, it can be concluded that the observed behaviour shows that the measured solution resistance measured is proportional to the electrolyte resistivity. The observed resistance is higher for the pHEMA-covered pair of electrodes because the volume, in which the electrical field between the electrodes is contained, is partially occupied by the insulating membrane.

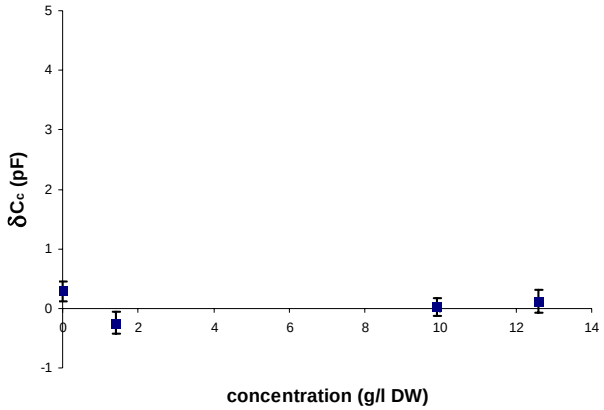

Figure 3- 8: Spectral capacitance change measured with a pHEMA-covered impedance sensor in yeast suspensions of various concentrations.

Figure 3-8 shows the difference in cell capacitance, δC_c, in two different frequency ranges (60-80 kHz and 1-2 MHz), measured with the pHEMA covered sensor as a function of the viable yeast concentration.

The observed spectral change in electrochemical capacitance is very small and there is no obvious relation with the viable yeast concentration. This indicates that the membrane is indeed impermeable to yeast cells.

To find the optimal pHEMA thickness, the electrical field distribution in this system was simulated using finite-element modelling. The width of all electrodes was defined as 200 μm, the length of the outer electrodes is set to 200 μm and the spacing between them to 400 μm. The length of the inner electrode is set to 2 μm because this is presumed to be the minimum feature size feasible with standard lithographic techniques. The spacing between the two most closely spaced electrodes is set to 2 μm as well. The electrodes are covered by a layer of varying thickness, which is assigned the electric properties of the hydrated pHEMA membrane, which were obtained from the measurements shown above. The volume outside this layer is assigned the dielectric properties of a cell suspension.

The current through the electrodes was simulated as a function of the membrane thickness. The result is depicted in figure 3-9.

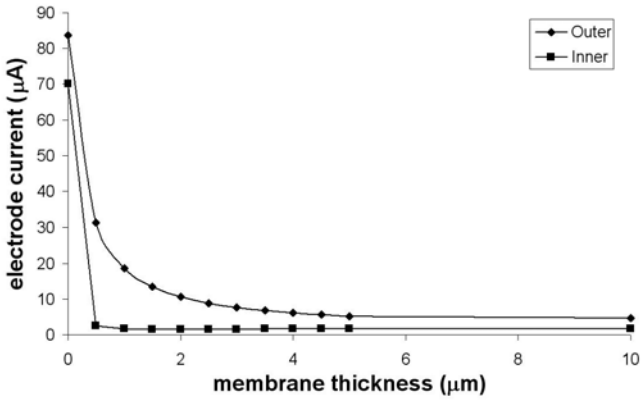

Figure 3- 9: Simulated relation between electrode current and membrane thickness

The current through the electrodes decreases with increasing membrane thickness, as the average electrolyte conductivity decreases. The current through the inner electrodes reaches a steady value at a thickness of 1 micron, indicating that for this thickness the electrical field lines do not penetrate the cell-containing solution so that the measured signal does not depend on the cell concentration.

Future sensor designs will be based on the optimal pHEMA thickness resulting from these finite-element simulations.

3.5 Conclusion

Using a micromachined impedance sensor, the characteristic frequency describing the dielectric dispersion in a S. *cerevisiae* cell suspension was determined to equal 2.8 MHz. This range corresponds well to empiric data in literature. The measured capacitance change due to dielectric dispersion shows a linear response to concentration and matches the calculations quite well for typical fermentor concentrations of yeast cells in a standard yeast buffer solution, confirming the relevance of the applied theory on microreactor scale.

The measurements with the pHEMA covered electrode pair show that the measured resistance does depend linearly on the actual electrolyte conductivity and that the measured cell capacitance is independent of the viable yeast cell concentration. This confirms that the pHEMA membrane gets hydrated, but is impermeable to yeast cells. This makes the proposed 3-electrode configuration suitable for determining the background electrolyte conductivity independent of the viable cell concentration. This signal can thus be used for compensating the measured impedance spectrum for changes in the background electrolyte.

The optimal hydrated membrane thickness arises from the observed electric properties of the membrane and finite element modelling and is found to equal 1 micron for the electrode configuration under study. The electric and transient properties of the membrane can be further optimized by altering the physical membrane properties.

References

Asami K. 2002. Characterization of biological cells by dielectric spectroscopy. Journal of Non-Crystalline Solids 305(1-3):268-277.

Asami K, Yonezawa T. 1995. Dielectric Analysis of Yeast-Cell Growth. Biochimica Et Biophysica Acta-General Subjects 1245(1):99-105.

Bockris JO, Reddy AKN. 1970. Modern Electrochemistry. New York: Plenum Press.

Gawad S, Cheung K, Seger U, Bertsch A, Renaud P. 2004. Dielectric spectroscopy in a micromachined flow cytometer: theoretical and practical considerations. Lab on a Chip 4(3):241-251.

Hauttmann S, Muller J. 2001. In-situ biomass characterisation by impedance spectroscopy using a full-bridge circuit. Bioprocess and Biosystems Engineering 24(3):137-141.

Maharbiz MM, Holtz WJ, Howe RT, Keasling JD. 2004. Microbioreactor arrays with parametric control for high-throughput experimentation. Biotechnology and Bioengineering 85(4):376-381.

Markx GH, Kell DB. 1995. The Use of Dielectric Permittivity for the Control of the Biomass Level during Biotransformations of Toxic Substrates in Continuous-Culture. Biotechnology Progress 11(1):64-70.

Olthuis W, Streekstra W, Bergveld P. 1995. Theoretical and Experimental-Determination of Cell Constants of Planar-Interdigitated Electrolyte Conductivity Sensors. Sensors and Actuators B-Chemical 24(1-3):252-256.

Schwan HP. 1957. Electrical properties of tissues and cell suspensions. Advances in Biological and Medical Physics 5:147.

Siano SA. 1997. Biomass measurement by inductive permittivity. Biotechnology and Bioengineering 55(2):289-304.

Szita N, Boccazzi P, Zhang ZY, Boyle P, Sinskey AJ, Jensen KF. 2005. Development of a multiplexed microbioreactor system for high-throughput bioprocessing. Lab on a Chip 5(8):819-826.

Varlan AR, Jacobs P, Sansen W. 1996. New design technique for planar conductometric haematocrit sensors. Sensors and Actuators B-Chemical 34(1-3):258-264.

Verduyn C, Postma E, Scheffers WA, van Dijken JP. 1992. Effect of benzoic acid on metabolic fluxes in yeasts: a continuous-culture study on the regulation of respiration and alcoholic fermentation. Yeast 8:501-517.

Chapter 4: Integrated electrochemical sensor array for on-line monitoring of yeast fermentations

This chapter describes the design, modelling and experimental characterization of an electrochemical sensor array for on-line monitoring of fermentor conditions in both miniaturized cell assays and in industrial scale fermentations. The viable biomass concentration is determined from impedance spectroscopy. As a miniaturized electrode configuration with high cell constant is applied, the spectral conductivity variation is monitored instead of the permittivity variation. The dissolved oxygen concentration is monitored amperometrically using an ultra micro electrode array, which is shown to have negligible flow dependence. pH is monitored using an ISFET and a platinum temperature resistance is included for temperature measurements. All sensors were shown to be sufficiently accurate within the range relevant to yeast fermentations. The sensor array is shown to be very stable and durable and withstands steam sterilization.

4.1 Introduction

In modern biotechnology, the products of micro-organisms are used for many applications (Gavrilescu and Chisti 2005). As fermentation in industrial scale fermentors is very money- and time consuming, it is very important that the right strains of cells are selected. For this purpose, rapid parallel screening of micro-organisms is needed. In conventional methods, this cell screening is done by first culturing the micro-organisms in Petri dishes or microtiter plates. Only the best performing strains of cells are selected for fermentation under industrially relevant conditions in a fermentor with working volumes typically varying from 0.5 – 2.0 liters. In order to make the cell screening faster, cheaper, more effective and less labor-intensive, there is a growing interest in the miniaturization and parallelization of these fermentors. This requires the development of small, integrated sensors suitable for the on-line assessment of fermentor conditions, such as biomass, temperature, pH and dissolved oxygen.

For application in yeast fermentations, these sensors should be sufficiently accurate under industrially relevant conditions. The sensors should remain stable for the duration of the fermentation process, which typically takes several days. The sensors need to be sterile when they are placed in the bioreactor. Sterilization can be done using gamma irradiation, but for reusable systems, sensors that can withstand steam sterilization are preferable. Moreover, in order to be applicable in miniaturized systems, the sensors should be small. This study aims at the development of sensors that can operate in systems compatible with the 96 well microtiter plate, which consists of 96 wells with a diameter of 6 millimeter.

In most miniaturization approaches, small and commercially available fiber-optical sensors are used (Balagadde et al. 2005; Maharbiz et al. 2004; Zanzotto et al. 2006; Zhang et al. 2006). In these sensors, the optical properties of one or more of the materials forming the waveguide respond to changes in the measurand.(Lambeck 2006) To achieve this, an active dye is usually immobilized at the tip of the fiber. Generally available fiber-optic pH sensors can not operate below pH 6 (Yotter et al. 2004), whereas S. *cerevisiae* yeast cells are usually fermented at pH 5 in industrial processes. Moreover, optical sensors are not very suitable for parallelization in a reusable system as they are expensive(Lambeck 2006), usually not steam-sterilizable and often suffer from dye-leaching (Gawad et al. 2001; Malins et al. 2000; O'Riordan et al. 2005). These problems can be overcome by using silicon-based electrochemical sensors instead. Therefore, integrated electrochemical sensors in silicon were developed for the on-line determination of fermentor conditions. The sensors are optimized for application in miniaturized fermentors, but can also be applied in larger

fermentor systems as in any other system where simultaneous pH, dissolved oxygen, viable biomass and temperature measurements are required.

4.2 Theory

The following subsections describe the fundamentals of sensors used for monitoring biomass, dissolved oxygen, pH and temperature, respectively.

4.2.1 Biomass

Measurement of biomass concentration is essential for successful operation of bioreactors. Conventional methods used for biomass concentration determination, like measurements of dry cell weight, packed cell volume and cell numbers counted under a microscope, often require samples of culture broth to be taken from the fermentor. Several on-line monitoring methods for biomass concentrations have been developed (Mishima et al. 1991), of which the measurement of optical density has frequently been applied in miniaturized cell assays. Impedance spectroscopy forms an electrochemical alternative to the aforementioned methods. A characteristic property of this technique is that the viable cell concentration is measured; dead cells do not contribute to the measurement output since they do not possess intact plasma membranes (Harris et al. 1987) and therefore do not polarize significantly (Carvell and Dowd 2006). It was shown by Markx and Kell (Markx and Kell 1995) that the dispersion signal indeed decreased when the cells were abruptly killed by adding benzaldehyde.

Impedance spectroscopy is based on conductivity measurements which consist of monitoring the impedance between two metallic electrodes placed in solution. For two equally large facing electrodes, the cell constant κ is written as:

$$\kappa = \frac{l}{A} \tag{4-1}$$

where l is the distance between the electrodes and A is the electrode area. A simple electrical equivalent circuit of such a conductivity cell and a typical impedance curve are shown in figure 4-1.

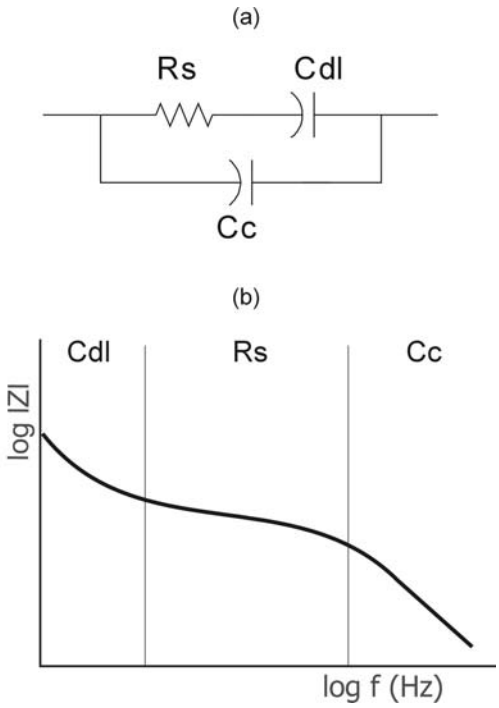

Figure 4-1: (a) Typical impedance model of a conductivity sensor, consisting of solution resistance R_s, combined double layer capacitance C_{dl} and electrochemical cell capacitance C_c (b) corresponding impedance spectrum

C_{dl} is the double layer capacitance that is attributed to the electrical double layers that build up at the electrode-electrolyte interfaces. The value of the electrolyte resistance R_s and the electrochemical cell capacitance C_c depend on the sensor dimensions and the conductivity σ and permittivity ε_r of the electrolyte, respectively, according to:

$$R_s = \frac{\kappa}{\sigma} \tag{4-2}$$

$$C_c = \frac{\varepsilon_0 \varepsilon_r}{\kappa} \tag{4-3}$$

where ε_0 is the permittivity of free space. For planar electrode configurations, the cell constant can be determined using conformal mapping of the electrodes (Olthuis et al. 1995).

The impedance spectra of biological micro-organism suspensions show three distinct dispersions in the frequency range of 1 Hz – 1 GHz, termed α-, β- and γ-dispersion

(Asami 2002). β-dispersion originates from interfacial polarization, that is the accumulation of charges at the boundaries between the micro-organism membrane and aqueous phases of different electrical properties. This polarization is frequency dependent and shows relaxation(Schwan 1957); the interfacial polarization effect can not follow the electric field when the frequency of the electric field exceeds a certain characteristic frequency. Therefore, the overall solution impedance, as measured by the conductivity sensor, changes above this frequency. The characteristic frequency above which interfacial polarization does not occur anymore, depends strongly on size and shape of the cells, the membrane capacitance, cytoplasm conductivity and background electrolyte conductivity(Hauttmann and Muller 2001). Previous studies showed characteristic frequencies in the order of a few MHz for viable S. *cerevisiae* cells (Asami and Yonezawa 1995a; Hauttmann and Muller 2001).

Asami et al.(Asami and Yonezawa 1995a) have described theoretically how β-dispersion causes the permittivity of the cell suspension to decrease and its conductivity to increase and how the viable cell concentration can be estimated from these data. The obtained analytical relation between the measured output and the viable cell concentration depends on the cell model used. Models for many different cell geometries, such as single shell or multilayer shell spherical cells, rod-like shaped cells(Fricke 1955), ellipsoid cells(Asami and Yonezawa 1995b) or cells accumulated as doublets(Asami et al. 1998) have been developed. Yeast cells are commonly spherical to egg shaped(Prescott et al. 1990). In previous studies, good results were obtained by modeling yeast cells as single shell spherical cells(Asami and Yonezawa 1995a; Krommenhoek et al. 2006). In his work, viable yeast cells are modeled as single-shell spherical cells. For a miniaturized electrode configuration with a high cell constant, the capacitance between the electrodes is very small. Small capacitance values are hard to measure accurately due to the influence of the parasitic capacitance of wiring and electronic circuitry; therefore determination of the conductivity is preferable. The theoretical relation between the conductivity change $\Delta\sigma$ and the viable biomass concentration (number of cells per unit volume) N_c is described by(Asami and Yonezawa 1995a):

$$\Delta\sigma \approx 6\pi R^3 N_c \sigma_a \left(\frac{\sigma_i / \sigma_a}{2 + \sigma_i / \sigma_a} \right) \qquad (4\text{-}4)$$

Here, R is the cell radius and σ_i and σ_a are the conductivities of the cell's cytoplasm and background medium, respectively. By assuming the cells are spherical in shape and $\sigma_i > \sigma_a$, a conductance difference of ~0.45% per g/l viable biomass can be expected. Depending on the accuracy of the impedance measurement setup, the detection limit could be well below 1 g/l.

4.2.2 Dissolved oxygen

Conventional methods for the electrochemical determination of the dissolved oxygen concentration in an electrolyte rely on amperometry, where oxygen is reduced at a working electrode and the resulting current is monitored. In aqueous acidic media, oxygen is reduced following(Hall 1990):

$$O_2 + 4H^+ + 4e^- \rightarrow 2H_2O \qquad \text{(4-5a)}$$

Similarly at alkaline pH, the reduction process is governed by:

$$2H_2O + O_2 + 4e^- \rightarrow 4OH^- \qquad \text{(4-5b)}$$

The relation between this current and the actual dissolved oxygen concentration in the solution is described by the Cottrell equation (Bard and Faulkner 1980; Rubinstein 1995):

$$I = nFAc_0\sqrt{\frac{D}{t\pi}} \qquad \text{(4-6)}$$

where n is the number of electrons being transferred, A is the electrode area, F is the Faraday constant, D is the diffusion constant of the reduced species, c_0 is the concentration of the redox active species in the bulk of the electrolyte and t is time. For macro electrodes in a stirred medium which is continuously supplied with oxygen, it might take up to several minutes before this concentration gradient is in equilibrium and the resulting diffusion boundary layer is subject to flow. Therefore, also the measured current *I* is flow-dependent. In conventional Clark oxygen probes, these problems are circumvented by letting the concentration gradient mainly build up in a membrane enclosing an internal

cavity containing the amperometric cell (Clark and Clark 1987). This structure, however, limits the response time of the sensor and makes the sensor difficult to miniaturize.

Another way to overcome the flow dependence of the current detection is by applying "ultra micro electrodes", which is a term generally denoting circular electrodes with a radius r below 2.5 μm. In this case, the equilibrium oxygen concentration profile builds up within a few milliseconds and the contribution of diffusion to the total mass transfer of oxygen becomes so high, that it is hardly influenced by convection (Brett and Brett 1983). For disc ultra micro electrodes, equation (4-6) therefore converts into:

$$I = nFAD\frac{c_0}{r} \tag{4-7}$$

As one can see, the measured current no longer depends on time. In addition, reducing the electrode area reduces the current magnitude. This potentially causes the achievable signal-to-noise ratio to decline. This problem can be circumvented by applying an array of ultra micro electrodes connected in parallel. Equation (4-7) can then be written as:

$$I = mnFAD\frac{c_0}{r} \tag{4-8}$$

Where m is the number of electrodes that constitute the array.

When an array of ultra micro electrodes is applied, the diffusion fields of the individual electrodes should not overlap. This would cause the diffusion lengths to increase, thereby reducing the benefits of applying small electrodes (Morf and de Rooij 1997). The minimally allowable spacing between the electrodes can be reduced by recessing the electrodes (Chen and Li 1993). Recessing the electrodes leads to a somewhat different diffusion profile compared to the case of inlaid electrodes. Mass transport to the electrode surface is reduced by an amount dependent on the height of the recess (Sandison et al. 2002). To a recessed ultra micro electrode array therefore applies:

$$I = mnFAD_O\frac{c_0}{r+h} \tag{4-9}$$

Where h is the height of the recess (Rubinstein 1995).

4.2.3 pH

The Ion-Selective Field Effect transistor (ISFET) was invented by Piet Bergveld in the 1970's (Bergveld 1970; Bergveld 2003). Its structure is very similar to that of a regular Metal Oxide Silicon FET, but there is no metallic gate. Therefore, the gate oxide is in direct contact with the electrolyte in which the sensor is placed and hydrogen ions in the solution can associate with or dissociate from the oxide groups. The surface charge of the gate oxide thus depends on the concentration of hydrogen ions in the solution, making the threshold voltage of the device a good measure for the solution pH.

The pH-dependent contribution to the threshold voltage of the device is defined by the surface potential, Ψ .

$$\Delta\Psi = -2.3\alpha \frac{RT}{F} \Delta pH_{bulk} \tag{4-10}$$

where R is the gas constant, T is the absolute temperature in Kelvin, F is the Faraday constant and ΔpH_{bulk} is the pH change of the bulk solution. α is a sensitivity factor described by:

$$\alpha = \frac{1}{2.3\left(\frac{kT}{q^2}\right)\left(\frac{C_s}{\beta_s}\right)+1} \tag{4-11}$$

where q is the unit charge, C_s is the differential double layer capacitance and β_s is a quantity describing the ability of the oxide surface to take up protons, also referred to as the intrinsic buffer capacity. For an ideally behaving device, $\alpha = 1$ and a maximum Nernstian sensitivity of 58.2 mV/pH unit at 20 ^{o}C is obtained. Ideality depends on the association and dissociation constants of the oxide sites and the site density (Faber et al.).

The main reason that ISFETs are not widely used for application in long-term pH measurements is that they exhibit transient behavior that is generally referred to as drift. Although the drift problem was intensively investigated since the first ISFETs were developed in the early 1970's, it is still not completely understood. Various effects add to the transient response of ISFETs.

It is believed that in the first few hours of operation, the transient response of ISFETs is dominated by the slow pH response of buried sites; reactive groups just

underneath the surface of the gate oxide (Jamasb et al. 1998b; Woias et al. 1998). After these first few hours of operation, the transient response of the ISFET is known to become nearly linear with time. It is known from MOSFET theory that non-idealities in the fabrication process lead to traps and charges inside or near the substrate/oxide interfaces. These charges can drift through the oxide layer, thereby increasing the overall oxide layer capacitance and thus decreasing the threshold voltage of the device (Campbell 1995; Masson et al. 2002). Another contribution to the long-term transient response of ISFETs is hydration of the top layer of the gate oxide when the device is immersed in an aqueous solution. This chemical modification of the oxide groups changes the overall gate oxide capacitance and resultantly the threshold voltage of the device. Even for very hard oxide types, like Ta_2O_5, chemical modification of the first few atomic layers as a result of exposure to electrolyte is highly conceivable (Jamasb et al. 1998a).

Although the slow pH response dominating in the first few hours of operation is unpredictable at present, the long-term drift rate of ISFETs is very constant and reproducible under constant temperature and around constant pH. Therefore, this rate can be determined prior to any long-term measurement and the measurement can be compensated for the transient response of the device on-line.

4.2.4 Temperature

The resistance of metallic thin films is often monitored as a measure for the temperature in a miniaturized device. The resistance of the metallic layer increases with increasing temperature, as the movement of free charge in the metal is increasingly hindered by thermal vibrations. For platinum, the relation between electrical resistance and temperature is nearly linear over a wide temperature range (Gong et al. 2006). The temperature coefficient of resistance (TCR) of platinum equals $3.9 \times 10^{-3} / °C$ (Cobbold 1974).

In this chapter, a new sensor array is presented. This electrochemical sensor array consists of sensors for the on-line measurement of viable biomass concentration, dissolved oxygen concentration, pH and temperature and is based on the measurement principles described above.

4.3 Experimental

4.3.1 Sensor design

The conductivity sensor must be able to monitor the electrolyte conductance above and below the characteristic frequency for β-dispersion of yeast cells. So the center of the plateau as indicated in the impedance curve in fig. 4-1b, must be localized near this characteristic frequency and the corresponding impedance value must be accurately determined. Assuming a background electrolyte conductivity of 1 S/m and with help of numeric simulations, the conductivity sensor was designed to consist of two 200 × 200 μm electrodes with 1200 μm spacing.

For the ultra micro electrode array, we do not need to address the electrodes individually, since they are operated in parallel and thus can have a common back-contact. We therefore fabricated the array by covering a platinum macro electrode with a photostructured layer of polyimide with a thickness of approximately 1 μm. This process results in recessed electrodes, which reduces the minimally allowable spacing between the electrodes. This minimally allowable spacing was determined from finite element simulations with CFD-ACE, from which the spatial oxygen distribution near the electrode is determined. These simulations show that the electrodes need to be separated by at least ~2.5 times the electrode diameter (figure 4-2a). If the recess of the electrodes equals the electrode diameter, this value can be reduced to ~1 time the electrode diameter (figure 4-2b), but this leads to a longer response time. For this application however, the space demand is not really stringent. The electrode array was therefore designed to comprise 114 electrodes with a radius of 2 μm and a minimal spacing of 50 μm. Using the Cottrell equation and assuming a polyimide layer thickness of 1 μm, one finds a theoretical current response at a dissolved oxygen concentration of 1 mg/l of 15.0 nA at a temperature of 25 ^{o}C. The counter electrode is formed by a 200 × 1000 μm platinum electrode.

The temperature resistor was designed to have a nominal resistance of 500 Ohm. Therefore, the design of the temperature sensor comprises a 150 nm thick platinum strip with a length of 4600 μm and a width of 10 μm.

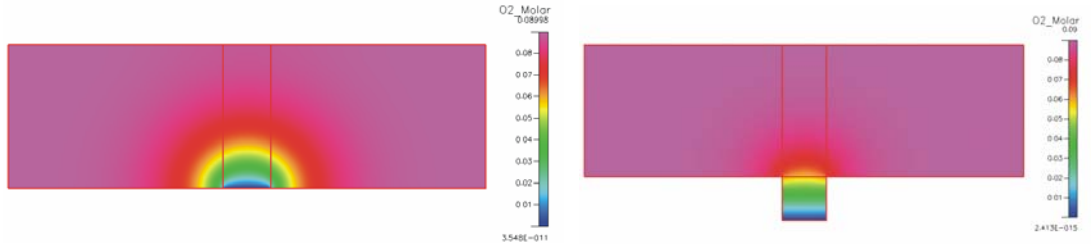

Figure 4-2: Finite element simulations of spatial distribution of oxygen near a (a) flat electrode and (b) recessed electrode with 2.5 μm radius

4.3.2 Device fabrication

The sensors were fabricated on an oxidized silicon substrate using standard microfabrication techniques. First, the ISFETs with Ta_2O_5 gate were manufactured by defining doped drain-and source regions using standard photolithographic processes and by deposition and oxidization of tantalum. Aluminum was sputtered to realize the electrical connection to the drain- and source regions. Details about ISFET fabrication were described by P. Bergveld et al.(Bergveld and Sibbald 1988) For the other metallic structures, platinum was sputtered. Tantalum was used as adhesion layer. A lift-off process was used for the creation of the Ta/Pt structures, as wet-etching possibly damages the sensitive parts of the ISFET.

The non-sensitive parts of the devices are covered with a photostructured layer of polyimide. Before the post-exposure bake of the polyimide, the devices were placed in oxygen plasma for 10 seconds. This roughens the polyimide surface and thereby improves the adhesion of the Hysol®, which is used to mount the devices on a PCB and to protect the bondwires used for making the electrical connections to the chip. A microscope picture of the fabricated device is shown in figure 4-3. The arch at the top of the sensor array is an alignment mark. It can be used for aligning the sensor array with a 6mm diameter well, like a microwell in a 96-well micro titer plate. The Pt heater, included for temperature studies, is not discussed in this chapter.

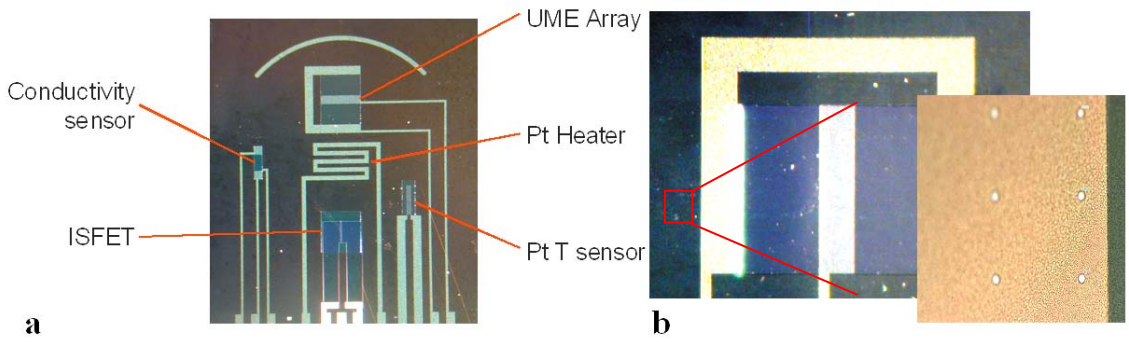

Figure 4-3: Microscope pictures of (a) sensor array and (b) dissolved oxygen sensor

4.3.3 Measurement setup

The response of the conductivity sensor in the range of 100 Hz – 10 MHz is measured using an impedance analyzer (4194A, Hewlett Packard). The sensor was calibrated in yeast suspensions of different concentrations which were made by suspending pressed baker's yeast in a standard yeast buffer solution (10 g/l $(NH_4)2(SO_4)$, 6 g/l KH_2PO_4, 1 g/l $MgSO_4.7H_2O$, pH was adjusted to 5 using 4M NaOH) and by approximating the impedance of the electrochemical cell by the equivalent electrical circuit shown in figure 1a. It is assumed that the ratio between the weight of pressed yeast and the dry weight of yeast cells is 3:1.

The dissolved oxygen sensor was connected to a potentiostat (Parstat 263A, Princeton Applied Research) in a three-electrode configuration. The measurements are preferably done at an electrode polarization corresponding to the beginning of the oxygen reduction plateau in the cyclic voltammogram. In this case, maximum selectivity at maximum sensitivity towards the dissolved oxygen concentration is obtained. The electrode polarization corresponding to this point depends on electrode material, temperature and solution pH. The proper polarization voltage with respect to an off-chip Ag/AgCl reference electrode was determined from cyclic voltammetry. Calibration of the sensor was done in a supernatant solution that was taken from a *Saccharomyces cerevisiae* fermentation under chemostat conditions in equilibrium. Dissolved oxygen concentration is varied by bubbling compressed air and nitrogen through the solution using mass flow controllers (El-Flow, Bronkhorst Hi-Tec). The dissolved oxygen concentration can be determined from Henry's gas law assuming the liquid is saturated with the gas bubbled through. The value is simultaneously measured with a conventional Clark oxygen sensor (810, Orion).

The output signal of the ISFET amplifier (home built) is acquired via a data acquisition device (DAQ USB 6009, National Instruments) and logged using LabVIEW. The ISFET was calibrated by placing the device in a standard pH 4 buffer solution (Radiometer Analytical). pH was increased by titrating a 0.1M TBAOH base solution using a piston burette (Titronic T200, Schott Instruments). pH was simultaneously monitored using a conventional pH meter (PHM83, Radiometer).

Temperature sensor impedance is measured using a digital multimeter (34401A, Agilent) and compared to the response of a Type K thermocouple (Tenma 72-6870). Temperature is controlled using a hotplate (RET B, Ika Werke). In all experiments, the solutions were mixed using a magnetic stirrer (RET B, Ika Werke).

4.4 Results

4.4.1 Biomass measurement results

Measurements in a 7 g/l dry weight (DW) *Saccharomyces cerevisiae* cell suspension show a clear conductivity increase for frequencies above 1 MHz, as depicted in figure 4-4a. This figure shows the observed conductivity increase, divided by the conductivity observed at 100 Hz, σ_l. The conductivity stabilizes at a higher value for frequencies at which interfacial polarization of the cell membrane does not occur. The increase scales linearly with the biomass concentration for yeast suspension of different dilutions. In figure 4-4b, the relative conductivity increase, normalized on the conductivity increase in a 4 g/l DW yeast suspension ($\delta\sigma_{4gl}$), is plotted as a function of the biomass concentration. These results were obtained by comparing the obtained solution resistance around 10 MHz to the value obtained around 100 kHz.

The obtained sensitivity equals 0.65% per g/l biomass. This is higher than the theoretically expected value of 0.45% per g/l. The differences could be caused by non-idealities of the single shell spherical model used to model the yeast cells, the estimation of dry cell weight and by non-homogeneity of the cell suspension.

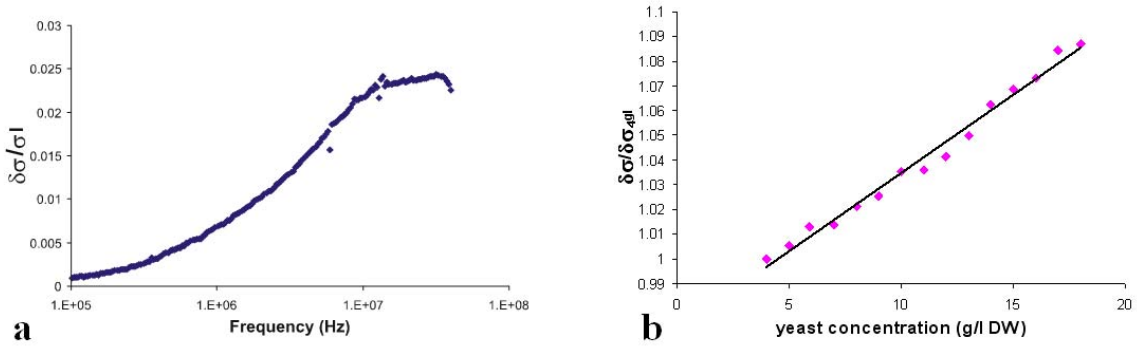

Figure 4-4: Conductivity change versus (a) frequency, normalized on the conductivity measured at 10 kHz and (b) biomass concentration, normalized on the conductivity change measured in a 4 g/l DW Saccharomyces cerevisiae cell suspension

4.4.2 Dissolved oxygen measurement results

Experimental results obtained in a supernatant solution show that the current through the ultra micro electrode array scales linearly with the dissolved oxygen concentration (figure 4-5a) with 3.7 nA per mg/l sensitivity. The extrapolated current value at zero concentration is very low, which indicates that at this polarization voltage (-0.4V vs. Ag/AgCl) the sensor exhibits high selectivity.

The obtained sensitivity is considerably lower than the theoretically expected value of 15.0 nA per mg/l. This is mainly explained by the polarization voltage being insufficient for maximum oxygen reduction. Furthermore, non-idealities in the fabrication of the sensor array and deviations from room temperature (25 ^{o}C) could be expected to lead to deviations. The achieved sensitivity is high enough for accurate process monitoring when the sensor is properly calibrated in advance, however.

The flow dependence of the sensor was tested and compared to the flow dependence of an amperometric sensor consisting of platinum macro electrodes with an area of 1 cm^2 at constant dissolved oxygen concentration (10 mg/l), as depicted in figure 4-5b. The results show that flow dependence is dramatically reduced by applying ultra micro electrodes.

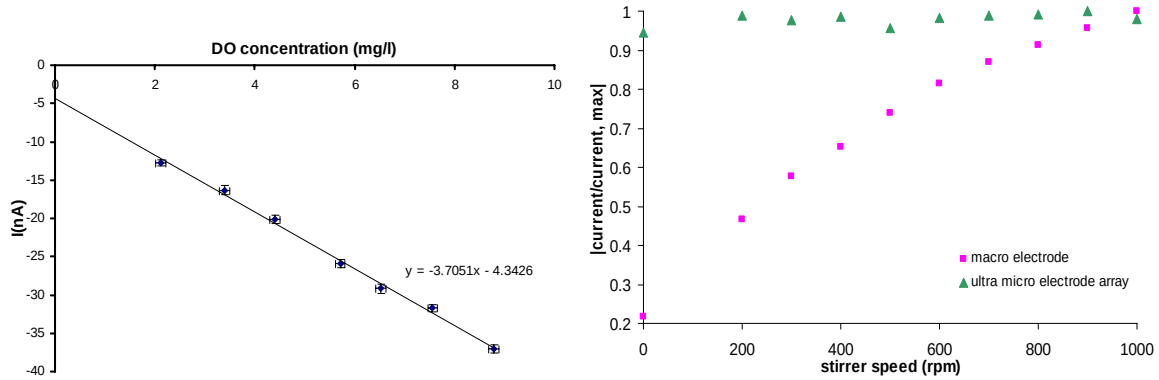

Figure 4-5: (a) Current response versus dissolved oxygen concentration as monitored using a Clark oxygen electrode (b) normalized current response versus rate of convection

4.4.3 pH measurement results

ISFET sensitivity equals -56 mV/pH unit at room temperature, as shown in figure 4-6a. Long-term drift rate was shown to be nearly linear and reproducible, indicating that long-term measurements can indeed be compensated for this behavior once the long-term drift rate has been determined. The long-term drift rate was very similar for ISFETs processed in the same batch. ISFET drift rate could be reduced to less than 0.002 pH unit/hr by measuring differentially between an ISFET placed in a constant pH environment and an ISFET which is exposed to pH changes, as depicted in figure 4-6b.

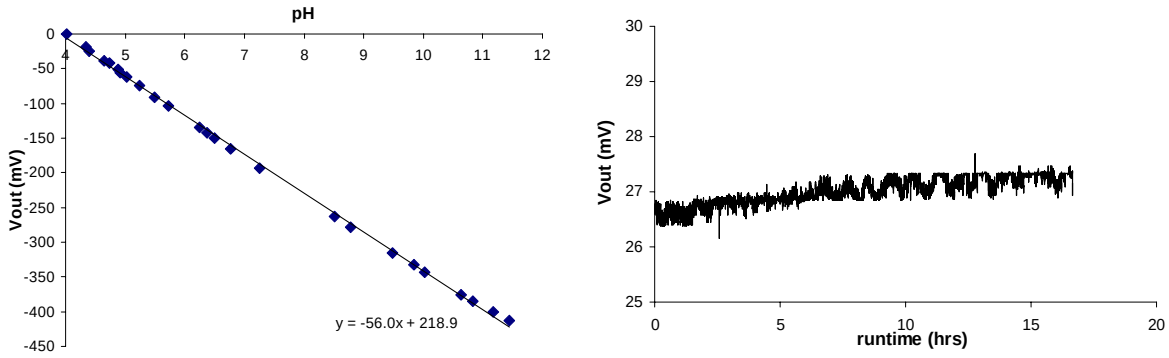

Figure 4-6: (a) ISFET pH response in the range of pH 4-11 and (b) transient behavior as observed in differential measurements at pH 7

4.4.4 Temperature measurement results

Characterization of the temperature sensor shows the resistance of the platinum strip to increase linearly with temperature in the range 20 – 45 ^{o}C with a TCR of $2.2\times10^{-3}/°C$, which is somewhat lower than the listed TCR of pure platinum. However, the TCR of platinum thin films is known to be lower (Mailly et al. 2001). Application of a tantalum adhesion layer is known to further reduce the TCR, compared to the case of pure platinum thin films (Tiggelaar et al. 2005). The obtained TCR compares well to values reported in these previous studies.

The resistance at room temperature equals 486 Ohm; this is slightly lower than expected and might have to do with the parallel conductance of the tantalum adhesion layer and non-idealities in the fabrication process.

Sensor response was shown to be stable for more than 72 hours, indicating that the sensors are stable enough for monitoring yeast growth processes. No response degradation was observed after steam sterilizing the sensor arrays several times.

4.5 Conclusions

This study shows the design, modeling and experimental characterization of an electrochemical sensor array suitable for on-line monitoring of the most relevant fermentor conditions, i.e. viable biomass concentration, dissolved oxygen concentration, pH and temperature. The sensors can be fabricated using standard cleanroom processes.

Experiments show the conductivity of a *Saccharomyces cerevisiae* cell suspension clearly increases for frequencies above 1 MHz. A calibration experiment shows the conductivity difference to scale linearly with the biomass concentration, which can be estimated with an accuracy of approximately 1 g/l. Dissolved oxygen calibration experiments in a supernatant solution shows the current through the ultra micro electrode array to scale linearly with the dissolved oxygen concentration with sensitivity close to its theoretical value. Flow dependence of the sensor was shown to be negligible compared to the flow dependence of macro electrodes. The ISFET and the temperature sensor were shown to be sufficiently sensitive in the desired range. The drift could be effectively compensated for.

Future work aims at calibration of the sensor array in lab-scale yeast fermentations (publication in preparation) and integration of the electrochemical sensor arrays in micro fermentors. The sensors will be operated sequentially in order to prevent crosstalk.

References

Asami K. 2002. Characterization of biological cells by dielectric spectroscopy. Journal of Non-Crystalline Solids 305(1-3):268-277.

Asami K, Gheorghiu E, Yonezawa T. 1998. Dielectric behavior of budding yeast in cell separation. Biochimica Et Biophysica Acta-General Subjects 1381(2):234-240.

Asami K, Yonezawa T. 1995a. Dielectric Analysis of Yeast-Cell Growth. Biochimica Et Biophysica Acta-General Subjects 1245(1):99-105.

Asami K, Yonezawa T. 1995b. Dielectric behavior of non-spherical cells in culture. Biochimica Et Biophysica Acta-General Subjects 1245(3):317-324.

Balagadde FK, You LC, Hansen CL, Arnold FH, Quake SR. 2005. Long-term monitoring of bacteria undergoing programmed population control in a microchemostat. Science 309(5731):137-140.

Bard AJ, Faulkner LR. 1980. Electrochemical Methods, Fundamentals and Applications. New York: J. Wiley & Sons.

Bergveld P. 1970. Development of an ion-sensitive solid-state device for neurophysiological measurements. IEEE Transactions on Biomedical Engineering 17:70-71.

Bergveld P. 2003. Thirty years of ISFETOLOGY - What happened in the past 30 years and what may happen in the next 30 years. Sensors and Actuators B-Chemical 88(1):1-20.

Bergveld P, Sibbald A. 1988. Analytical and biomedical application of ion-selective field-effect transistors. Amsterdam: Elsevier.

Brett CMA, Brett AMO. 1983. Electrochemistry: Principles, Methods and Applications. New York: Oxford University Press. 81-90 p.

Campbell SA. 1995. The Science and Engineering of Microelectronics Fabrication. Oxford: Campbell.

Carvell JP, Dowd JE. 2006. On-line measurements and control of viable cell density in cell culture manufacturing processes using radio-frequency impedance. Cytotechnology 50(1-3):35-48.

Chen YQ, Li GA. 1993. A Mathematical-Model with Finite-Element Analysis of Recessed Dissolved-Oxygen Cathode Array. Sensors and Actuators B-Chemical 10(3):223-228.

Clark LC, Clark EW. 1987. A personalized history of the Clark oxygen electrode. International Anesthesiology Clinics 25:1-29.

Cobbold RSC. 1974. Transducers for Biomedical Measurements. New York: John Wiley & Sons. 58-73 p.

Faber EJ, Sparreboom W, Groeneveld W, de Smet LCPM, Bomer JG, Olthuis W, Zuilhof H, Sudhölter EJR, Bergveld P, van den Berg A. pH Sensitivity of SiC Linked Organic Monolayers on Crystalline Silicon Surfaces (p NA) ChemPhysChem article in press.

Fricke H. 1955. The Complex Conductivity of a Suspension of Stratified Particles of Spherical or Cylindrical Form. Journal of Physical Chemistry 59(2):168-170.

Gavrilescu M, Chisti Y. 2005. Biotechnology - a sustainable alternative for chemical industry. Biotechnology Advances 23(7-8):471-499.

Gawad S, Schild L, Renaud P. 2001. Micromachined impedance spectroscopy flow cytometer for cell analysis and particle sizing. Lab on a Chip 1(1):76-82.

Gong JW, Chen QF, Lian MR, Liu NC, Daoust C. 2006. Temperature feedback control for improving the stability of a semiconductor-metal-oxide (SMO) gas sensor. Ieee Sensors Journal 6(1):139-145.

Hall EAH. 1990. Biosensors. Bryant JA, Kennedy JF, editors. Buckingham: Open University Press. 110 p.

Harris CM, Todd RW, Bungard SJ, Lovitt RW, Morris JG, Kell DB. 1987. Dielectric Permittivity of Microbial Suspensions at Radio Frequencies - a Novel Method for the Real-Time Estimation of Microbial Biomass. Enzyme and Microbial Technology 9(3):181-186.

Hauttmann S, Muller J. 2001. In-situ biomass characterisation by impedance spectroscopy using a full-bridge circuit. Bioprocess and Biosystems Engineering 24(3):137-141.

Jamasb S, Collins S, Smith RL. 1998a. A physical model for drift in pH ISFETs. Sensors and Actuators B-Chemical 49(1-2):146-155.

Jamasb S, Collins SD, Smith RL. 1998b. A physical model for threshold voltage instability in Si3N4-gate H+-sensitive FET's (pH ISFET's). Ieee Transactions on Electron Devices 45(6):1239-1245.

Krommenhoek EE, Gardeniers JGE, Bomer JG, van den Berg A, Li X, Ottens M, van der Wielen LAM, van Dedem GWK, van Leeuwen M, van Gulik WM and others. 2006. Monitoring of yeast cell concentration using a micromachined impedance sensor. Sensors and Actuators B-Chemical 115(1):384-389.

Lambeck PV. 2006. Integrated optical sensors for the chemical domain. Measurement Science & Technology 17(8):R93-R116.

Maharbiz MM, Holtz WJ, Howe RT, Keasling JD. 2004. Microbioreactor arrays with parametric control for high-throughput experimentation. Biotechnology and Bioengineering 85(4):376-381.

Mailly F, Giani A, Bonnot R, Temple-Boyer P, Pascal-Delannoy F, Foucaran A, Boyer A. 2001. Anemometer with hot platinum thin film. Sensors and Actuators a-Physical 94(1-2):32-38.

Malins C, Glever HG, Keyes TE, Vos JG, Dressick WJ, MacCraith BD. 2000. Sol-gel immobilised ruthenium(II) polypyridyl complexes as chemical transducers for optical pH sensing. Sensors and Actuators B-Chemical 67(1-2):89-95.

Markx GH, Kell DB. 1995. The Use of Dielectric Permittivity for the Control of the Biomass Level during Biotransformations of Toxic Substrates in Continuous-Culture. Biotechnology Progress 11(1):64-70.

Masson P, Autran JL, Munteanu D. 2002. DYNAMOS: a numerical MOSFET model including quantum-mechanical and near-interface trap transient effects. Solid-State Electronics 46(7):1051-1059.

Mishima K, Mimura A, Takahara Y, Asami K, Hanai T. 1991. Online Monitoring of Cell Concentrations by Dielectric Measurements. Journal of Fermentation and Bioengineering 72(4):291-295.

Morf WE, de Rooij NF. 1997. Performance of amperometric sensors based on multiple microelectrode arrays. Sensors and Actuators B-Chemical 44(1-3):538-541.

O'Riordan TC, Voraberger H, Kerry JP, Papkovsky DB. 2005. Study of migration of active components of phosphorescent oxygen sensors for food packaging applications. Analytica Chimica Acta 530(1):135-141.

Olthuis W, Streekstra W, Bergveld P. 1995. Theoretical and Experimental-Determination of Cell Constants of Planar-Interdigitated Electrolyte Conductivity Sensors. Sensors and Actuators B-Chemical 24(1-3):252-256.

Prescott LM, Harley JP, Klein DA. 1990. Microbiology. Dubuque: Wm. C. Brown Publishers. 501 p.

Rubinstein I. 1995. Physical Electrochemistry, Principles, Methods and Applications. New York: Marcel Dekker, Inc. 134-182 p.

Sandison ME, Anicet N, Glidle A, Cooper JM. 2002. Optimization of the geometry and porosity of microelectrode arrays for sensor design. Analytical Chemistry 74(22):5717-5725.

Schwan HP. 1957. Electrical properties of tissues and cell suspensions. Advances in Biological and Medical Physics 5:147.

Tiggelaar RM, Berenschot JW, de Boer JH, Sanders RGP, Gardeniers JGE, Oosterbroek RE, van den Berg A, Elwenspoek MC. 2005. Fabrication and characterization of high-

temperature microreactors with thin film heater and sensor patterns in silicon nitride tubes. Lab on a Chip 5(3):326-336.

Woias P, Meixner L, Frostl P. 1998. Slow pH response effects of silicon nitride ISFET sensors. Sensors and Actuators B-Chemical 48(1-3):501-504.

Yotter RA, Lee LA, Wilson DM. 2004. Sensor technologies for monitoring metabolic activity in single cells - Part I: Optical, methods. Ieee Sensors Journal 4(4):395-411.

Zanzotto A, Boccazzi P, Gorret N, Van Dyk TK, Sinskey AJ, Jensen KF. 2006. In situ measurement of bioluminescence and fluorescence in an integrated microbioreactor. Biotechnology and Bioengineering 93(1):40-47.

Zhang ZY, Szita N, Boccazzi P, Sinskey AJ, Jensen KF. 2006. A well-mixed, polymer-based microbioreactor with integrated optical measurements. Biotechnology and Bioengineering 93(2):286-296.

Chapter 5: Lab-scale fermentation tests of micro chip with integrated electrochemical sensors for pH, temperature, dissolved oxygen and viable biomass concentration

This chapter shows the development and testing of a microchip with integrated electrochemical sensors for measurement of pH, temperature, dissolved oxygen and viable biomass concentration under yeast cultivation conditions. Measurements were done both under dynamic batch conditions as well as under prolonged continuous cultivation conditions. The response of the sensors compared well with conventional measurement techniques. The biomass sensor was based on impedance spectroscopy. The results of the biomass sensor matched very well with dry weight measurements and showed a limit of detection of ~1 g/l. The dissolved oxygen concentration was monitored amperometrically using an ultra micro electrode array, which showed an accuracy of ~0.2 mg/l and negligible drift. pH was monitored using an ISFET with an accuracy well below 0.1 pH unit. The platinum thin-film temperature resistor followed temperature changes with ~0.1 ^{o}C accuracy. The dimensions of the multi sensor chip are chosen as such that it is compatible with the 96-well plate format.

5.1 Introduction

Screening and testing of micro-organisms is crucial for both companies and research institutes operating in the field of biotechnology. High-throughput screening programs generate large amounts of mutants in order to find new and highly productive micro-organisms for industrial applications. Tools like metabolic engineering and genomics only increase the amount of mutants but these tools also raise opportunities to gain insight in the functioning of micro-organisms under different environmental conditions at a molecular and genetic level. The main challenge lies in the evaluation of this enormous amount of possible permutations of both genetic origin and culture conditions by means of cell cultivation (Boccazzi et al. 2005; Sauer 2004). Clearly, the ability to measure and control the environmental conditions as well as the high-throughput is crucial for success.

Lab-scale bioreactors are state of the art for the controlled cultivation of micro-organisms under well defined conditions. They have typical working volume ranging from a few hundred millilitres up to several litres and are equipped with sensors and fluid- and gas-handling systems for the online-measurement and tight control of important parameters like pH, dissolved oxygen concentration and temperature. Feed and effluent pumps make it possible to control the substrate concentration. The control of the substrate concentration is important in many industrial processes in order to prevent substrate inhibition or overflow metabolism but substrate control is also crucial in many fundamental studies, for example the effect of different substrate limitations on a metabolic and genetic level. However, operating lab-scale bioreactors is laborious and operation and investment costs are high, thus limiting parallelization and throughput.

Microtiter plates are attractive for high-throughput cell cultivation because of the small working volumes, the high degree of parallelization and the already available robotics, shakers and liquid handling equipment (Duetz et al. 2000; Warringer and Blomberg 2003). Although smaller working volumes and higher numbers of wells per plate are available, microtiter plates for the high-throughput cultivation of micro-organisms typically contain 24 or 96 parallel wells with working volumes of 0.1 to 3 ml. However, microtiter plates have limited possibilities for online measurement of environmental condition in the individual wells and generally only the temperature is controlled. Poor measurement and control possibilities of microtiter plates reduce the selectivity in high-throughput screening of micro-organisms for industrial application and significantly reduce the possibilities for high-throughput testing of micro-organisms under different environmental conditions.

Microbioreactor technology aims at combining the small working volume and the high-throughput possibilities of microtiter plates with the monitoring and control features of lab-scale bioreactors (Kumar et al. 2004; Lye et al. 2003). Small and reliable sensors for important environmental parameters are a first prerequisite for the success of microbioreactor technology. The sensors should preferably fit underneath a 96-well plate in order to make use of high-throughput instrumentation that is already available, like robotics, shakers and liquid handling systems. Although individual sensors that can potentially fit in a 96-well plate exist, a multi sensor chip that has a 96-well plate footprint and combines the online measurement of pH, dissolved oxygen concentration, temperature and biomass concentration is to the authors' knowledge currently not available.

5.1.1 pH

Most micro-organisms grow optimally in a small pH range only. Because many micro-organisms produce or consume acids, online measurement and control of the pH is very important in cell cultivations. Glass electrodes remain state of the art, but are bulky. Optodes measure the pH by means of either absorbance or fluorescence of an immobilized pH sensitive dye. 24- and 96-well plates with integrated optodes were commercialized (e.g. PreSens, precision sensing GmbH Regensburg, Germany) and successfully applied (John et al. 2003a). However, optodes suffer from a small measurement range. Industrially relevant species like the yeasts *Candida utilis* and *Saccharomyces cerevisiae* are cultivated at a pH around 5, which is outside the working range of the optodes. The best option for pH measurement in microbioreactors when cultivating yeast is the Ion-Selective field effect transistor (ISFET), a FET-based device with a reference electrode in a solution acting as gate contact. Site-binding processes at the oxide surface lead to a pH-dependent threshold voltage (Bergveld 1970; Faber et al.). ISFETs can cover a wide pH spectrum (Bergveld 2003). ISFETS were already successfully applied in miniaturized cultivation systems (Maharbiz et al. 2004; Walther et al. 2000). A known drawback of ISFETS is that they exhibit transient behavior generally referred to as drift. After 2-3 hours of operation, however, the drift is known to become linear with time and reproducible (Jamasb et al. 1998a; Jamasb et al. 1998b; Woias et al. 1998). Therefore the measurement could be compensated for the drift.

5.1.2 Dissolved oxygen concentration

Oxygen is one of the substrates in an aerobic cultivation. Oxygen supply is often a bottleneck owing to the low oxygen solubility in water. Oxygen-limiting conditions are unfavorable for most aerobic bioconversions. The Clark cell remains the most reliable sensor for the measurement of the dissolved oxygen concentration but miniaturization is complicated. Optodes that are sensitive to oxygen are based on the quenching of fluorescence (Kostov et al. 2001b; Papkovsky 1995). Optodes for oxygen were integrated in titerplates, commercialized (e.g. PreSens, precision sensing GmbH Regensburg, Germany) and successfully used in research (Deshpande and Heinzle 2004; John et al. 2003b; Zimmermann et al. 2003). The sensitivity of optodes is optimal at low oxygen concentrations. Ultra micro electrode arrays (UMEA) are a viable electrochemical alternative for the measurement of the dissolved oxygen concentration in small volume although they are not yet applied in microbioreactors. The measurement of the dissolved oxygen concentration with the UMEA is based on amperometric detection of oxygen reduction and the signal of the UMEA is known to be flow insensitive (Brett and Brett 1983; Chen and Li 1993; Morf and de Rooij 1997; Rubinstein 1995).

5.1.3 Biomass concentration

The biomass concentration is an important process indicator. Micro-organisms catalyze the desired reactions but are also self-catalyzing, generally referred to as microbial growth. Several techniques exist to measure the biomass concentration but all have limitations. Dry weight measurement is an accurate but off-line technique. Because this technique involves sampling, drying and weighing, it is nearly impossible to miniaturize. Online measurement of the biomass concentration is possible by both optical and electrochemical means. Turbidity measurements are already applied in microbioreactors. However, miniaturization leads to a decrease in sensitivity and particles and air bubbles can interfere with measurement.

An alternative technique for the online measurement of biomass is impedance spectroscopy. In impedance spectroscopy an alternating current (AC) electrical field is applied to a cell culture and the conductivity is measured as a function of the frequency. For living cells present in an AC electrical field, interfacial polarization of the insulating cell membrane occurs. When the frequency of the electric field exceeds a so called characteristic frequency, the interfacial polarization cannot follow the electric field (Schwan 1957). Therefore the conductivity of the cell suspension increases at frequencies above the

characteristic frequency and approaches the conductivity of the background electrolyte (Asami and Yonezawa 1995). The characteristic frequency, describing the dielectric dispersion effect, typically equals a few MHz for viable yeast cells (Hauttmann and Muller 2001). The total increase in conductivity around the characteristic frequency scales linearly with the viable biomass concentration. The conductivity increase can be determined from impedance measurements performed at signal frequencies below and above the characteristic frequency of the cells under investigation (further details about the method can be found in an earlier paper (Krommenhoek et al. 2007)).

5.1.4 Temperature

Temperature is probably the easiest parameter to measure in bioreactors but is of great importance. The conventional way to measure the temperature is by means of a thermistor. For such a device, the resistance of a metallic layer increases with increasing temperature, as the movement of free charge in the metal is increasingly hindered by thermal vibrations. For platinum, the relation between resistance and temperature is nearly linear over a wide temperature range (Gong et al. 2006; Tiggelaar et al. 2005).

5.1.5 Sensor integration

Optical sensors received a great deal of attention and several attempts were made to integrate multiple optical sensors in microbioreactors, both on millilitre (Harms et al. 2006; Kostov et al. 2001a; Lamping et al. 2003) and microliter scale (Lee et al. 2006; Szita et al. 2005). Promising growth kinetics data were presented, showing the potential of microbioreactor technology. However, these systems have several limitations especially for our main interest: the high-throughput cultivation of yeast. First of all the inability to measure the pH around a value of 5 with the current optodes is a major bottleneck. Moreover, electrochemical sensors fabricated on a silicon substrate using standard lithographic processes are more attractive for application in parallelized systems. This is because sensors of different types can easily be integrated in a single substrate and the fabrication techniques allow for cheap mass fabrication (Moore 1998). Furthermore we believe that the 96-well format has major advantages, because of the already available robotics, shakers and liquid handling equipment.

In order to improve the current high-throughput cultivation system, the 96-well plates,

we developed a multi sensor chip that has a 96-well plate footprint. The sensor chip integrates electrochemical sensors for the online measurement of pH, dissolved oxygen concentration, temperature and biomass concentration. In an earlier publication, we have described the design, fabrication and showed test results of the calibration of each individual sensor (Krommenhoek et al. 2007). In that paper, it was also shown that the sensor array is able to withstand autoclaving. In this contribution we present a thorough test of the sensor chip under conditions where the sensor ultimately should function, i.e. under yeast cultivation conditions.

5.2 Materials and methods

5.2.1 Design and fabrication of the multi-sensor chip

Chips with integrated sensors for the measurement of pH, temperature, dissolved oxygen and viable biomass concentration were fabricated on an oxidized silicon substrate. The sensor array fits within a 6 mm diameter circle, making it small enough for implementation in the microwells of a 96-well microtiter plate. First, the Ta_2O_5 ISFETs were manufactured. Next, a lift-off process was used for the creation of the platinum structures for the other sensors. The impedance sensor used for the biomass measurements consists of 200 × 200 µm electrodes with a spacing of either 1200 µm (*type A*) or 400 µm (*type B*). The ultra micro electrode array (UMEA) consists of a platinum macro electrode, covered by a photostructured layer of polyimide as to create arrays of recessed ultra micro electrodes with a radius of 2 µm. The temperature resistor was designed to have a nominal resistance of 500 Ohm. The sensor chips were bondwired to a printed circuit board. Hysol® was used for packaging and for protection of the bondwires. Details about the design, fabrication and packaging of the sensor chips have been described previously (Krommenhoek et al. 2007).

Two packaged sensor chips were inserted in a 23.6 cm long stainless steel tube (ID: 1.7 mm, OD: 1.9 mm), together with a Ag/AgCl reference electrode (Radiometer Analytical, Copenhagen, Denmark). The sensors and the reference electrode were sealed to the tube and the probe was made leak-tight with one component silicon sealant (Dow Corning, Michigan, USA).

5.2.2 Readout of the sensor chip

The readout of the individual sensors on the sensor chip was accomplished through the use of a relay switch board controlled by a DAQ device (USB DAQ 6009, National Instruments, Austin, USA). The electromechanical relays sequentially coupled and uncoupled the sensors to the appropriate analyzer in order to prevent crosstalk. The outputs of the DAQ device were buffered using bipolar junction transistors in order to deliver enough switching power. A DC voltage supply (E015-2, Delta Elektronika, Zierikzee, The Netherlands) delivered the switching power.

An impedance analyzer (HP4194A, Hewlett Packard, USA) was used to measure the response of the impedance sensor in the range of 10 kHz – 15 MHz. The dissolved oxygen sensor was connected to a potentiostat (Parstat 263A, Princeton Applied Research, Oak Ridge, USA). The proper polarization voltage was determined from cyclic voltammetry and chosen high enough to ensure oxygen reduction, but not too high as to prevent interference from other redox reactions taking place. The ISFET was connected to an ISFET amplifier (home built). Both the output of the ISFET amplifier and the resistance of the temperature resistor were measured using a digital multimeter (34401A, Agilent, Santa Clara, USA).

A labVIEW ^{TM} (National Instruments, Austin, USA) software routine controlled the relays, communicated with the impedance analyzer and the digital multimeter and logged the signals. The LabVIEW^{TM} routine was coupled to a Powersuite® (Princeton Applied Research, Oak Ridge, USA) software routine, in order to control and log the dissolved oxygen measurements. With this experimental setup a complete measurement cycle, comprising the time taken to record the four parameters in duplo, lasted 5 minutes.

5.2.3 Batch and continuous cultivation

A preculture (0.5 liters) of *Candida utilis* CBS 621 was grown overnight in a shake flask at 30 ºC on mineral medium (Verduyn et al. 1992) which contained 15 g/l glucose*1 H_2O. The preculture served as inoculum for the 7 liter bioreactor (Applikon, Schiedam, The Netherlands) with a working volume of 4 liters. For both the batch and continuous cultivation experiments in the bioreactor the concentrations of all components in the medium were increased to twofold the concentrations of the shake flask medium, and ethanol (1.4 g/l) was added as a second substrate. In the continuous cultivation experiment the dilution rate was set at 0.05 h^{-1}. The reactor was placed on a balance and the weight was controlled by means of an effluent pump. Besides the multi sensor chip, the bioreactor

was equipped with sensors for pH (Inpro 3030/120, Mettler-Toledo GmbH, Switzerland), temperature (PT-100), dissolved oxygen tension (DOT, Mettler-Toledo GmbH, Switzerland) and foam (level sensor). The pH was controlled at pH 5 with a 4M KOH solution. A thermo circulator (ADI 1018 Applikon, Schiedam, the Netherlands) controlled the temperature of the reactor content at 30 ^{o}C. The foam was controlled with a 10 (v/v) silicone antifoam solution (BDH, VWR International Ltd. Poole, England). Two Rushton turbine stirrers were applied for mixing of the broth with a rotation speed of 450 rpm. Air was sparged through the reactor with a flow rate of 3 l/min by means of a mass flow controller (Brooks Instruments B.V. Veenendaal, The Netherlands). The off-gas of the bioreactor was cooled in a condenser connected to a cryostat at 2 ^{o}C to reduce evaporation. The bioreactor was operated at an overpressure of 0.27 bars. A process control system (DCU3, Sartorius AG, Melsingen, Germany) controlled the entire fermentation and MFCS software (Sartorius AG, Melsingen, Germany) logged the data to a computer.
The entire reactor setup, without the probe with the sensor chip, was autoclaved at 121 ^{o}C for 20 minutes. Because the reference electrode could not withstand autoclaving, the probe was sterilized separately in 70 % ethanol and mounted in the bioreactor just before inoculation.

The batch cultivations of *Candida utilis* were performed in duplicate. In Batch I, a sensor array with a type A impedance sensor was used. Along with this sensor array, the dissolved oxygen sensor of a second multi-sensor chip was used. From this second chip, the polyimide layer on top of the UMEA was removed to expose the entire area of the underlying macro electrode. Batch II preceded the continuous cultivation and in both cultivations a sensor array with a type B impedance sensor was used.

Cell culture samples (5 ml, in duplicate) were filtered through pre-dried and pre-weight nitrocellulose filters (pore size 0.45 µm, Gelman Science, Ann Arbor, MI, USA). The filters were washed three times with 5 ml demineralized water and dried in a stove at 70 ^{o}C for 48 hours and then weighed.

5.3 Results and discussion

5.3.1 Sensor chip

Figure 5-1 shows microscopic pictures of (a) the multi-sensor chip and (b) the ultra micro electrode array. All the separate sensors on the chip are clearly visible and no defects could be detected. *Figure 5-1* (c) shows that the sensor dimensions meet the floor plan of 96-well microtiter plates.

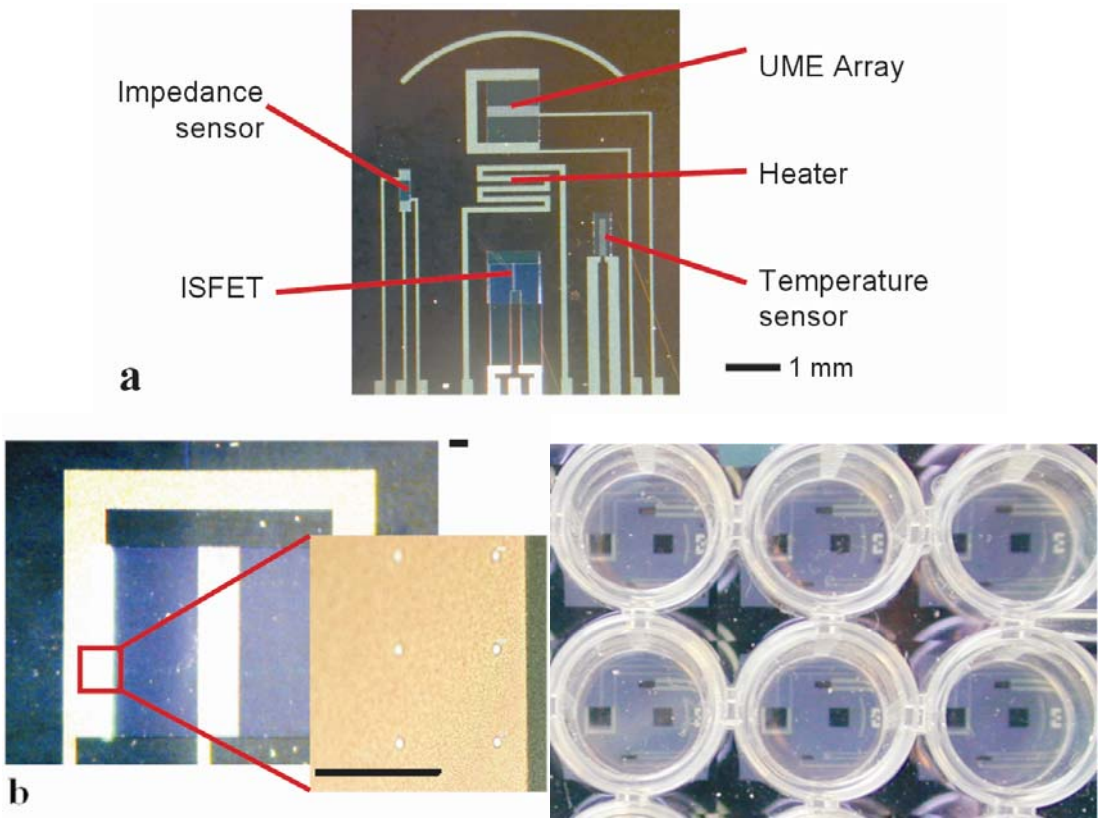

Figure 5-1: Microscope pictures of: (a) the sensor chip with the integrated sensors for the measurement of temperature (T sensor), pH (ISFET), dissolved oxygen concentration (UMEA) and the viable biomass concentration (impedance sensor). The arch at the top of the sensor array is an alignment mark, indicating the edge of a well if the sensor would be placed underneath a 96-well microtiterplate. The Pt heater, included for temperature studies, is not discussed in this paper. (b) the dissolved oxygen sensor (UMEA) in detail. The length of the scale bars corresponds to 100 μm (c) The sensor dimensions meet the floor plan of a 96-well microtiter plate

Examination of the sensor surface under a microscope after the yeast cultivations showed no visible damage to the surface and no biofilm formation on the sensor surface.

5.3.2 Dissolved oxygen measurements

Batch cultivation

During the batch cultivation the dissolved oxygen concentration decreased in time due to the increasing oxygen demand of the exponentially growing yeast. At 7.5 hours in Batch I and 8 hours in Batch II, the dissolved oxygen concentration curve showed a sharp increase followed by a sharp decrease (see *Figure 5-2* and *Figure 5-3*). This characteristic spike in the dissolved oxygen curve indicated that the glucose was depleted and that the yeast switched to growth on ethanol. The batch experiments finished at approximately 9 hours after inoculation.

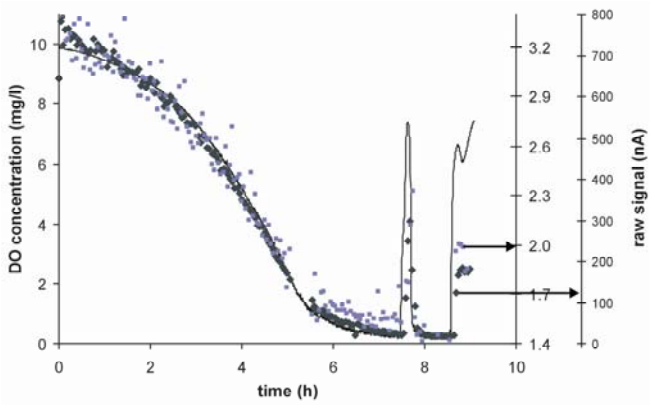

Figure 5-2: Comparison between the dissolved oxygen signals from the conventional Clark cell (—), the UMEA on the multi-sensor chip (■) and the dissolved oxygen sensor with large working electrode surface on the multi-sensor chip during (♦) Batch I

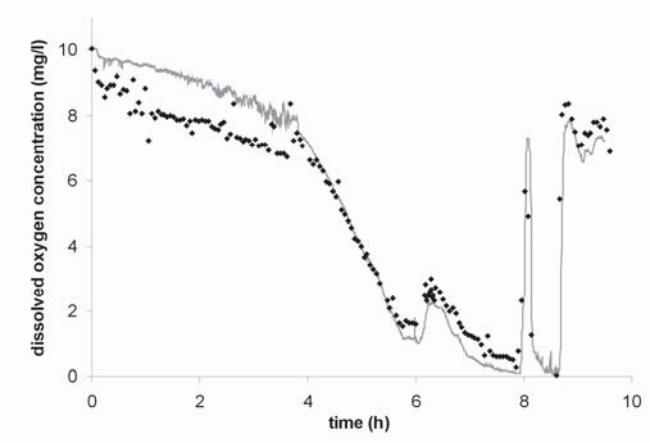

Figure 5-3: Comparison between the dissolved oxygen signals from the conventional Clark cell (—) and the UMEA (♦) on the multi-sensor chip during Batch II

Figure 5-2 shows the dissolved oxygen signals from both the conventional Clark cell and the ultra micro electrode array (UMEA) on the multi sensor chip, measured simultaneously in Batch I. It can be seen from this figure that the signal of the UMEA closely matches the signal of the Clark cell. Also the spike was clearly visible in the UMEA profile but less pronounced compared to the profile of the Clark cell due to the lower sampling rate of the UMEA signal. It can also be seen that the signal of the UMEA contained more noise than the Clark cell signal. This is probably due to the low current levels combined with electromagnetic interference from the environment. A way to improve the signal to noise ratio of the UMEA would be by increasing the electrode area and thus the measured current level.

This hypothesis was tested by removing the polyimide layer of the UMEA electrode area of the second sensor chip present in Batch I. *Figure 5-2* shows the signal of this oxygen sensor, together with the signal of the Clark cell in Batch I. The current measured with the sensor with the enlarged electrode surface area was roughly 200 fold higher compared with the UMEA with the 2 µm radius holes (i.e. from ~3 nA to ~700 nA at a dissolved oxygen concentration of 9.9 mg/l). A comparison between the signals plotted in *Figure 5-2* shows that an increased surface area significantly increased the signal to noise ratio. However, this way to achieve a better signal to noise ratio goes at the expense of increased flow independency and oxygen consumption of the sensor. Since reduction of 1 oxygen molecule is associated with the transport of 4 unit charges q, one can calculate that the maximum current of 700 nA corresponds to an oxygen consumption of 6.5 nmol/h when measuring continuously. Even when the multi-sensor chip would be mounted under a 96-well microtiterplate, with a typical working volume of 100 µl and operated under high

oxygen demands of typically 40-80 mmol/l/h, the oxygen consumption of the sensor is negligible to the oxygen consumption of the biomass at high biomass concentrations.

The recorded UMEA signal during Batch I was reproduced nicely during Batch II (see *Figure 5-3*). Just before the batch cultivation a two point in situ calibration (0 and 7.9 mg/l) was performed. The calibration resulted in a sensitivity of 0.96 nA/mg O_2/l and an offset of 0.9 nA. Also in Batch II, the dissolved oxygen concentration measured by the UMEA corresponded very well with the data from the Clark cell with about 0.2 mg/l sensitivity. Roughly 4 hours after inoculation, however, the sensitivity of the UMEA suddenly seems to increase. A few minutes before the increase in sensitivity of the UMEA, accidentally several milliliters of concentrated antifoam solution was added to the bioreactor. Most likely the antifoam has a negative effect on the sensitivity of the UMEA.

Remarkably, in Batch II the noise on the UMEA data was significantly reduced compared to Batch I. This could be explained by reduced electromagnetic interference due to improved wiring.

Continuous cultivation

The drift and robustness of the newly developed oxygen sensor were tested in a continuous cultivation experiment. In this experiment all the environmental conditions were kept constant. A continuous cultivation experiment is the best option for a drift test under conditions under which the sensor ultimately should function. *Figure 5-4* shows a comparison between the oxygen concentration measured by the UMEA and the conventional Clark cell over a period of 15 hours of continuous cultivation.

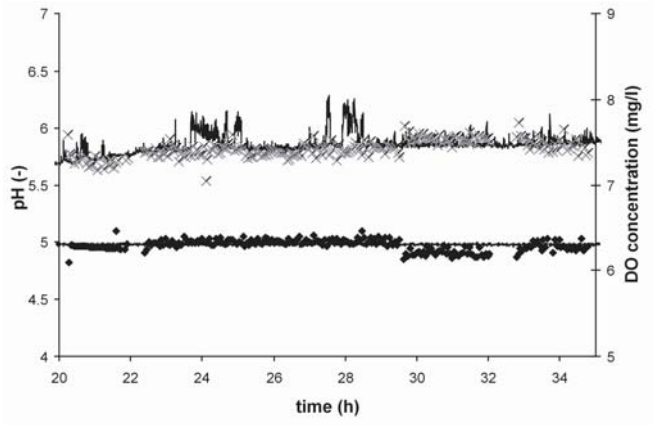

Figure 5-4: Comparison between the dissolved oxygen signals from the Clark cell (—) and the UMEA (×) on the multi-sensor chip and between the conventional pH sensor (—) and the ISFET 1(♦) during the continuous cultivation of Candida utilis

From a comparison of the slopes of the two curves in *Figure 5-4*, it can be observed that the drift rate of the UMEA is insignificant, i.e. 2 µg/l/hr with respect to the Clark cell.

5.3.3 pH measurements

Batch cultivation

During Batch I, the ISFET signal was logged using the DAQ device instead of the digital multimeter. As the DAQ device was not electrically floating, the reference electrode was unintentionally grounded when the ISFET was connected. As the fermentor housing is grounded as well, a ground loop problem occurred and the pH measurements failed.

In Batch II, the ISFET signal was logged by the electrically floating digital multimeter and this solved the ground-loop problem. For this reason, the pH was measured by the sensor chip in Batch II only and therefore only sensor chip measurements for the pH of Batch II are presented here. Prior to the batch experiment, a two point calibration was performed. The calibration resulted in a sensitivity of -58 mV/pH unit, which is close to the ideal Nernst sensitivity (Bergveld 2003; Faber et al.). The long-term drift rate was determined to equal 1.2 mV/hr. The measurements in both the batch and continuous cultivations were compensated for this transient behavior.

The pH during the batch cultivation was controlled at pH 5 by an automatic titration of a 4M KOH solution. To make sure that the ISFET was working correctly, the pH control

was started 0.75 hours after inoculation. At the end of the batch, when the glucose and ethanol were depleted, the yeast consumed the acids that were formed during the batch. Since there was no acid control, the pH increased because of this.

Figure 5-5 compares the pH measured by the ISFET, obtained using the sensitivity and drift corrections described above, to the conventional pH sensor present in the bioreactor. The performance of the ISFET was very good under these test conditions and accuracy was well below 0.1 pH unit.

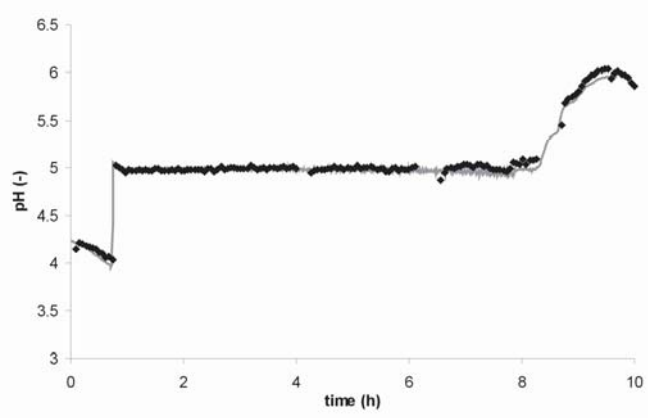

Figure 5-5: comparison between the conventional glass pH sensor (—) and ISFET 1 (♦) in Batch II

Continuous cultivation

Figure 5-4 shows the prolonged measurement of pH during continuous cultivation of *Candida utilis*. It can be observed from these measurements that the drift of the ISFET could indeed be successfully corrected with a drift rate and therefore remained constant in a controlled environment. Therefore, the applied compensation method is very effective.

5.3.4 Biomass concentration measurements

Batch cultivation

The conductivity of the cell culture was determined from impedance measurements in the range of 10 kHz – 15 MHz. The conductivity values for the non-dispersive and dispersive frequency range were obtained for 10 spectral measurement points around 100 kHz and 10 MHz, respectively. As explained above, the high-frequency conductance is a measure for

the background electrolyte conductivity. The low-frequency conductance is lower due to interfacial polarization of the cell membranes.

The impedance signals at 100 kHz and 10 MHz showed significant noise levels. Noise was presumably caused by interference of environmental electromagnetic fields, i.e. those presented by the conventional electrochemical probes inside the fermentor. The measurements furthermore show that background electrolyte conductivity remained very constant throughout the cultivation experiments (data not shown). The low-frequency conductance significantly decreased during the batch growth of *C. utilis*, indicating that interfacial polarization increasingly took place. Both conductance values were normalized with respect to their initial values. The difference between both values was used as a measure for the biomass concentration.

Figure 5-6 and *Figure 5-7* show the dispersion signals thus obtained for batch I and batch II, respectively and compare the signals with a conventional technique to determine the biomass concentration i.e. off-line dry weight measurement. A moving average over 10 measurements was plotted in order to reduce noise. Monitoring a moving average leads to a delay in response time. This was not considered to be a major issue, because the biomass concentration is not a parameter used for the control of fermentation processes.

The results depicted in *Figure 5-6* and *Figure 5-7* scale linearly with the measured cell dry weight. This indicates that the sensitivity of the sensor does not change during the experiment. Both measurements show an exponential growth curve until (almost all) the glucose is depleted and then levels off. The obtained accuracy for the biomass sensor is ~ 1g/l. The signals seem to show a sort of cyclical variation with time. The magnitude of this variation is comparable to the obtained noise magnitude and could not be related to the biomass concentration. It was therefore considered as an artifact of the measurement.

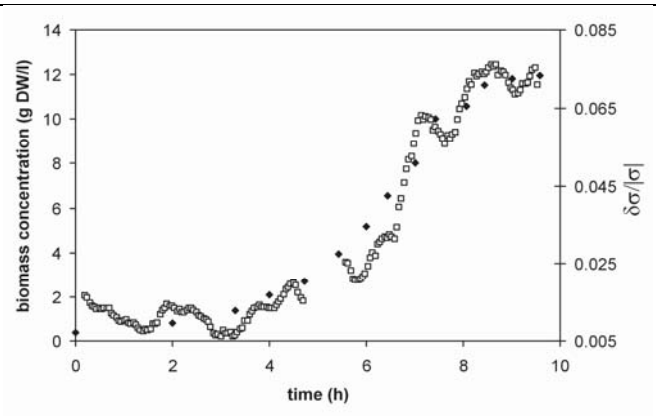

Figure 5-6: comparison of biomass concentration measurements using dry weight (♦) and biomass sensor (□) in Batch I

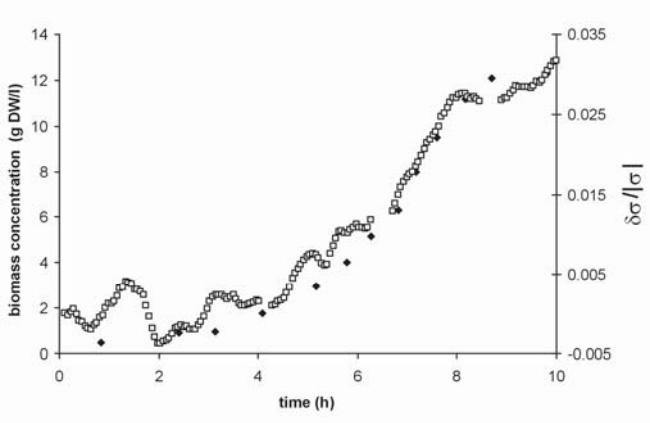

Figure 5-7: comparison of biomass concentration measurements using dry weight (♦) and biomass sensor (□) in Batch II

The sensitivity of the biomass sensor as obtained during Batch II appeared considerably lower than the sensitivity obtained during Batch I. This difference might be due to the different geometries of the type A and type B conductivity sensors, used for obtaining the measurement results in Batch I and Batch II, respectively. The electrode spacing is lower in case of the type B conductivity sensor, meaning that the electrical field distribution between the electrodes is located relatively more close to the sensor surface. It is conceivable that the yeast cell distribution close to this surface is inhomogeneous and less dense, resulting in a lower signal for the type B conductivity sensor (Yeung et al. 2006).

Continuous cultivation

Figure 5-8 shows the sensor response during the continuous cultivation of yeast cells. The figure shows that the sensor response is stable and exhibits low drift during long-term measurements.

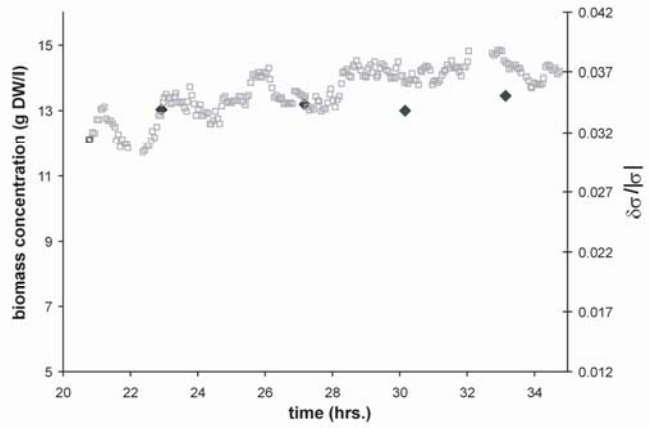

Figure 5-8: comparison of biomass concentration measurement using dry weight (♦) and biomass sensor (□) during continuous cultivation of Candida utilis

5.3.5 Temperature measurements

During both batch experiments the temperature was controlled at 30 °C. The temperature was measured by a standard Pt100, which is a commercially available thermistor consisting of a platinum wire with a nominal resistance of 100 Ohm. The measured temperature was compared to the signal from the platinum thin-film resistor on the multi-sensor chip. Prior to the measurements, the thin film resistor was calibrated and showed a linear sensitivity of 0.22%/ °C in the temperature range 25– 40 °C. As can be seen in *Figure 5-9*, the signal from the thin-film resistor nicely follows the signal measured by the conventional Pt100 with ~0.1 ^{o}C accuracy.

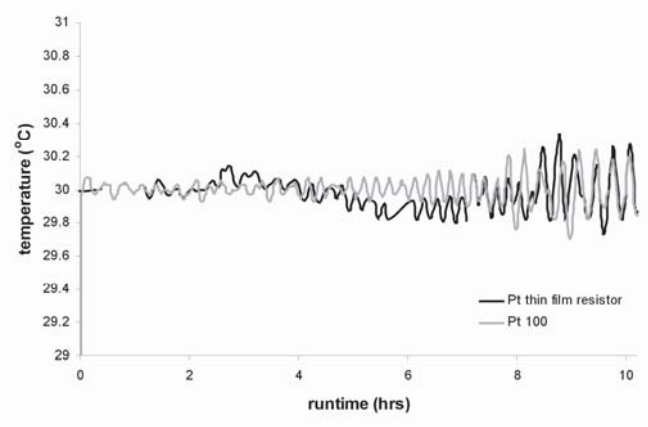

Figure 5-9: comparison of temperature measurement between conventional PT100 (—) and the temperature resistor on chip (♦) in Batch I

Both temperature signals in *Figure 5-9* exhibit increased instability as time proceeds. This is due to a shortcoming of the temperature controller that does not adequately counteract small changes in environmental temperature. *Figure 5-9* shows that even these small and relatively fast temperature changes could be accurately monitored by the thermistors on the sensor array. Deviations between both temperature sensor signals are likely to be due to the fact that both sensors are located on different positions inside the fermentor.

5.4 Conclusions

The electrochemical multi sensor chip turned out to be robust and give reliable and producible reading. All sensors were shown to be sufficiently accurate within the range relevant to yeast fermentations under conditions the sensor ultimately should function.

The ultra micro electrode array used for monitoring the dissolved oxygen concentration showed an accuracy of ~0.2 mg/l and negligible drift. Oxygen consumption was shown to be insignificant, even for the sensor with enlarged electrode area applied in a microreactor with a 200 µl volume. The results of the biomass sensor matched very well with dry weight measurements and showed a limit of detection of ~1 g/l. Impedance measurements suffered from significant noise levels. An important potential noise source is formed by the conventional electrochemical probes present in the fermentor and is cancelled if no other electrochemical sensors operate in parallel in the final application. Sensor performance can be further improved by better shielding of electrical wires and connections and by fitting the impedance data on more advanced electrical circuit models.

pH was monitored using an ISFET with an accuracy well below 0.1 pH unit. Measurements performed during the continuous cultivation experiments show ISFET drift could effectively be compensated for using a device-specific constant factor. The platinum thin-film temperature resistor followed temperature changes with ~0.1 ^{o}C accuracy.

Examination of the sensor surface under a microscope showed no visible damage or defects caused during the performed experiments. In combination with previously reported results showing that no signal degradation is observed after autoclaving the sensor several times (Krommenhoek et al. 2007), it can be concluded that the sensor array has high potential for implementation in reusable systems.

The time required to monitor all 4 parameters in duplo was set to 5 minutes during these experiments. Because only a small fraction of this interval is required for the measurements themselves, measurement resolution can be improved significantly by optimizing the software controlling the data communication between the measurement equipment and the computer.

References

Asami K, Yonezawa T. 1995. Dielectric Analysis of Yeast-Cell Growth. Biochimica Et Biophysica Acta-General Subjects 1245(1):99-105.

Bergveld P. 1970. Development of an ion-sensitive solid-state device for neurophysiological measurements. IEEE Transactions on Biomedical Engineering 17:70-71.

Bergveld P. 2003. Thirty years of ISFETOLOGY - What happened in the past 30 years and what may happen in the next 30 years. Sensors and Actuators B-Chemical 88(1):1-20.

Boccazzi P, Zanzotto A, Szita N, Bhattacharya S, Jensen KF, Sinskey AJ. 2005. Gene Expression Analysis of Escherichia Coli Grown in Miniaturized Bioreactor Platforms for High-Throughput Analysis of Growth and genomic Data Applied Microbiology and Biotechnology 68(4):518-532.

Brett CMA, Brett AMO. 1983. Electrochemistry: Principles, Methods and Applications. New York: Oxford University Press. 81-90 p.

Chen YQ, Li GA. 1993. A Mathematical-Model with Finite-Element Analysis of Recessed Dissolved-Oxygen Cathode Array. Sensors and Actuators B-Chemical 10(3):223-228.

Deshpande RR, Heinzle E. 2004. On-line oxygen uptake rate and culture viability measurement of animal cell culture using microplates with integrated oxygen sensors. Biotechnology Letters 26(9):763-767.

Duetz WA, Rüedi L, Hermann R, O'Connor K, Büchs J, Witholt B. 2000. Methods for intense aeration, growth, storage, and replication of bacterial strains in microtiter plates. Applied and Environmental Microbiology 66:2641-2646.

Faber EJ, Sparreboom W, Groeneveld W, de Smet LCPM, Bomer JG, Olthuis W, Zuilhof H, Sudhölter EJR, Bergveld P, van den Berg A. pH Sensitivity of SiC Linked Organic Monolayers on Crystalline Silicon Surfaces (p NA) ChemPhysChem article in press.

Gong JW, Chen QF, Lian MR, Liu NC, Daoust C. 2006. Temperature feedback control for improving the stability of a semiconductor-metal-oxide (SMO) gas sensor. Ieee Sensors Journal 6(1):139-145.

Harms P, Kostov Y, French JA, Soliman M, Anjanappa M, Ram A, Rao G. 2006. Design and performance of a 24-station high throughput microbioreactor. Biotechnology and Bioengineering 93(1):6-13.

Hauttmann S, Muller J. 2001. In-situ biomass characterisation by impedance spectroscopy using a full-bridge circuit. Bioprocess and Biosystems Engineering 24(3):137-141.

Jamasb S, Collins S, Smith RL. 1998a. A physical model for drift in pH ISFETs. Sensors and Actuators B-Chemical 49(1-2):146-155.

Jamasb S, Collins SD, Smith RL. 1998b. A physical model for threshold voltage instability in Si3N4-gate H+-sensitive FET's (pH ISFET's). Ieee Transactions on Electron Devices 45(6):1239-1245.

John GT, Goelling D, Klimant I, Schneider H, Heinzle E. 2003a. PH-sensing 96-well microtitre plates for the characterization of acid production by dairy starter cultures. Journal of Dairy Research 70(3):327-333.

John GT, Klimant I, Wittmann C, Heinzle E. 2003b. Integrated optical sensing of dissolved oxygen in microtiter plates: A novel tool for microbial cultivation. Biotechnology and Bioengineering 81(7):829-836.

Kostov Y, Harms P, Randers-Eichhorn L, Rao G. 2001a. Low-cost microbioreactor for high-throughput bioprocessing. Biotechnology and Bioengineering 72(3):346-352.

Kostov Y, Harms P, Rao G. 2001b. Ratiometric sensing using dual-frequency lifetime discrimination. Analytical Biochemistry 297(1):105-108.

Krommenhoek EE, Gardeniers JGE, Bomer JG, Li X, Ottens M, van Dedem GWK, van Leeuwen M, van Gulik WM, van der Wielen LAM, Heijnen JJ and others. 2007. Integrated Electrochemical Sensor Array for On-Line Monitoring of Yeast Fermentations. Anal. Chem. 79(15):5567-5573.

Kumar S, Wittmann C, Heinzle E. 2004. Minibioreactors. Biotechnology Letters 26(1):1-10.

Lamping SR, Zhang H, Allen B, Shamlou PA. 2003. Design of a prototype miniature bioreactor for high throughput automated bioprocessing. Chemical Engineering Science 58(3-6):747-758.

Lee HLT, Boccazzi P, Ram RJ, Sinskey AJ. 2006. Microbioreactor arrays with integrated mixers and fluid injectors for high-throughput experimentation with pH and dissolved oxygen control. Lab on a Chip 6(9):1229-1235.

Lye GJ, Ayazi-Shamlou P, Baganz F, Dalby PA, Woodley JM. 2003. Accelerated design of bioconversion processes using automated microscale processing techniques. Trends in Biotechnology 21(1):29-37.

Maharbiz MM, Holtz WJ, Howe RT, Keasling JD. 2004. Microbioreactor arrays with parametric control for high-throughput experimentation (vol 85, pg 376, 2004). Biotechnology and Bioengineering 86(4):485-490.

Moore GE. 1998. Cramming more components onto integrated circuits. Proceedings of the IEEE 86(1):82-85.

Morf WE, de Rooij NF. 1997. Performance of amperometric sensors based on multiple microelectrode arrays. Sensors and Actuators B-Chemical 44(1-3):538-541.

Papkovsky DB. 1995. New Oxygen Sensors and Their Application to Biosensing. Sensors and Actuators B-Chemical 29(1-3):213-218.

Rubinstein I. 1995. Physical Electrochemistry, Principles, Methods and Applications. New York: Marcel Dekker, Inc. 134-182 p.

Sauer U. 2004. High-throughput phenomics: experimental methods for mapping fluxomes. Current Opinion in Biotechnology 15(1):58-63.

Schwan HP. 1957. Electrical properties of tissues and cell suspensions. Advances in Biological and Medical Physics 5:147.

Szita N, Boccazzi P, Zhang ZY, Boyle P, Sinskey AJ, Jensen KF. 2005. Development of a multiplexed microbioreactor system for high-throughput bioprocessing. Lab on a Chip 5(8):819-826.

Tiggelaar RM, Berenschot JW, de Boer JH, Sanders RGP, Gardeniers JGE, Oosterbroek RE, van den Berg A, Elwenspoek MC. 2005. Fabrication and characterization of high-temperature microreactors with thin film heater and sensor patterns in silicon nitride tubes. Lab on a Chip 5(3):326-336.

Verduyn C, Postma E, Scheffers WA, van Dijken JP. 1992. Effect of benzoic acid on metabolic fluxes in yeasts: a continuous-culture study on the regulation of respiration and alcoholic fermentation. Yeast 8:501-517.

Walther I, van der Schoot BH, Boillat M, Cogoli A. 2000. Performance of a miniaturized bioreactor in space flight: Microtechnology at the service of space biology. Enzyme and Microbial Technology 27:778-783.

Warringer J, Blomberg A. 2003. Automated screening in environmental arrays allows analysis of quantitative phenotypic profiles in Saccharomyces cerevisiae. Yeast 20(1):53-67.

Woias P, Meixner L, Frostl P. 1998. Slow pH response effects of silicon nitride ISFET sensors. Sensors and Actuators B-Chemical 48(1-3):501-504.

Yeung ES, He Y, Li H, Kang SH, Isailovic D, Zheng J. Sub-Diffraction Limit Imaging of Single Molecules and Single Cells. In: Kitamori T, Fujita H, Hasebe S, editors; 2006; Tokyo, Japan. p 1-3.

Zimmermann HF, John GT, Trauthwein H, Dingerdissen U, Huthmacher K. 2003. Rapid evaluation of oxygen and water permeation through microplate sealing tapes. Biotechnology Progress 19(3):1061-1063.

Chapter 6: Fermentation monitoring in a batch micro bioreactor array

In this chapter, the development and testing of a an array consisting of 2 micro bioreactors suitable for on-line monitoring yeast fermentations, is presented. The reactors have a working volume of 100 µl and incorporate the electrochemical sensor arrays presented in chapters 4 and 5. Mixing is achieved by means of a magnetic stirrer bar fixated on an axle. A saltbridge consisting of a Nafion hollow fiber membrane for ensuring proper electrical connection between the micro bioreactors and the reference electrode reservoir is presented. The developed system was tested for the batch cultivation of *Candida utilis* yeast cells. The results are presented and discussed.

6.1 Introduction

The goal of biotechnology is to obtain useful metabolic products from biological material (Crueger and Crueger 1990; Gavrilescu and Chisti 2005). Fermentation procedures must be developed for the cultivation of microorganisms under optimal conditions and for the production of the desired metabolites or enzymes by the microorganisms. Batch fermentation procedures, where cells are cultured in a vessel with an initial charge of medium that is not altered by further nutrient addition or removal, are simple and widely used in laboratories and industrially (Shuler and Kargi 2002). After inoculation of a sterile nutrient solution with microorganisms and cultivation under physiological conditions, the four typical phases of growth as depicted in figure 6-1 can be observed (Crueger and Crueger 1990).

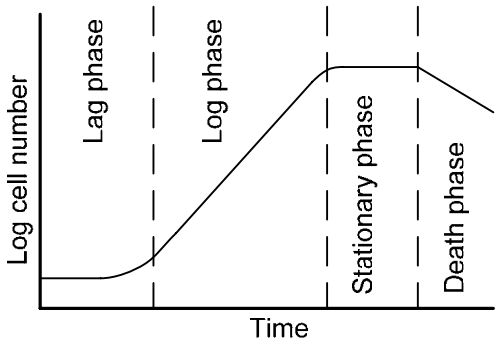

Figure 6-1: typical growth curve

During the *lag phase*, which typically takes several hours for yeast cultures, the microorganisms adapt to their new environment and there is no increase in the number of cells. When the cells have adapted to their new environment, growth of biomass can be described as a doubling of biomass per unit time, hence the term *log phase*. The lag phase and the log phase will be referred to as the *batch phase* in the following sections. At the end of the batch phase, the substrate is metabolized and growth slows down or completely stops, although the composition of the cells may change. This phase is referred to as the *stationary phase*. In the *death phase*, the energy reserves of the cells are exhausted and cells die at an exponential rate.

As fermentation in industrial scale fermentors is very money- and time consuming, it is very important that the right strains of cells are selected. For this purpose, there is a growing interest in the miniaturization and parallelization of bioreactors (Lee et al. 2006).

Microbioreactor technology aims to combine the small working volume and the high-throughput possibilities of microtiter plates with the monitoring and control features of lab-scale bioreactors (Kumar et al. 2004; Lye et al. 2003). Two complementing approaches can be distinguished. The first is trying to understand in a more sophisticated manner the quantitative process features of shaken bioreactors (hydrodynamics and mass transfer) as well as the performance of bioprocesses in shaken bioreactors by introducing sensors for the parallel online measurement of dissolved oxygen (DO) and pH. The second approach is trying to miniaturize the industrial cultivation technology by scale-down of more or less complete stirred-tank reactors with gas supply, control of relevant state variables and fed-batch operation capability (Weuster-Botz et al. 2005).

In this chapter, the development and testing of parallelized microbioreactors with 200 µl volume and means for mixing, gas supply and on-line sensing of temperature, pH, dissolved oxygen and viable biomass concentrations is presented. In section 6.2, the design of the microfermentor array is discussed. Section 6.3 shows the fabrication of the device and explains the experiments that are performed to study its functionality. The measurement results are shown in section 6.4 and are followed by a discussion and conclusions in section 6.5

6.2 Microreactor design

This section shows the design of the micro bioreactor array under study and explains its theoretical background. The design of this micro bioreactor array is based on the electrochemical sensor array presented in chapters 4 and 5 of this thesis and the 96-well microtiter plate format.

For operating the sensor arrays on this format, it was explained in chapter 2 that microfluidic means are needed to ensure electrical connection between the micro bioreactors and a separate reservoir containing a reference electrode. The design of these microfluidic connections is described in section 6.2.1. Section 6.2.2 describes the means used for mixing in the micro bioreactors. In 6.2.3, the resulting design of the complete microfermentor array is described.

6.2.1 Reference electrode configuration

For proper functioning of the pH sensors and the dissolved oxygen sensors, an electrode of known potential which approaches ideal non-polarizability, generally referred to as a

reference electrode (Bard and Faulkner 2001), is needed. Although several microfabricated solid-state reference electrodes have been developed (Bakker and Qin 2006; Polk et al. 2006), aqueous electrodes, like the aqueous silver/silver chloride reference electrode, remain the most suitable reference electrode when long-term stability is required.

Therefore, it was proposed in chapter 2 to apply a single, aqueous reference electrode in a separate reservoir filled with medium and ensure electrical connection to the microfermentors by microfluidic means. When an electrical connection between two electrochemical half cells needs to be established, use of saltbridges can be made. A salt bridge usually consists of a suitably shaped tube closed at both ends by a porous material.

The filling solution is usually chosen such that the liquid junction potential arising from cation and anion diffusion across the junction between electrolytes with different ion concentrations is minimized (Koryta and Dvořák 1987). Since in the system under study, cation and anion concentrations on both sides of the salt bridge are assumed to be equal and remain constant throughout the process, no diffusion occurs and thus no liquid junction potentials build up if the salt bridge is filled with medium as well.

The junction device closing the salt bridge should be designed in such a way that leakage of filling electrolyte into the sample solution is prevented as much as possible, and the electrical resistance of the junction is minimized (Sawyer et al. 1995). In case of the system under study, the porous junction device closing the salt bridge is constituted by an ion-selective Nafion hollow fiber membrane. In this case, no fluid leakage is to be expected and the electrical resistance of the junction is low because of cation permeability. The voltage drop across the membrane is linear with the difference in anion concentrations in the electrolyte solutions on both sides of the membrane. Since the ion concentrations in both liquid phases are assumed to be practically equal and remain constant throughout the process, this voltage drop is expected to be very low and stable.

6.2.2 Mixing method

At present, observations on mixing within microwells have mainly been reported for systems using the aid of shaking (Duetz and Witholt 2001; Micheletti et al. 2006; Weiss et al. 2002). Many applications though, like biological assays, are best carried out using static microwells (Kostov et al. 2001; Nealon et al. 2006). Moreover, in case of static microwells, the system is not exposed to immense vibrations which could limit its durability.

Although recent developments in microfluidics offer promising methods for mixing in microreactor arrays, this research confined itself to finding a rapidly applicable method

for mixing. Therefore, use is made of a magnetic stirrer bar. As to prevent mechanical contact between the stirrer bar and the sensor array located at the bottom of the microreactor, the stirrer bar is fixated on elevated height.

Shear stress, being defined as the internal distribution of force per unit area parallel to the face of a material, is characterized by a so-called shear factor. For a parallel-plate flow chamber, the shear factor is defined as (Bacabac et al. 2005):

$$T = \frac{h}{\lambda_v} \tag{6-1}$$

where h is the distance between the parallel plates and λ_v is the viscous penetration depth. For agitated small-scale bioreactors, an integrated shear factor, ISF, was derived as (Chen et al. 2003):

$$ISF = \frac{2\pi N D_I}{D_T - D_I} \tag{6-2}$$

Here, N is the angular speed of the impeller, D_I is the impeller diameter and D_T is the vessel diameter. Since $v_I \equiv \pi N D_I$ represents the impeller tip speed and $d \equiv (D_T - D_I)/2$ represents the distance between the impeller tip and the vessel wall, equation (6-2) can be rewritten as:

$$ISF = \frac{v_I}{d} \tag{6-3}$$

The mean fluid velocity, v_F, required for sufficient oxygen transfer depends on the Reynolds number of the vessel, according to:

$$v_F = \frac{N D_I}{Re} \tag{6-4}$$

Based on these relations and $v_I \sim v_F$, it was estimated that the magnitude of shear induced in the micro bioreactors is of comparable order of magnitude as those obtained in larger

scale fermentors if the headspace of the reactors is filled with pure oxygen and the stirring speed is adjusted to a rate enabling sufficient oxygen transfer.

6.2.3 Complete micro bioreactor array design

The above subsections explained the design of specific parts of the system under study. A schematic overview of the complete setup can be found in figure 6-2. This figure shows the setup for operation and monitoring of a single micro bioreactor only. However, the micro fermentors were built in duplo, placed on a single stirrer motor as described above and connected to the same relays board as to allow for the control of two reactors in parallel.

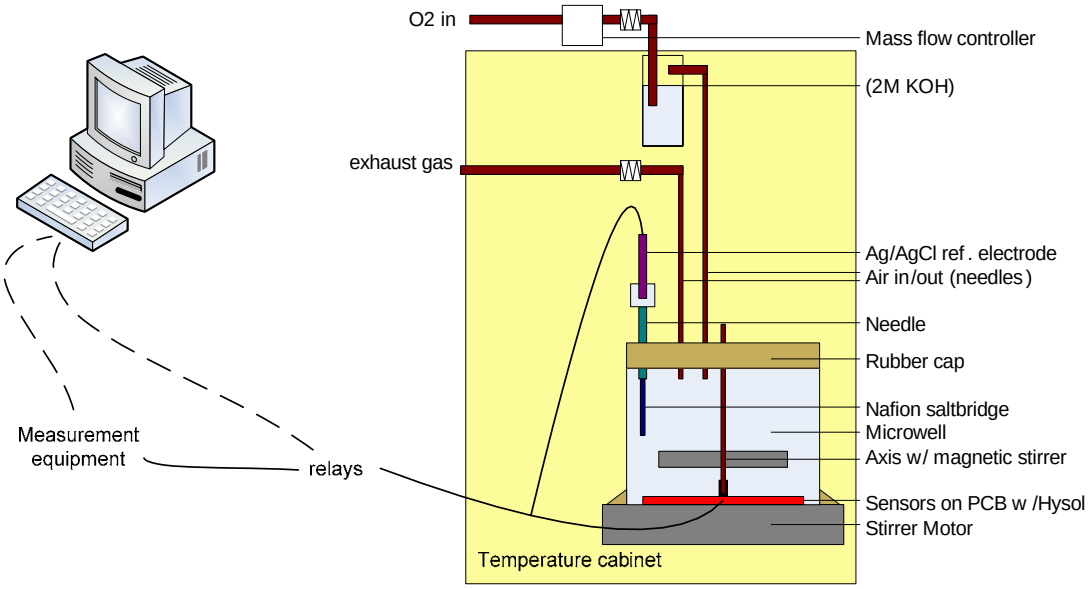

Figure 6-2: Schematic representation of micro bioreactor setup

The micro bioreactors are equipped with a magnetic stirrer bar which is fixated on elevated height by means of an axle. The reactors are placed on a single stirrer motor. The electrochemical sensor arrays described in chapters 4 and 5 are located on the bottom of the micro bioreactors and controlled as described previously. The reactors are closed by a rubber cap containing air in- and outlets and the tip of the salt bridge described above. The rate at which pure oxygen flows into the reactors is controlled by means of mass flow controllers. The gas is bubbled through 2M KOH solutions for humidification and CO_2 removal. The air outlets can be connected to an off-gas analysis system. Filters help to ensure sterility. The saltbridges are connected to a reservoir filled with medium and

containing an aqueous Ag/AgCl reference electrode. The complete setup is placed in a thermostatically controlled cabinet which uses light bulbs as heating elements.

6.3 Experimental

The following subsections describe the fabrication of the micro bioreactor array and the measurements performed to study its functionality.

6.3.1 Device fabrication

Electrochemical sensor arrays were mounted on a printed circuit board as described in chapter 4. Single wells were taken from 96-well microtiter plates and glued on top of the sensor arrays using Hysol®. The wells were closed using rubber caps. Needles were pinched through as to create gas in- and outlets. A Nafion hollow fiber membrane was shifted over the tip of a third needle and filled with medium using a syringe. The salt bridge was closed using a droplet of glue. The saltbridges were connected to a reservoir filled with medium using silicone tubing. An aqueous Ag/AgCl reference electrode (REF 201, Radiometer Analytical) was immersed in this reservoir.

Holes were drilled in magnetic stainless steel stirrer bars of 1.67 mm x 2.01 mm x 4.80 mm in size (VP 711-1, V&P Scientific). Needles were pinched through the rubber caps and these holes. The tips of the needles were bent as to fixate the stirrer bars at elevated height. The microreactors were placed on a single stirrer motor (RET B, IKA Werke). A closeup picture of two microreactors constructed in this way can be obtained in figure 6-3.

Figure 6-3: closeup picture of two micro bioreactors, the coin on the left has a diameter of 25 mm

The inflow of pure oxygen gas is controlled by means of mass flow controllers (Brooks Instruments). Before entering the reactor chamber, the gas is bubbled through a 4M KOH solution for humidification and CO_2 removal, and filtered.

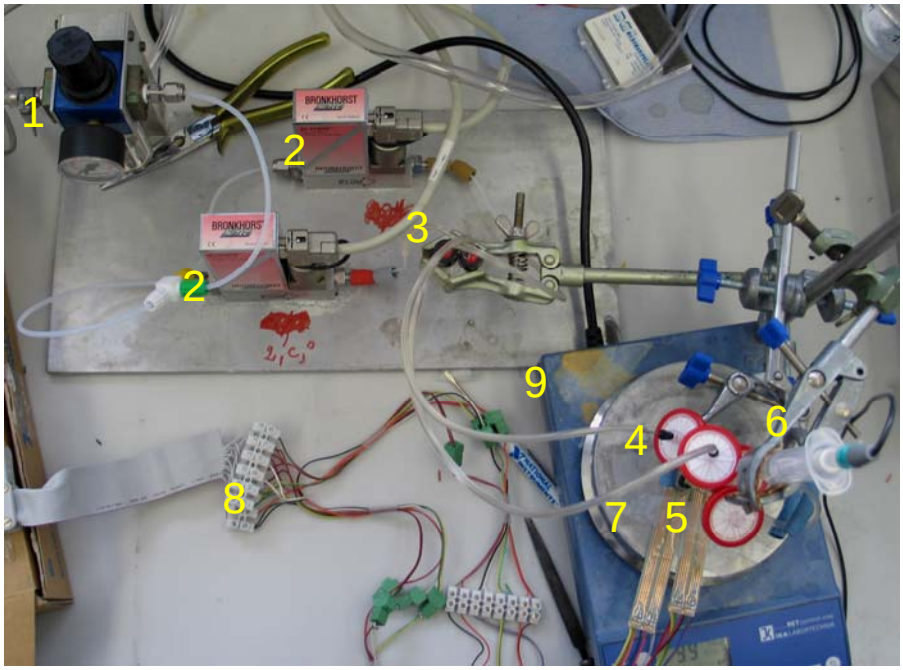

Figure 6-4: Photograph of the complete measurement setup with (1) oxygen gas supply (2) mass flow controllers (3) humidifying bottles (4) gas inlets (5) gas outlets (6) reference electrode in separate reservoir connected to the reactors by saltbridges (7) printed circuit boards (8) cable towards relays and measurement equipment and (9) stirrer motor

The complete setup is placed in a temperature controlled cabinet. The sensor chips are connected to the measurement equipment via a relays board. Both this relays board as the equipment are controlled through a custom written Labview program. More details about the readout of the sensor chip can be found in the next section. A photograph of the complete setup can be found in figure 6-4.

6.3.2 Measurements

The measurement setup was built as described above. Before having the ability to run and monitor yeast fermentations with it, the functionality of the saltbridge required validation by means of experimental tests.

Saltbridge

First, the stability of the salt bridge was investigated by placing the tip of the bridge in a beaker filled with medium. The voltage drop across the bridge was measured by monitoring the voltage drop between aqueous reference electrodes (REF 201, Radiometer Analytical) placed in the beaker and the reservoir at the beginning of the salt bridge using a multimeter (34401A, Agilent).

pH changes of the sample solution implicate that the anion concentration of the sample solution changes. Therefore, the stability of the voltage drop across the salt bridge was also studied at different pH values. This was done by comparing ISFET calibrations obtained with and without intervention of the salt bridge. In the first case, the ISFET was placed in the sample solution and the reference electrode was placed in the reservoir at the beginning of the salt bridge. In the latter case, both the ISFET and the reference electrode were placed in the sample solution. Furthermore, sample solution pH was varied by pipetting in acid (1M HCl) or base (1M KOH) solutions. The ISFET was connected to a home built ISFET amplifier whose output signal was logged using a digital multimeter (34401A, Agilent). Solution pH was simultaneously measured using a glass pH electrode (PHM83, Radiometer). The solution was stirred using a magnetic stirrer (RET B, Ika Werke) and the calibrations were performed at room temperature.

A peculiar characteristic of the duplo micro bioreactor configuration is that the salt bridge in either one of the fermentor can be bypassed by the salt bridge in the other fermentor, as depicted in figure 6-5.

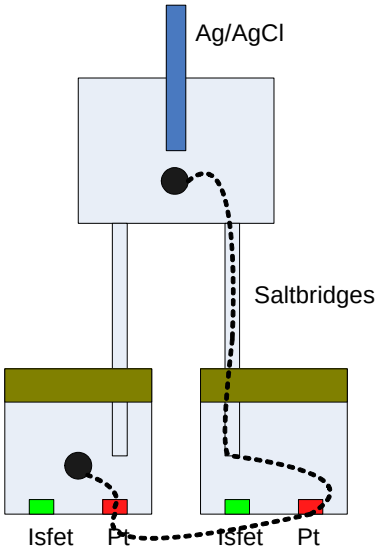

Figure 6-5: salt bridge "bypass"

The bypass arises because the counter electrodes of the oxygen sensors on the sensor arrays in both micro bioreactors are interconnected. Since the DAQ device had no output available to control an additional relay abolishing this interconnection, it was investigated whether the impedance of the bypass path, basically constituted by the impedance of the salt bridge plus the impedance of two platinum-electrolyte junctions, was high enough to neglect its influence on the measurements. This is done by first calibrating one of the ISFETs while all other sensors are uncoupled and the reference electrode is immersed directly into the sample solution. The result is compared to a calibration that is obtained by using the full measurement setup described in section 6.3.1. The signal related to the ISFET placed in the second microwell, at constant pH, is simultaneously monitored as to investigate whether it is influenced by pH changes in the first well.

Cell cultivation experiments

Prior to these experiments, ISFET sensitivity was determined from two point calibrations in pH4 and pH7 buffer solutions (Radiometer Analytical). The sensitivity of the dissolved oxygen sensor was determined from a single point calibration obtained by filling the microreactors with medium and blowing pure oxygen gas over the headspace. Temperature sensor sensitivity was obtained from two point calibrations

A preculture (0.5 liters) of *Candida utilis* CBS 621 was grown overnight in a shake flask at 30 ºC on mineral medium (Verduyn et al. 1992), which contained 7 g/l glucose*1 H_2O. The preculture served as inoculum for the micro bioreactors with a working volume of 150 µl. For the batch cultivation experiments in the bioreactors the concentrations of all

components in the medium were increased to twofold the concentrations of the shake flask medium, and ethanol (1.4 g/l) was added as a second substrate. Just before inoculation, the reactors were rinsed with 70% ethanol. This was the only means of sterilization used for the micro bioreactors. The stirring rate was set to approximately 200 rpm. Pure oxygen gas was blown over the headspace of the microreactors at a rate of around 2 ml/min. The bioreactors were placed in a cabinet which was thermostatically controlled at 30 °C.

The sensor arrays located inside the micro bioreactors were connected to the measurement setup described in chapter 5. The sensors are operated sequentially, as to prevent crosstalk. A full measurement cycle lasts almost 2 minutes. Therefore the time interval between subsequent measurements is set to 150 seconds. Since the duration of the measurement cycle is mainly determined by the time needed for data communication between computer and the measurement equipment and not by the measurements themselves, this time interval can be reduced significantly by adjusting the configuration.

6.4 Results

This section shows the measurement results obtained from the setup and protocols described above. In section 6.4.1, the results obtained from the salt bridge characterization experiments are shown. Section 6.4.2 shows the results obtained from yeast cell cultivation experiments.

6.4.1 Salt bridge characterization

The stability of the salt bridge was investigated by measuring the voltage drop across the bridge, as described above. The measurement results are shown in figure 6-6.

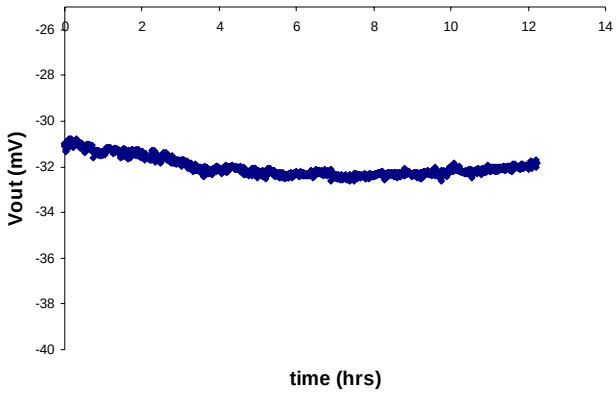

Figure 6-6: voltage drop across the salt bridge

The measured voltage drop was approximately -30 mV. This may be due to charge separations across the membrane, but could also have other causes such as the inequality of the voltage drops across the reference electrodes used. It can also be observed that the measured voltage drop was stable within 1.5 mV throughout the 12 hour-lasting experiment, even though the experiment was not performed at controlled temperature. This is acceptable for the intended application.

As described in the previous section, ISFET calibration was performed in the pH range relevant to yeast fermentations, i.e. pH3 – pH7. The results are depicted below.

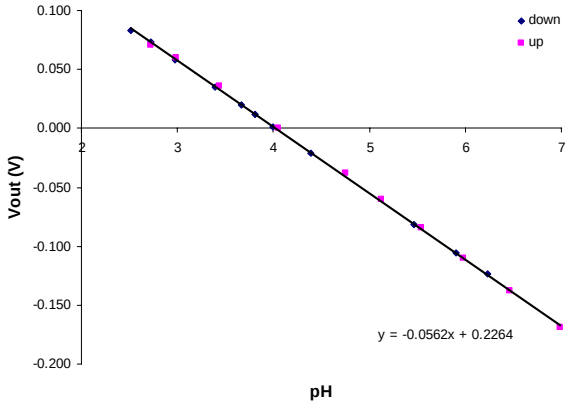

Figure 6-7: ISFET calibration

As can be observed from these results, the output signal of the ISFET amplifier shows a linear relation with solution pH and negligible hysteresis over the whole measurement range. This indicates that sample solution pH has negligible influence on the voltage drop across the Nafion membrane constituting the salt bridge.

In order to determine the influence of the salt bridge "bypass" described in section 6.3.2, the ISFET in one of the wells was monitored without and with this bypass being present. The results are depicted in figure 6-8a. For the latter case, the signal from the ISFET located in the second well, which remained at constant pH, is depicted in figure 6-8b.

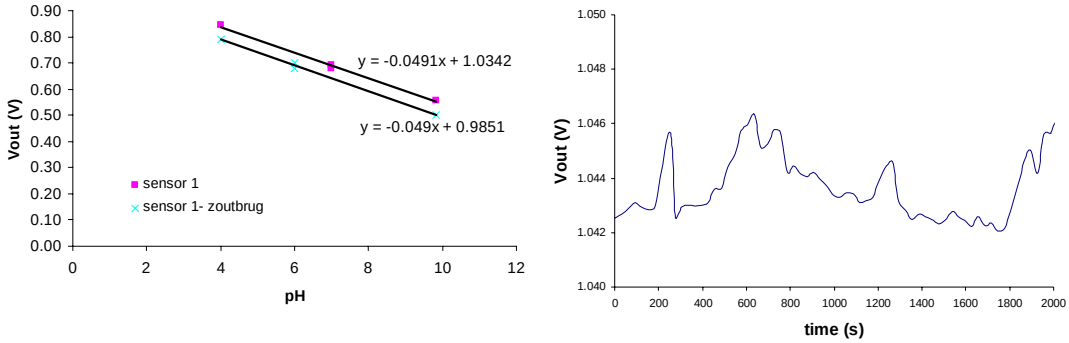

Figure 6-8: (a) ISFET calibration with and without salt bridge "bypass" (b) Interference between both ISFET signals

The measurement results in figure 6-8 show that the obtained ISFET sensitivity is not affected by the presence of the "bypass" and that the measurements performed in both microwells do not interfere with each other. It was therefore concluded that the impedance of this bypass was high enough to have no significant influence on the measurement results obtained with the measurement setup described previously.

6.4.2 Cell cultivation

The microfermentor array was constructed and used for on-line monitoring of cell cultivations, as described in section 6.3. The software controlling the sensor readout tended to stop responding when long-term communication with the potentiostat connected to the dissolved oxygen sensor was required. Therefore, oxygen concentrations were not monitored when the cell cultivation experiments were performed unattended.

In the following subsections, measurement results obtained during and after the batch growth of *Candida utilis* will be shown.

During the batch phase

Batch cultivations of *Candida utilis* cells were performed and monitored on-line in two micro bioreactors simultaneously. As shown in chapter 5, the end of the batch phase is characterized by stagnation of biomass growth, pH increase and increase in dissolved

oxygen concentration. It could therefore be determined that in all cell cultivations performed, the batch phase ended 6-8 hours after inoculation.

Solution resistance was determined from impedance measurements under the assumption that the conductivity between the platinum electrodes constituting the sensor could be modeled with a simple C(RC) circuit. The thus obtained solution resistances of buffer at zero concentration, and one obtained during a typical batch fermentation process are depicted below for a signal frequency ranging from 0.3 MHz - 2.3 MHz.

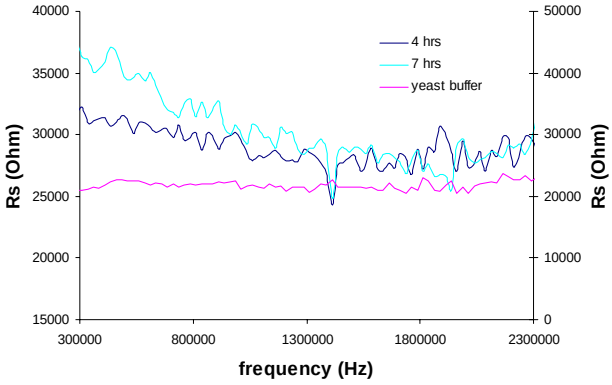

Figure 6-9: determined solution resistance versus signal frequency

The impedance curves show considerable random noise levels, resulting from a noisy environment and relatively complex wiring. However, it can clearly be observed that at zero concentration, a very constant resistance value is obtained in this frequency range. For higher cell concentrations (i.e. after 4 – 7 hrs of cultivation), the obtained resistance clearly increases at lower signal frequencies, whereas it remains stable at higher frequencies. Dispersion magnitude was therefore determined by comparing the resistance obtained at 10 spectral points around 0.3 MHz to 10 spectral points around 2 MHz.

The dispersion signals obtained during three duplo batch growth processes are plotted in figure 6-10. The figures show dRs/Rs as a function of time, with dRs being the difference between both solution resistance values and Rs being the solution resistance determined around 2 MHz. The individual reactors constituting the reactor arrays are addressed by supplements *a* and *b*, respectively.

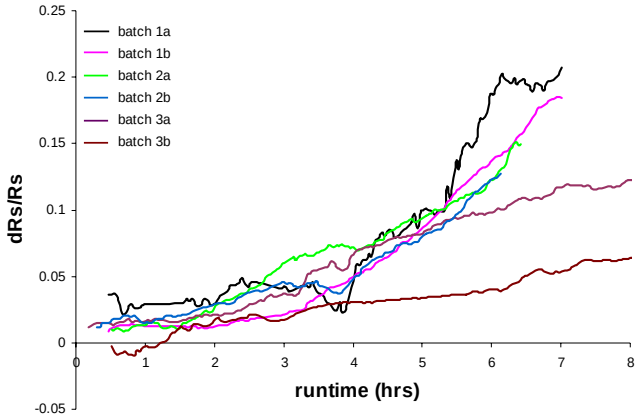

Figure 6-10: dispersion signal during batch phase

From this figure, it can be concluded that dispersion as obtained during the batch growth of *Candida utilis* increases exponentially with time, after a lag phase of approximately 2 hours. All signals obtained during batch 1 and batch 2 compare well. Only the duration of the batch phase and thereby the attained end values differ. Probably, the glucose concentrations were not equal for each growth process.

The signal obtained in batch 3a looks somewhat deformed. At the end of this batch, that took place unattended, it was observed that the magnetic stirrer bar had got stuck somewhere during the cultivation process and, resultingly, cell sedimentation had occurred. Since the sensor array is located at the bottom of the reactor, its surface got fouled and this presumably led to erroneous signals.

The signal measured in batch 3b increases very slowly. Moreover, the signal increase has not ended at the end of the experiment. It could be presumed that batch growth took place very slowly during this cultivation process. Since the salt bridge in the concerning micro reactor appeared to be malfunctioning, probably because of an air bubble in the tubing, no adequate measurement data was obtained from the ISFET or the dissolved oxygen sensor to verify this.

Solution pH was simultaneously monitored as shown in figure 6-11. This figure shows the moving average of 10 subsequent measurements in order to reduce the influence of random noise generated by the saltbridges, wiring, light interference or interfering electromagnetic fields in the environment. No stable pH measurements could be performed in batch 2a and 3b, since in both cases the salt bridge malfunctioned. This was probably due to an air bubble in the tubing.

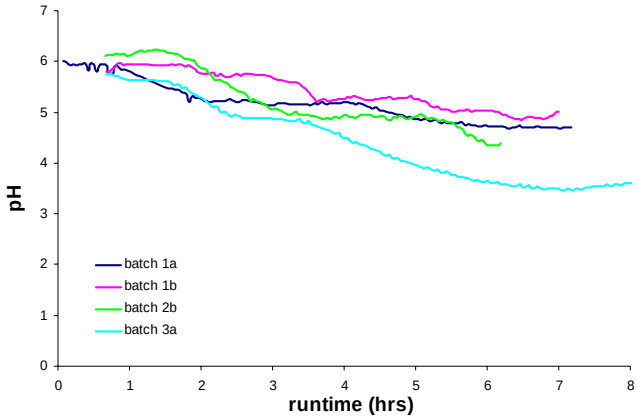

Figure 6-11: pH signal during batch phase

As can be observed from this figure, pH gradually decreases by about 1 pH unit during the batch phase. For batch 3a, the pH decrease is considerably higher, i.e. over 2 pH units. In this case, however, the stirrer bar got stuck and cell sedimentation occurred. This presumably led to divergent sensor signals.

Dissolved oxygen concentration was simultaneously monitored during batch 1a and 1b only because the other cell cultivations were performed unattended. As explained above, oxygen was not monitored during cultivations that were performed unattended because communication with the potentiostat connected to the dissolved oxygen sensors tended to cause the software controlling the sensor readout to stall. The dissolved oxygen concentrations as measured during batch 1a and batch 1b are depicted in figure 6-12.

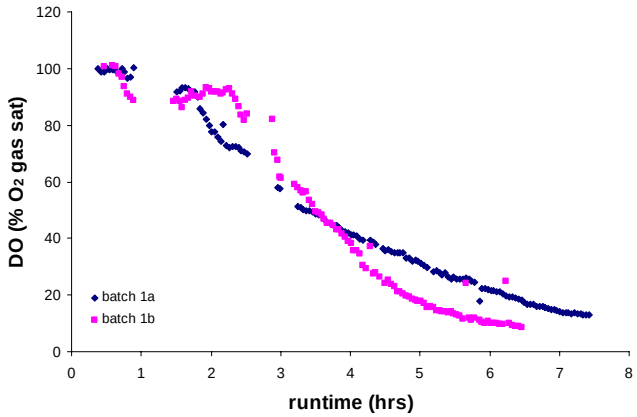

Figure 6-12: DO sensor signal during batch phase

The dissolved oxygen concentration clearly decreases to a close to zero value during the batch growth of *Candida utilis*. The shape of the curves is somewhat different from those

reported in chapter 5, where exponential decays were observed. The difference may be due to fouling; if the polyimide layer that defines the geometry of the ultra micro electrode array gets fouled, the effective electrode area decreases thereby leading to a reduced response. Fouling may be due to sedimentation or other effects such as proteins sticking to its surface. The measured signals do not reach zero value. This may be due to cross sensitivity of the electrochemical sensor to other species in the culture. It may also be, however, that oxygen limitation does not occur at all during the batch phase. This is confirmed by the fact that the signals still decay at the end of the batch phase.

At the end of the batch phase, the micro organisms are expected to change over to ethanol consumption thereby giving rise to a dissolved oxygen concentration peak. Although one of the "spikes" at the end of the signal acquired in batch 1b might result from this concentration peak, it could not clearly be distinguished. It may well be that this is due to the limited temporal resolution of the measurements.

The fourth parameter simultaneously monitored using the sensor array located inside the reactor chambers is temperature. The measurement results obtained during the cultivation processes are depicted in figure 6-13.

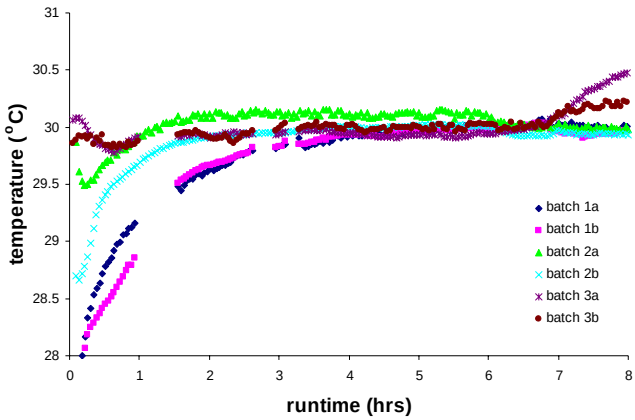

Figure 6-13: Temperature measurements during batch phase

The measurements indicate that the temperature was ~30 °C throughout the fermentation process. This corresponds to the setpoint of the thermostatically controlled cabinet. The obtained temperature measurements also indicate that it takes up to several hours before this temperature is reached. There is no measurable overshoot, however.

After the batch phase

The measurement results shown above indicate that the batch growth of *Candida utilis* could successfully be monitored in multiple wells using the developed system. The batch phase ends when all glucose present in the growth medium has been metabolized by the cells. As explained in section 6-1, the cell culture is expected to enter the stationary phase where biomass concentrations hardly change.

The dispersion signal that was monitored throughout the complete experiment is shown in figure 6-14.

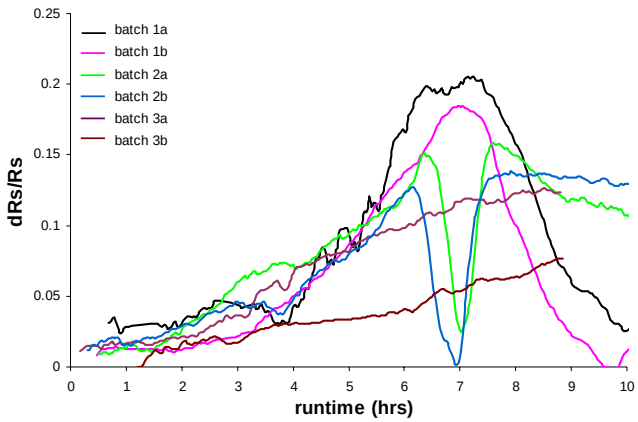

Figure 6-14: dispersion signal until the end of experiment

After the exponential growth phase has stopped, the dispersion signal as obtained in batch 1a and batch 1b is stable for only a short period of time and then rapidly decreases. This behavior was not observed in the 4L fermentations shown in chapter 5. As to further investigate the dispersion signals observed in the microreactors, the solution resistance values measured at both high and low frequencies during batch 1, are depicted in figure 6-15.

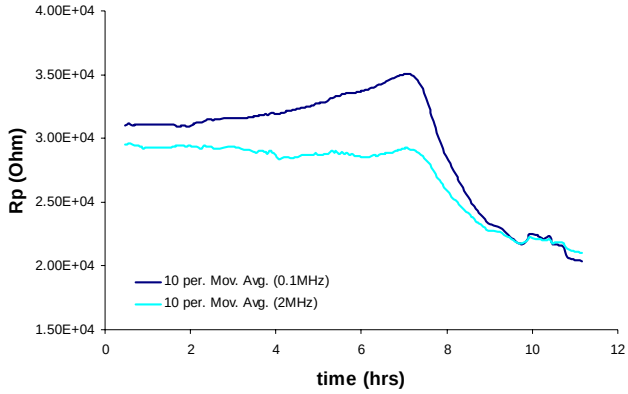

Figure 6-15: R_s as obtained at low and high frequencies

The signals as observed during the batch phase compare well to those obtained in the large scale fermentations discussed in chapter 5. After this batch phase however, the observed solution resistance rapidly decreases and so does the dispersion signal.

The dispersion signals obtained in batch 2a and batch 2b show even more curious behavior; dispersion rapidly decreases after batch growth has finished, and then rapidly returns. The dispersion curve obtained for batch 3a does not show a decrease. The curve looks somewhat deformed however, because cell sedimentation occurred during this batch. For batch 3b, it seems that the culture was still in the batch phase at the end of the experiment.

The pH signals monitored throughout the experiments are depicted in figure 6-16.

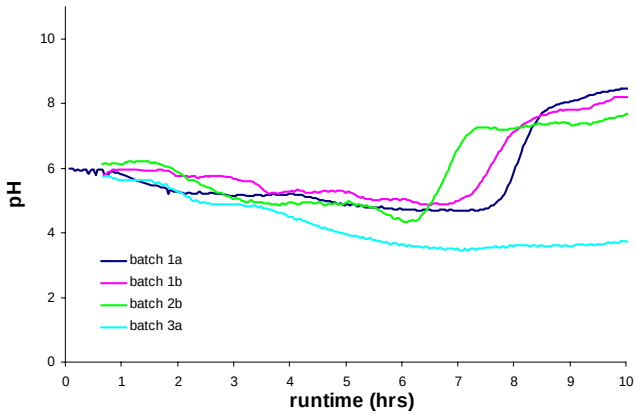

Figure 6-16: pH signal until the end of experiment

From this figure, it can be observed that pH considerably increases shortly after the exponential growth phase has finished. Similar behavior was observed during the large-scale fermentations shown in chapter 5 and can be ascribed to uptake of acidic compounds.

The dissolved oxygen measurements performed until the end of the experiments are depicted in figure 6-17.

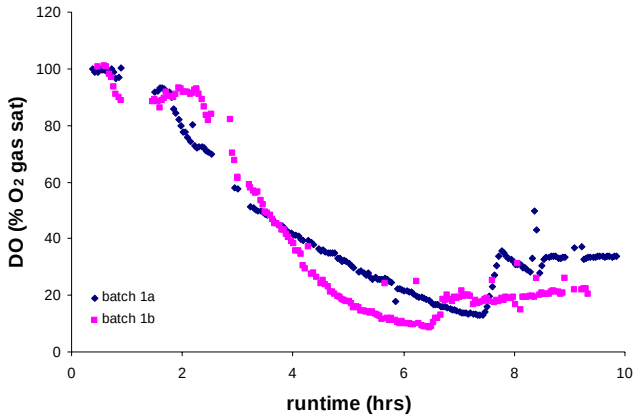

Figure 6-17: DO sensor measurements until the end of experiment

Based on the measurement results obtained in chapter 5, the measured signal is expected to return to close to the initial value after the batch phase has ended. Although the measurements do show an increase at the end of the batch phase, the increase is much smaller than expected.

6.5 Discussion & conclusions

From feasibility studies on the salt bridge comprising a Nafion hollow fiber membrane filled with medium, it can be concluded that the thus created electrical connection between the micro wells and the reservoir containing the reference electrode shows high stability in the pH range relevant to yeast fermentations.

Based on this salt bridge, a micro bioreactor array comprising two micro wells suitable for the batch fermentation and on-line monitoring of micro organisms was constructed and tested. The measurement results shown above indicate that viable biomass, dissolved oxygen, pH and temperature could successfully be monitored in multiple wells during the batch growth of *Candida utilis*. The oxygen measurements look somewhat deformed though; this may be due to fouling as explained above.

When the batch phase has ended, all substrate is metabolized and the culture is expected to enter the stationary phase, where growth slows down or completely stops. pH rapidly increases due to acid consumption which corresponds to the measurements shown above.

The increase in dissolved oxygen signals obtained after the batch growth of *Candida utilis* is smaller than expected from the experiments shown in chapter 5. This could indicate that the cells still show metabolic activity. Another explanation for the lower-than-expected signals acquired from the dissolved oxygen sensors, is that the electrode area is reduced. This can be due to either fouling or physical degradation of the electrodes. Physical degradation of the electrodes could not be observed by microscopic inspection. The electrodes did look dirty, though. Sensor response did not return to the calibrated value at oxygen gas saturation after rinsing it with ethanol. After rinsing with acetone, however, the response did return to the calibrated value. This confirms that fouling caused the observed response of the sensor.

The same fouling effect might also explain why the dispersion signals obtained during batch 1 and batch 2 rapidly decrease after the batch phase has ended: if the sensor gets fouled, the electrical field between the electrodes might get deformed and consequently does not penetrate the cell-containing solution. Signal recovery obtained in batch 2, could be due to re-suspension of sedimentated species. Another explanation for the observed behavior of the biomass sensor is that the cells die shortly after the batch phase has ended. However, this effect can not explain why the signal decreases obtained during batch 2 largely recover. Since the results in figure 6-15 indicate that the solution resistance changes dramatically after the batch phase has finished, it may also be that the impedance model used is not accurate anymore in the frequency range studied. This hypothesis could however not unambiguously be sustained by testing with other impedance models or by looking at other frequencies.

The above reasoning suggests the odd behavior observed for both sensors is caused by the same fouling effect. The dissolved oxygen sensor seems more sensitive to this fouling effect as its response seems to be influenced by fouling not only after, but also during the batch phase. A possible explanation is that the polyimide layer defining the geometry of the oxygen sensor is very rough and therefore very sensitive to fouling effects.

The fouling effect described above might have a biological cause. As explained in section 6-1, the composition of the cells might change significantly when the culture enters the stationary phase. Cells become less robust and a significant part of the cells might die.

Similar effects did not (or less pronounced) take place in the large scale fermentations shown in chapter 5. This may be due to the positioning of the sensors; the sensors were placed in upright position in the lab-scale fermentor. In case of the microreactor experiments, however, the sensors were located on the bottom of the reactor and therefore more sensitive to sedimentation. Moreover, the microreactors suffer from worse mixing conditions compared to the lab-scale fermentors. Sedimentation is therefore more likely to occur. As mixing and oxygen transfer capabilities of the microreactors are worse compared to the large scale fermentors, presumably a larger fraction of the cells dies after the batch phase has ended. In that case, membrane parts and cell contents such as proteins might become subject to sedimentation or sticking thereby explaining the observed sensor response.

The reasoning above indicates that the developed microreactor system can be further improved by improving mixing. Adequate mixing should prevent the occurrence of sedimentation. It should be further investigated whether excessive cell death takes place when the culture enters the stationary phase and if so, the origin of this effect should be found and solved. Electrochemical cleaning steps might help in further reducing fouling effects.

References

Bacabac RG, Smit TH, Mullender MG, Van Loon JJWA, Klein-Nulend J. 2005. Initial stress-kick is required for fluid shear stress-induced rate dependent activation of bone cells. Annals of Biomedical Engineering 33(1):104-110.

Bakker E, Qin Y. 2006. Electrochemical sensors. Analytical Chemistry 78(12):3965-3983.

Bard AJ, Faulkner LR. 2001. Electrochemical Methods, Fundamentals and Applications: John Wiley & Sons, Inc.

Chen AK, Latz MI, Frangos JA. 2003. The use of dinoflagellate bioluminescence to characterize cell stimulation in bioreactors. Biotechnology and Bioengineering 83(1):93-103.

Crueger W, Crueger A. 1990. Biotechnology: a textbook of industrial microbiology. Haessly C, translator. Brock TD, editor. Sunderland: Sinauer Associates, Inc. 64-73 p.

Duetz WA, Witholt B. 2001. Effectiveness of orbital shaking for the aeration of suspended bacterial cultures in square-deepwell microtiter plates. Biochemical Engineering Journal 7(2):113-115.

Gavrilescu M, Chisti Y. 2005. Biotechnology - a sustainable alternative for chemical industry. Biotechnology Advances 23(7-8):471-499.

Koryta J, Dvořák J. 1987. Principles of Electrochemistry. Chichester: John Wiley & Sons Ltd. 125-126 p.

Kostov Y, Harms P, Randers-Eichhorn L, Rao G. 2001. Low-cost microbioreactor for high-throughput bioprocessing. Biotechnology and Bioengineering 72(3):346-352.

Kumar S, Wittmann C, Heinzle E. 2004. Minibioreactors. Biotechnology Letters 26(1):1-10.

Lee HLT, Boccazzi P, Ram RJ, Sinskey AJ. 2006. Microbioreactor arrays with integrated mixers and fluid injectors for high-throughput experimentation with pH and dissolved oxygen control. Lab on a Chip 6(9):1229-1235.

Lye GJ, Ayazi-Shamlou P, Baganz F, Dalby PA, Woodley JM. 2003. Accelerated design of bioconversion processes using automated microscale processing techniques. Trends in Biotechnology 21(1):29-37.

Micheletti M, Barrett T, Doig SD, Baganz F, Levy MS, Woodley JM, Lye GJ. 2006. Fluid mixing in shaken bioreactors: Implications for scale-up predictions from microlitre-scale microbial and mammalian cell cultures. Chemical Engineering Science 61(9):2939-2949.

Nealon AJ, O'Kennedy RD, Titchener-Hooker NJ, Lye GJ. 2006. Quantification and prediction of jet macro-mixing times in static microwell plates. Chemical Engineering Science 61(15):4860-4870.

Polk BJ, Stelzenmuller A, Mijares G, MacCrehan W, Gaitan M. 2006. Ag/AgCl microelectrodes with improved stability for microfluidics. Sensors and Actuators B-Chemical 114(1):239-247.

Sawyer DT, Sobkowiak A, Roberts J, J. L. 1995. Electrochemistry for Chemists. New York: John Wiley & Sons, Inc.

Shuler ML, Kargi F. 2002. Bioprocess engineering - basic concepts. Guerrierri P, editor. Upper Saddle River: Prentice Hall PTR. 156-175 p.

Verduyn C, Postma E, Scheffers WA, Van Dijken JP. 1992. Effect of Benzoic-Acid on Metabolic Fluxes in Yeasts - a Continuous-Culture Study on the Regulation of Respiration and Alcoholic Fermentation. Yeast 8(7):501-517.

Weiss S, John GT, Klimant I, Heinzle E. 2002. Modeling of mixing in 96-well microplates observed with fluorescence indicators. Biotechnology Progress 18(4):821-830.

Weuster-Botz D, Puskeiler R, Kusterer A, Kaufmann K, John GT, Arnold M. 2005. Methods and milliliter scale devices for high-throughput bioprocess design. Bioprocess and Biosystems Engineering 28(2):109-119.

Chapter 7: Microfluidics for pH control and fed-batch functionality

This chapter shows the development of microfluidics for pH control and fed-batch functionality. A brief overview of microvalve fabrication and actuation techniques reported in literature is given. Then, a new technique for fabrication of PDMS microvalves with a semicircular cross section is presented. The fabricated microvalves are characterized using three different actuation techniques, i.e. by means of electromagnetic actuation, Braille display actuation and pneumatic actuation. The results are shown and discussed at the end of the chapter.

7.1 Introduction

Demands for consistent high yeast quality and yield require an accurate control of commercial fermentations. Critical process parameters such as temperature, aeration and pH are usually under closed-loop control. Feed rates frequently are controlled according to preset schedules (Verachtert and de Mot 1990). For both closed loop pH control and open loop feed control, pumps and fluidic connections to the fermentors are required. In order to achieve a good resemblance with industrial scale fermentations, it thus is desirable to expand the microreactor platform under development with fluidics enabling pH control and fed-batch functionality.

In case of variable volume fed-batch fermentations, where the total culture volume increases due to feeding with a substrate solution, the volume increase may be a multiple of the initial culture volume (Posten 1993). To reduce the volume increase, it is common that the substrate concentration is as high as practically possible (Envors 2006).

Since the pump rates required to control pH are usually much lower, feeding is determinative for the maximum pump rate required. The feeding substrate is utilized for both cell growth and maintenance. Cellular maintenance is represented by a maintenance coefficient, describing the feed uptake required to repair damaged cellular components, to transfer nutrients and products in and out of cells, for motility and to adjust the osmolarity of the cell's interior volume (Shuler and Kargi 2002). Under the assumptions of a constant cell yield on substrate $Y_{X/S}$ and a constant maintenance coefficient m throughout the fermentation, the nutrient feeding rate $F_m(t)$ can be determined by (Lee et al. 1999):

$$F_m(t) = \left(\frac{\mu}{Y_{X/S}} + m \right) M_X(0) e^{\mu t} \qquad (7\text{-}1)$$

Here, μ is the specific growth rate and $M_X(0)$ is the total amount of biomass at the moment feeding is started. It is assumed that $\mu \approx 0.2\ hr^{-1}$, $Y_{X/S} \approx 0.55\ g/g$ (Ejiofor et al. 1994a), $m \approx 0.02\ g/g \cdot hr$ (Ejiofor et al. 1994b) and that the targeted biomass concentration at the end of the fermentation process is ~100 g/l. If the feed solution has a glucose concentration of 100 g/l (the solubility of glucose equals 479.2 g/l in water at 20 °C (Yalkowsky and He 2003)), it can be estimated that a flow rate of a few hundreds of $\mu l/hr$ is required to control a fed-batch fermentation in a single 200 μl volume. The feed solution can be added continuously or in pulsed mode, which would require considerably

higher momentary feed rates. Therefore, it seems reasonable to assume the maximum flow rates required to control the microreactors under study is a few ml/hr.

To achieve such feed rates for micro bioreactors, several groups applied external pumps like osmotic pumps (Gmunder et al. 1988), piezo-electric silicon membrane pumps (Walther et al. 2000), conventional peristaltic pumps (Gu et al. 1999) or syringe pumps (Zhang et al. 2006). Balagaddé et al. (Balagaddé et al. 2005) developed a microchemostat reactor consisting of integrated poly(dimethylsiloxane) (PDMS) peristaltic pumps and valves.

Since there is a strong demand for micro bioreactor arrays that allow many parallel experiments to be performed on cells or organisms under identical conditions (Weibel and Whitesides 2006), our work focuses on strategies to develop an integrated microfluidic platform that can be used to feed large arrays of micro bioreactors. It is required that this platform allows for accurate and robust fluid control and that it can be fabricated and actuated at low cost.

As microvalves are less complex to fabricate and actuate than micropumps, it is preferred to use a configuration as depicted in figure 7-1 for feeding and controlling pH in the microreactor array under development.

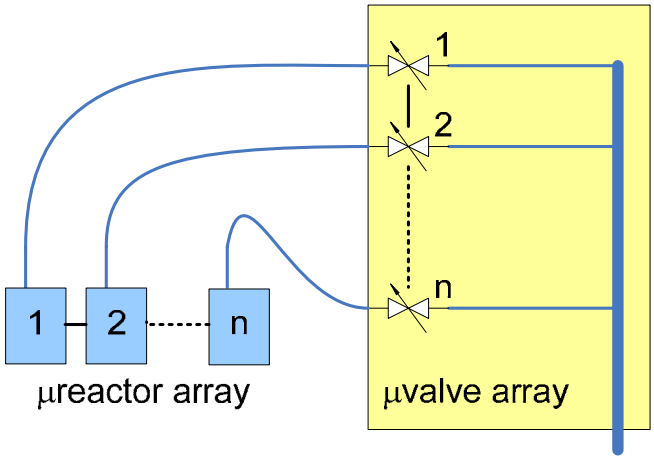

Figure 7-1: Proposed configuration for feeding an array of n microreactors

Here, the feed solution is contained in a single reservoir and pumped in a microchannel with a single macroscale pump. The microfluidic platform required to regulate the fluid flows to an array of n microreactors individually now consists of n microvalves only. Although full integration of such a microvalve array in the microreactor array could be considered, this research focuses on the development of a separate microfluidic module. This subdivision allows for independent fabrication and testing of the separate modules.

This chapter discusses the feasibility of such a microfluidic platform. A new method for fabrication of PDMS microvalves containing a flow channel with semicircular cross section is presented and a comparison between different means for actuation of these microvalves is shown.

In section 7.2, current fabrication and actuation principles for microvalve arrays are described. Section 7.3 shows the actual design, fabrication and actuation methods explored for the microvalves that were developed in this study. Measurement results are shown in section 7.4 and are followed by discussions in section 7.5.

7.2 Theory

The research on lab-on-a-chip systems has increased dramatically over the past two decades (van den Berg and Bergveld 2006). As a consequence, there has been a growing interest in the development of active microvalves. The many different types of active microvalves that have been developed so far can be categorized on their actuation principle (Oh and Ahn 2006).

In mechanical microvalves, usually a mechanically movable membrane is coupled to for instance a magnetic (Terry et al. 1979), electrostatic (Sato and Shikida 1994; Shikida et al. 1994), electrokinetic (Kirby et al. 2002), electromagnetic (Bohm et al. 2000), piezoelectric (van Lintel et al. 1988) or thermal (Jerman 1994) microactuator (Shoji and Esashi 1994). Non-mechanical active microvalves may hold membranes, but these membranes are actuated by the use of smart materials such as deformable hydrogels (Beebe et al. 2000) or phase change materials which are influenced by means of, for instance, electrically controlled microheaters (Carlen and Mastrangelo 2002; Lee and Lucyszyn 2007) or optically illuminated nanoheaters (Park et al. 2007). A third group is formed by externally actuated microvalves. These microvalves may hold membranes, but actuation is achieved by the aid of external systems, such as pneumatic means (Ohori et al. 1998).

For the fabrication of microfluidic devices, rapid prototyping using “soft lithography”, a term generally denoting a set of polymer-based micromolding and micropattern-transfer techniques, has gained much popularity over the past few years (Whitesides et al. 2001). Soft lithography’s advantages include the capacity for rapid prototyping, easy fabrication without expensive capital equipment, and forgiving process parameters (Unger et al. 2000). Multiple layers of polymer substrate can easily be bonded

after oxidizing their surfaces with oxygen plasma (Duffy et al. 1998), which enables easy, rapid fabrication of very complex microfluidic networks consisting of thousands of microvalves (Thorsen et al. 2002).

Due to these advantages, PDMS microvalves fabricated using soft lithography form an attractive candidate for the system under study. This study therefore focuses on this type of microvalves. In section 7.2.1, various methods for fabrication of PDMS microvalves will be discussed. Section 7.2.2 discusses operation principles for actuation of PDMS microvalves.

7.2.1 Microvalve fabrication

Although the structure and configuration of actual prototypes may vary, a PDMS microvalve basically consists of a microchannel which is enclosed by a deformable membrane. Deformation of the membrane by some actuation means will partially or completely close the microchannel, thereby tuning the rate at which liquid flows through the microchannel. Valve performance depends strongly on the cross sectional shape of the microchannel; it was shown that valve closure is much more easily achieved for a microchannel with a semicircular or bell-shaped cross section, than for microchannels with rectangular or trapezoidal cross sections (Unger et al. 2000).

In order to achieve this, Unger et al. molded PDMS channels from a master containing inverse microchannel structures. The inverse structures were fabricated by patterning photoresist on top of a silicon wafer. The molds were baked at 200 °C after development of the photoresist, as to make the photoresist reflow thereby rounding the structure of the inverse channels. This fabrication method is very simple, but the resulting channel shape is quite poorly defined and usually not really semicircular or bell-shaped.

In order to improve the resulting channel shape, Futai et al. fabricated the inverse microchannel structures on top of a glass wafer using a technique they call “backside diffused-light photolithography” (Futai et al. 2004; Gu et al. 2004; Song et al. 2005). In this method, a layer of SU-8 is spun on a glass wafer. The SU-8 layer is exposed from the backside of the glass substrate through a photomask by the diffuse light produced by an UV transilluminator. The spatial intensity distribution of the diffracted light then leads to a bell-shaped channel. The exact shape can be tuned by adjusting the exposure time and the photomask aperture.

Other methods to create a photoresist layer with variable height on a flat substrate is by using grayscale masks (Waits et al. 2003; Waits et al. 2005; Yuan et al. 2001) or molding of bulged UV-curable glue (Go and Shoji 2004).

7.2.2 Microvalve actuation

Many different ways for actuation of microvalves comprising a PDMS membrane have been reported in literature.

In pneumatically actuated microvalves (Unger et al. 2000), two crossing channels are separated by the membrane. The membrane deflects in response to the pressure applied to a control channel, thereby altering the fluid flow in a flow channel. A schematic representation of the microvalves developed by this group is depicted in figure 7-2.

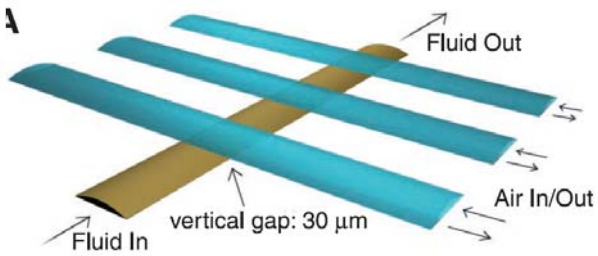

Figure 7-2: Schematic representation of pneumatically actuated PDMS microvalve

In case of thermopneumatic actuation (Knight and House 2004; Yang et al. 1998), this pressure is applied by on-chip heaters instead of an external pressure source. In electro-rheological-fluid-based valves (Niu et al. 2005), the control channel is filled with electro-rheological fluid which shows solid-like behavior under application of an electric field.

Large arrays of pneumatically actuated PDMS microvalves have been reported in literature (Balagadde et al. 2005; Thorsen et al. 2002; Urbanski et al. 2006). This actuation method requires a pneumatic valving system and numerous leakproof interconnections allowing for the individual pressures of the control channels. The number of control channels, however, can be reduced by varying the width of the control channel as to implement a binary tree (Thorsen et al. 2002).

A completely different approach for PDMS microvalve actuation is by the use of externally actuated pins which can deform the membrane, thereby altering the fluid flow. In previous studies, this was done with the aid of commercially available Braille displays actuator

components holding pins which are individually driven piezoelectrically (Gu et al. 2004; Song et al. 2005).

Since commercially available Braille display actuators hold up to 1600 individually addressable pins, this actuation method is a very attractive low-cost alternative for actuation of microvalve arrays.

There are some limitations in the use of Braille displays, however. The pins are usually placed in a grid, thereby limiting device density and the flexibility in organization of the placement of pumps and valves. Moreover, this actuation method lacks multiplexing capability. Each pin actuates only a single valve while for pneumatically actuated systems, each actuator can control multiple valves by application of binary trees (Thorsen et al. 2002).

As to benefit from the advantages of both actuation strategies described above, it has been proposed to combine the two methods (Gu et al. 2007). In this case, the PDMS microvalves are designed as hydraulic valves that are analogous to the pneumatic microvalves described above, but the control lines are pressurized mechanically by movable Braille pins rather than by externally delivered and gated high pressure gas. This configuration requires fewer leak free connections and no compressed air source is needed.

7.3 Experimental

7.3.1 Microvalve fabrication

For convenient valve functionality, the microchannels comprising the microvalves should have a semicircular to bell-shaped cross section. Smoothening the inverse channel structures by post-development baking of the mold is an easy method to effectuate this. However, this method does not allow for accurate control of the resulting channel shape and results in smoothened rectangular channels instead of channels with a semicircular cross section. Other methods to control the geometrical shape of the microchannels require expensive grayscale masks or special equipment such as a UV transilluminator. Therefore, a new fabrication method to fabricate microchannels with a semicircular cross section using standard clean room equipment was investigated. The process flow is schematically depicted in figure 7-3.

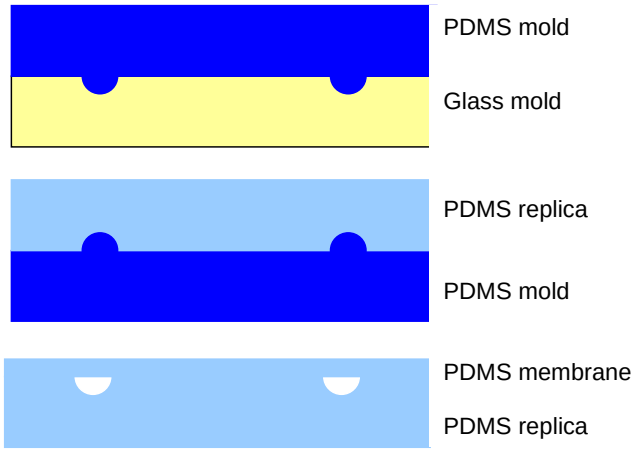

Figure 7-3: PDMS microvalve fabrication

First, microchannels with 20 µm depth and a maximum width ranging from 42 µm to 100 µm are isotropically etched in glass. This is done by first sputtering Cr/Au on the glass wafer. The metallic layers are structured using photolithography and chemical wet etching. Hydrophobic fluor carbon coating is deposited as to prevent PDMS from sticking to the glass surface. A brim is formed by sticking tape to the side of the wafer. Then, the prepolymer solution is made in a 1:10 curing agent-to-base ratio (Sylgard 184, Dow Corning). The prepolymer solution is stirred for 10 minutes using a stirring plate, degassed and cast onto the glass mold. The prepolymer solution is degassed again before it is cured at 100 °C for 2 hours.

The PDMS slab created contains the inverse channel features and can be used as a mold for fabrication of PDMS microchannels. Therefore, the PDMS mold was dipped in a hydrophobic coating solution (EGC 1700, 3M Corporation) and a brim was formed using adhesive tape. Prepolymer solution was prepared, cast and cured similar to how the PDMS mold was fabricated. A photograph of the cross section of a microchannel fabricated this way is depicted in figure 7-4.

Figure 7-4: Cross section of PDMS microchannel

Channel depth was estimated to equal 22 µm and maximum width was found to equal 56 µm, whereas values of 20 µm and 42 µm were expected, respectively, based on the design of the microchannels. Deviations may be due to the coatings used, softened edges and due to PDMS shrinkage resulting from gel-to-solid transition (Orhan et al. 2006). As to enable microfluidic connections to the created microvalves, holes are pinched at the beginning and at the end of each microchannel.

A PDMS membrane was formed by first spin-coating a silicon dummy wafer with hydrophobic coating (EGC 1700, 3M Corporation). A prepolymer solution was prepared according to the protocol described above and spin-coated on the dummy wafer for 20 seconds at 2000 rpm. A relation between the spin speed and the resulting membrane thickness can be obtained from previous studies (Herber 2005). From these studies, the membrane thickness under the conditions mentioned is expected to equal 25 µm.

The surfaces of the PDMS substrate containing the microchannels and the membrane which is still on the dummy wafer are then treated with oxygen plasma for 4 minutes and pressed together as to form an irreversible bond. The PDMS can now be peeled off of the dummy wafer and the separate microvalves can be cut out using a knife. Silicone tubing is shifted into the inlet holes as to enable fluidic connectivity to the outside world. The connection is made leakproof by sealing the joints with one component silicone sealant (Dow Corning).

A photograph of the PDMS microvalves fabricated in this manner is depicted in figure 7-5.

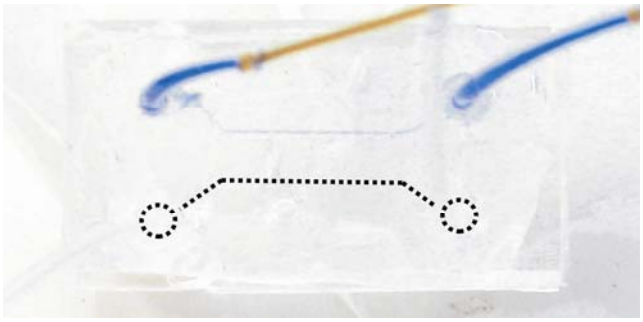

Figure 7-5: Microfluidic device containing 2 PDMS microvalves. The upper microchannel is filled with ink and the in- and outlets are connected using fused silica capillaries. The dotted line indicates the position of the second microchannel.

The picture shows a microfluidic device containing two PDMS microvalves from the backside. The upper channel is connected to reservoir using fused silica capillaries, as to fill the channel with blue ink. Dotted lines mark the location of the second, empty fluidic channel.

7.3.2 Microvalve actuation

Three methods were investigated for actuation of the fabricated microvalves. Initially, microvalves were controlled using an electromagnetically actuated pin readily available from stock. As a more practical approach towards the actuation of an entire array of microvalves is by using a commercial Braille display or pneumatic actuation, these methods were investigated subsequently.

Electromagnetic pin actuation

Actuation by means of an electromagnetically controlled pin readily available from stock was investigated. This method of actuation allows a study of the feasibility of pressing a membrane mechanically by means of a pin similar to the Braille displays, and will also give information about the elastic properties of the PDMS material. A photograph of the available electromagnetic actuator is depicted in figure 7-6.

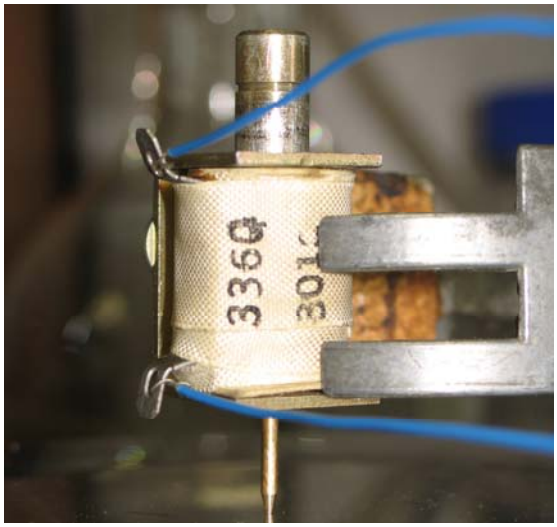

Figure 7-6: Electromagnetic actuator

The actuator consists of an electromagnetic coil which has a pin with a rounded tip attached to the freely movable core. The device is controlled using a DC power supply (E030-1, Delta Elektronika) for voltages ranging from 0-15V. The applied voltage is simultaneously monitored using a digital multimeter (34401A, Hewlett Packard). The mechanical forces generated by means of this actuator are characterized by fixing the pin directly above a weight balance (PJ3600 Datarange, Mettler) using a lab holder.

The generated force was characterized as a function of the applied potential as well as of the part of the core extending into the coil. From these measurements, the setpoint needed to mimic actuation by means of commercially available Braille displays can be determined. Microvalves are actuated around this setpoint by positioning the tip of the actuator straight above the microfluidic channel.

Braille display actuation

As to investigate the feasibility of valve actuation by means of commercially available Braille displays, several Braille display units consisting of 8 piezo-electrically actuated pins were acquired (Modul B11, Metec). The maximum force that can be delivered by these pins is specified to be 17 cN. A photograph of such a module is depicted in figure 7-7.

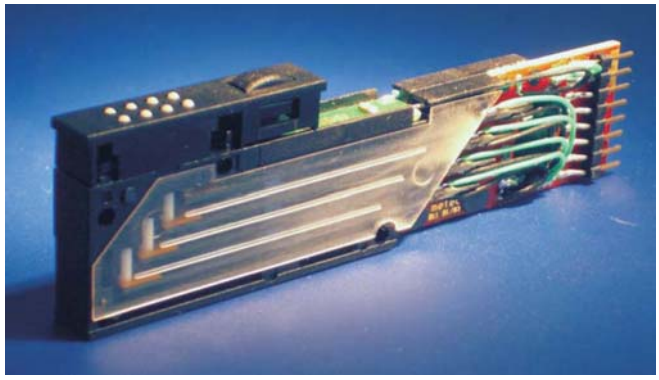

Figure 7-7: Braille display unit with 8 piezo-electrically activated pins

Customized Labview (National instruments) software was written to individually address and control the pins. The required signals were delivered to the modules using a data acquisition device (USB 6009, National Instruments). Power required to drive the piezoelectric elements was delivered by means of a high voltage power supply (6515A, Hewlett Packard) and simultaneously monitored using a digital multimeter (34401A, Hewlett Packard).

The force generated by the pins was characterized as a function of the applied potential by fixing the module in upside-down position above a weight balance (PJ3600 Datarange, Mettler). Microvalves were actuated by alignment of the microfluidic channel with one of the tips of the module.

Pneumatic actuation

For pneumatically actuated microvalves, another PDMS slab is fabricated on a dummy wafer spin-coated with hydrophobic coating (EGC 1700, 3M Corporation). Holes are pinched in as to enable connection to an external pressurized air gating system. The substrate is bonded to fabricated microvalves, in the course of which the holes pinched in the top substrate are aligned with the microchannels. Silicon tubing is shifted into the holes of this top substrate. As to ensure a leakfree connection, joints are sealed with one component silicon sealant (Dow Corning). The control pressure inlets can be connected to an external pressurized air gating system as to control the pressure applied to the membrane of the microvalve. A photograph of a microfluidic device fabricated in this way is depicted in figure 7-8.

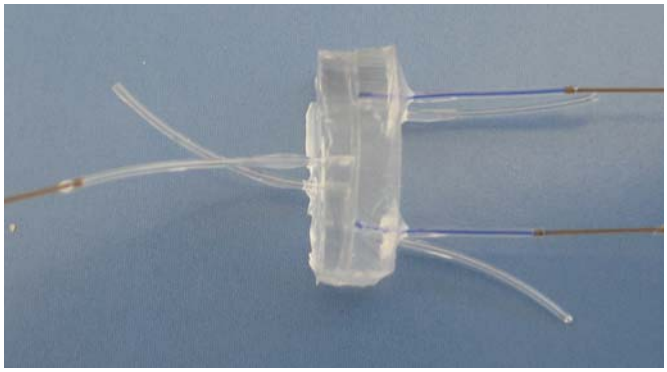

Figure 7-8: Microfluidic device containing 2 pneumatic microvalves

On the right side, connections of the microfluidic channels are visible. One of the channels is connected using fused silica capillaries and filled with blue ink. On the left side, the control pressure inlets can be observed. These inlets can be connected to a pneumatic control valve (Sempress) which is used to reduce the pneumatic pressure of compressed air.

7.3.3 Microvalve characterization

Although valve characterization based on measuring the conductance of an electrolyte solution through the microvalve section has been reported (Galas et al. 2005), the most common method for valve characterization is by studying the relation between the pressure drop across the valve and the flowrate (Oosterbroek et al. 1999). In this study, this was done using the measurement setup which is schematically depicted in figure 7-9.

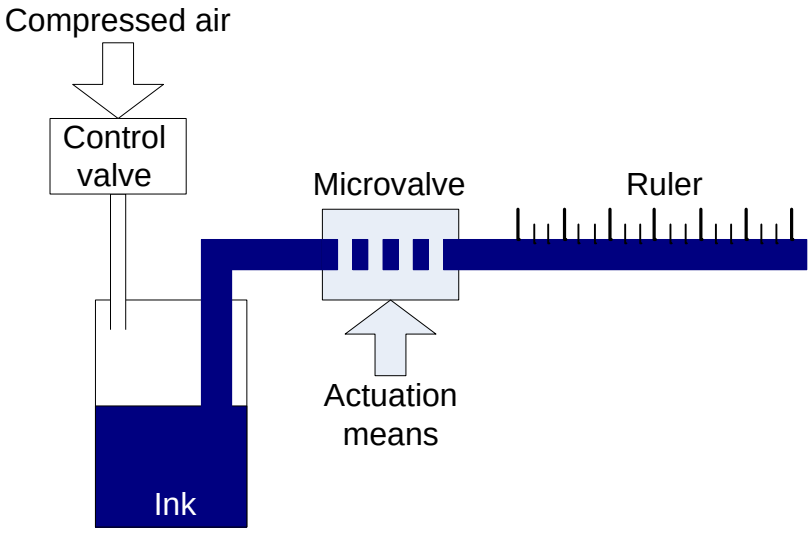

Figure 7-9: Microvalve characterization setup

The pressure of compressed air is reduced by means of a pneumatic control valve (Sempress). The set overpressure is applied to the solution entering the microvalve. Transparent tubing is connected to the outlet and placed along a ruler.

The pressure drop across the microvalve equals the set overpressure at the inlet, under the assumption that the pressure drop across the fluidic connections is negligible. The rate at which water flows through the microvalve can be determined by measuring the displacement of the liquid front in the transparent tube connected to the outlet of the microvalve after a set period of time. In order to make the liquid front clearly visible, some ink was added to the water flowing through the microvalve.

The relation between the measured velocity of the water front and the flow rate is determined by the inner diameter of the tubing connected to the outlet of the microvalve. A fixed error of ~0.5 mm is expected in the determination of dye movement. Therefore, measurement accuracy increases with increasing time interval or decreasing tube diameter. Tubing used in this study had an internal diameter of 0.85 mm. This suggests a measured velocity of 1 cm/min corresponds to a flow rate of 3.84 µl/min.

The setup described above is used to characterize the developed microvalves at different rates of actuation for each actuation method, i.e. electromagnetic-, Braille display- and pneumatic actuation. Hysteresis measurements, where the rate of actuation is varied along a triangular curve, and on-off measurements, where the rate of actuation is repeatedly varied between its minimum and maximum values, will be used to determine whether the membrane undergoes temporary or permanent deformation.

7.4 Measurement results

This section shows the measurement results obtained from the setup and protocols described above. The following subsections describe the results as obtained for electromagnetic actuation, Braille display actuation and pneumatic actuation subsequently.

7.4.1 Electromagnetic actuation

As described above, the electromagnetic actuator was positioned above a balance with a defined part of the core extending into the coil. A DC voltage signal was applied and the

resulting force was measured by the balance by using the relation $1\,kg = 9.8\,N$. The results are depicted in figure 7-10a and b.

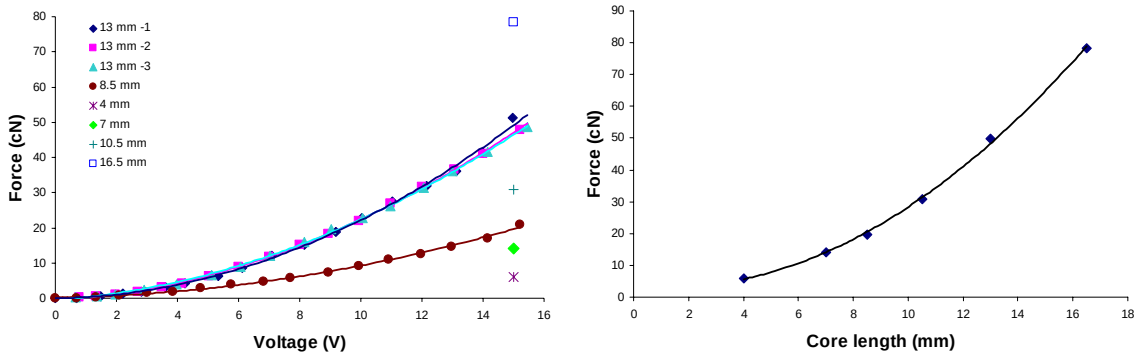

Figure 7-10: Generated force as a function of (a) applied voltage and (b) core length

As can be seen from figure 7-10a, the generated electromagnetic force increases with increasing voltage applied to the coil. The increase is more than linear which is probably due to the fact that for increasing force, the surface of the weight balance is slightly pressed downwards thereby increasing the part of the core that extends into the coil. This is confirmed by figure 7-10b, which shows that the force generated at constant potential increases with an increase of the part of the core extending into the coil.

From the results in figure 7-10a and b, it can thus be concluded that using this actuator, the generated force can be accurately controlled in a range defined by the core length. As to mimic the situation where the microvalves are actuated by Braille displays which generate a force of at most 17 cN, the microvalves are first actuated electromagnetically with the core length of the actuator adjusted to 13 mm and the applied voltage is varied in a range of 0-5 V. The pin of the actuator is aligned above the 80 µm-wide fluidic channel and flow-pressure characteristics are measured as a function of the voltage applied to and thus the force generated by the coil. The results are depicted in figure 7-11.

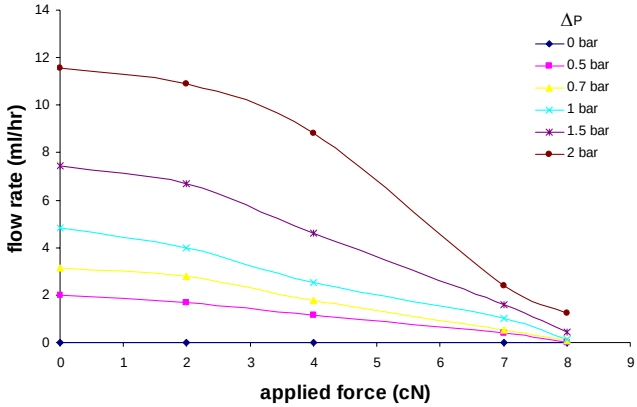

Figure 7-11: Flow-pressure characteristics obtained with electromagnetic actuator

From figure 7-11, it can be observed that valve closure is easily obtained for an applied voltage of 5V, as long as the inlet pressure is kept below 1 bar. The results are very difficult to reproduce, however, since they strongly depend on accurate alignment between the actuator and the microfluidic channel.

7.4.2 Braille display actuation

Measurements performed with the electromagnetic actuator indicated that the forces that can be generated with a Braille display, according to its specifications, are high enough to suitably regulate the flow resistance in the fabricated microfluidic devices. As to verify this, the force generated by a single pin from such a module was measured as a function of the applied voltage. The result is depicted in figure 7-12.

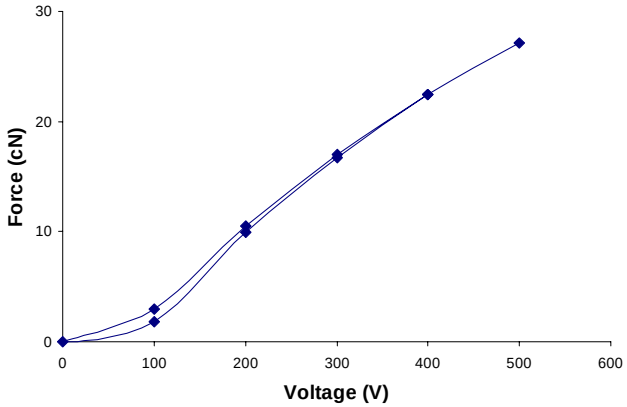

Figure 7-12: Force generated using a Braille display versus applied voltage

It can be seen that the forces generated using the module are in the same range as those generated by means of the electromagnetic actuator. Hysteresis, presumably caused by the hysteretic nature of the electro-mechanical behavior of piezo-electric materials (Mayergoyz and Bertotti 2005), is low. The force generated at a voltage of 200 V is slightly above 10 cN, which is somewhat lower than the specified value of 17 cN. Higher voltages may cause damage to the piezo bimorphs, according to its specifications. In practice, however, no problems were observed for voltage signals up to 500 V.

Braille display actuated microvalve characterization was performed by fixing a Braille pin straight above the microfluidic channels. The measurement results as obtained for a 42 µm-wide microchannel are depicted in figure 7-13.

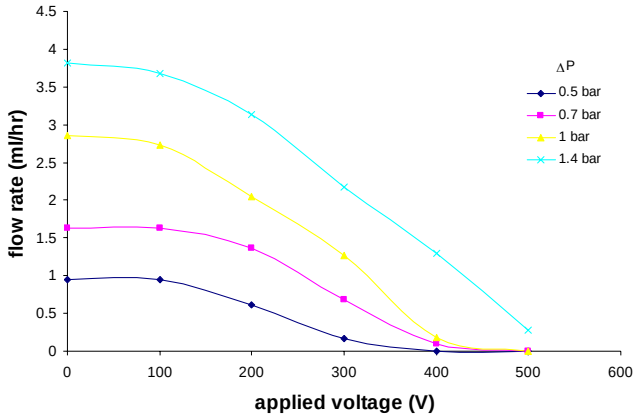

Figure 7-13: Flow-pressure characteristics obtained with Braille display actuation

As could be expected, the flowrate decreases with decreasing inlet channel pressure and increasing voltage applied to the actuator. The valve is completely closed for an applied voltage of 500 V and an inlet pressure below 1 bar. Compared to the tests with the electromagnetic actuator, the measured flow rates are considerably lower, which is due to the fact that the microchannel is smaller. Moreover, the required actuation force appears to be slightly higher. This is expected to be due the differences in channel dimensions, tip shape and alignment.

In order to study hysteresis, the voltage applied to the bimorphs was first gradually increased and then gradually decreased and the resulting flow rate was measured. The measurement results obtained for 42 and 80 µm-wide microchannels are depicted in figure 7-14a and 7-14b, respectively.

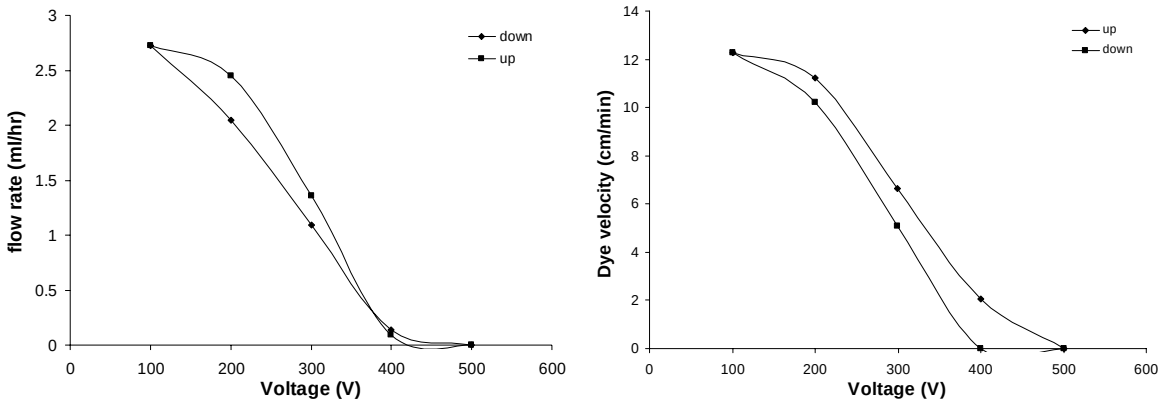

Figure 7-14: hysteresis measurements for (a) 42 and (b) 80 µm-wide microvalves

These measurements indicate that microvalves consisting of small microchannels show less hysteresis in the lower flow regime, indicating the valves open more easily after complete closure. In the higher flow regime, both types of microvalves seem to show hysteresis. This may be due to the limited elasticity of the membrane; after the membrane has been pressed and thus stretched out, it might require some time to completely re-contract.

On-off experiments were performed to further investigate device stability in time. Therefore, the inlet pressure was set to 1 bar while the voltage applied to the Braille module was switched between 0 V and 500 V. The result is depicted below.

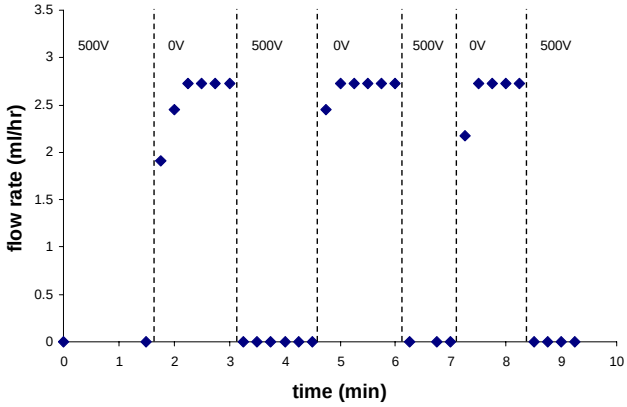

Figure 7-15: flowrate as a function of time

From figure 7-15, it can be observed that maximum and minimum flowrates remain very stable while the voltage applied to the piezoelectric pins is switched between 0 V and 500 V. This indicates that the membrane is not permanently deformed during these tests. The tests also indicate that valve closure happens considerably faster (within 15 seconds) than valve opening (between 15 and 30 seconds). This confirms the above hypothesis that valve

opening by contraction of the membrane requires a considerable amount of time. It can not be excluded that this is an artifact of the measurement, however; the flowrate is determined from the movement of the liquid front in an external tube. Due to compressibility of the liquid or (unobserved) gas bubbles in the tube, this measurement method might lead to a delayed response.

7.4.3 Pneumatic actuation

Microvalves which enable pneumatic actuation were fabricated as described above. Flowrates at set fluid flow pressures were determined at different control pressures by measuring dye movement. The results obtained for a microvalve comprising an 80 µm-wide microfluidic channel are depicted below.

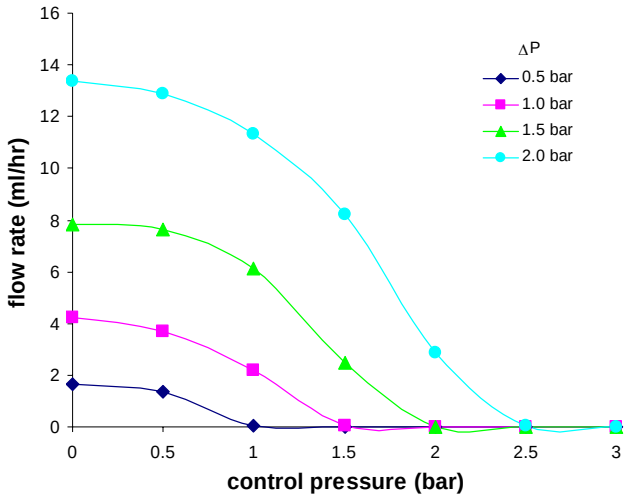

Figure 7-16: flowrate versus control pressure

As can be seen from this figure, flowrate decreases with decreasing fluid flow pressure and increasing control pressure. Control pressure needed for full valve closure increases with increasing fluid flow pressure. The flow rates observed in this experiment compare nicely to those observed in figure 7-11.

The results obtained with pneumatic actuation are very robust and reproducible since there is no need to align the microchannel with an external actuator.

7.5 Discussion & conclusion

In order to expand the microreactor array under study with pH control and fed-batch functionality, the development of a microvalve array was proposed. A new method for fabrication of microvalves with rounded cross sections and high control of channel dimensions was proposed. The microvalves were tested in combination with three different actuation principles as to investigate the feasibility of both Braille display actuation and pneumatic actuation for microvalve array control.

The desired microchannel structures were isotropically etched in glass. After casting and curing PDMS, a PDMS mold containing negative relief features was formed. This mold was coated and PDMS was cast and cured as to create a PDMS substrate with the desired channel structures which could be bonded to a PDMS membrane spun on a dummy wafer. This simple fabrication method was verified to result in microchannels with rounded to semicircular cross section with accurate control of channel dimensions.

An electromagnetic actuator with rounded tip was verified to generate forces similar to those generated by the piezo-electrically activated pins of commercially available Braille displays. Experiments with both electromagnetic actuation as with Braille display actuation showed that the flowrate in the fabricated microchannels can be accurately controlled in the desired range using Braille display pins. The experiments also showed that accurate control of pin shape and pin alignment is needed to achieve satisfying reproducibility.

Valve closure could always be achieved at a sufficiently high rate of actuation. Moreover, the flow rate at zero actuation is nearly independent of tip shape and alignment, since in this case the force exerted on the membrane is negligible. This indicates that reproducibility could be increased by operating the valves in on/off modes such that the effective flow rate is determined by the duty cycle of the applied signal. On/off measurements with the developed microvalves show that valve opening occurs considerably slower than valve closure. This limits the controllability of the effective flow rate when the microvalve is operated in pulse mode, although the effect could be compensated for analytically or by applying microvalves with smaller channels.

In case of pneumatic actuation, the effective flowrate can be controlled in the desired range in an accurate manner. The results are very reproducible, since the alignment of the control channel is fixed once it is bonded to the membrane-covered microchannel. Valve closure happens considerably faster compared to Braille display actuation. The reason for this presumably is that the total force exerted on the membrane is more equally distributed over its surface.

For further development of a microfluidic platform which enables for pH control and fed-batch functionality, the use of pneumatic actuation is recommended since this method allows for more robust and reproducible control of fluid flow. Although Braille display actuation is an attractive alternative for actuation of small microvalve arrays, pneumatic actuation seems to be favorable for the actuation of large arrays of microvalves, since use of multiplexing principles can be made.

References

Balagadde FK, You LC, Hansen CL, Arnold FH, Quake SR. 2005. Long-term monitoring of bacteria undergoing programmed population control in a microchemostat. Science 309(5731):137-140.

Beebe DJ, Moore JS, Bauer JM, Yu Q, Liu RH, Devadoss C, Jo B-H. 2000. Functional hydrogel structures for autonomous flow control inside microfluidic channels. Nature 404(6778):588-590.

Bohm S, Burger GJ, Korthorst MT, Roseboom F. 2000. A micromachined silicon valve driven by a miniature bi-stable electro-magnetic actuator. Sensors and Actuators a-Physical 80(1):77-83.

Carlen ET, Mastrangelo CH. 2002. Surface micromachined paraffin-actuated microvalve. Journal of Microelectromechanical Systems 11(5):408-420.

Duffy DC, McDonald JC, Schueller OJA, Whitesides GM. 1998. Rapid prototyping of microfluidic systems in poly(dimethylsiloxane). Analytical Chemistry 70(23):4974-4984.

Ejiofor AO, Posten CH, Solomon BO, Deckwer WD. 1994a. A Robust Fed-Batch Feeding Strategy for Optimal Parameter-Estimation for Bakers-Yeast Production. Bioprocess Engineering 11(4):135-144.

Ejiofor AO, Solomon BO, Posten C, Deckwer WD. 1994b. Analysis of the Respiro-Fermentative Growth of Saccharomyces-Cerevisiae on Glucose in a Fed-Batch Fermentation Strategy for Accurate Parameter-Estimation. Applied Microbiology and Biotechnology 41(6):664-669.

Envors S. 2006. Basic Biotechnology. Ratledge C, Kristiansen B, editors. Cambridge Cambridge University Press. 470-471 p.

Futai N, Gu W, Takayama S. 2004. Rapid prototyping of microstructures with bell-shaped cross-sections and its application to deformation-based microfluidic valves. Advanced Materials 16(15):1320-+.

Galas JC, Studer V, Chen Y. 2005. Characterization of pneumatically activated microvalves by measuring electrical conductance. Microelectronic Engineering 78-79:112-117.

Gmunder FK, Nordau CG, Tschopp A, Huber B, Cogoli A. 1988. Dynamic Cell-Culture System - a New Cell Cultivation Instrument for Biological Experiments in Space. Journal of Biotechnology 7(3):217-228.

Go JS, Shoji S. 2004. A disposable, dead volume-free and leak-free in-plane PDMS microvalve. Sensors and Actuators A: Physical 114(2-3):438-444.

Gu MB, Gil GC, Kim JH. 1999. A two-stage minibioreactor system for continuous toxicity monitoring. Biosensors & Bioelectronics 14(4):355-361.

Gu W, Chen H, Tung YC, Meiners JC, Takayama S. 2007. Multiplexed hydraulic valve actuation using ionic liquid filled soft channels and Braille displays. Applied Physics Letters 90(3):-.

Gu W, Zhu XY, Futai N, Cho BS, Takayama S. 2004. Computerized microfluidic cell culture using elastomeric channels and Braille displays. Proceedings of the National Academy of Sciences of the United States of America 101(45):15861-15866.

Herber S. 2005. Development of a hydrogel-based carbon dioxide sensor. Enschede: University of Twente. 99 p.

Jerman H. 1994. Electrically-Activated, Normally-Closed Diaphragm Valves. Journal of Micromechanics and Microengineering 4(4):210-216.

Kirby BJ, Shepodd TJ, Hasselbrink EF. 2002. Voltage-addressable on/off microvalves for high-pressure microchip separations. Journal of Chromatography A 979(1-2):147-154.

Knight M, House J. 2004. Design, fabrication, and test of a peristaltic micropump. Microsystem Technologies-Micro-and Nanosystems-Information Storage and Processing Systems 10(5):426-431.

Lee J, Lee SY, Park S, Middelberg APJ. 1999. Control of fed-batch fermentations. Biotechnology Advances 17(1):29-48.

Lee JS, Lucyszyn S. 2007. Design and pressure analysis for bulk-micromachined electrothermal hydraulic microactuators using a PCM. Sensors and Actuators a-Physical 133(2):294-300.

Mayergoyz I, Bertotti G. 2005. The Science of Hysteresis. New York: Elsevier Academic Press.

Niu XZ, Wen WJ, Lee YK. 2005. Electrorheological-fluid-based microvalves. Applied Physics Letters 87(24).

Oh KW, Ahn CH. 2006. A review of microvalves. Journal of Micromechanics and Microengineering 16(5):R13-R39.

Ohori T, Shoji S, Miura K, Yotsumoto A. 1998. Partly disposable three-way microvalve for a medical micro total analysis system (mu TAS). Sensors and Actuators a-Physical 64(1):57-62.

Oosterbroek RE, Berenschot JW, Schlautmann S, Krijnen GJM, Lammerink TSJ, Elwenspoek MC, van den Berg A. 1999. Designing, simulation and realization of in-plane operating micro valves, using new etching techniques. Journal of Micromechanics and Microengineering 9(2):194-198.

Orhan JB, Parashar VK, Sayah A, Gijs MAM. 2006. Fabrication and characterization of three-dimensional microlens arrays in sol-gel glass. Journal of Microelectromechanical Systems 15(5):1159-1164.

Park JM, Cho YK, Lee BS, Lee JG, Ko C. 2007. Multifunctional microvalves control by optical illumination on nanoheaters and its application in centrifugal microfluidic devices. Lab on a Chip 7(5):557-564.

Posten CHC, C. L. 1993. Biological Fundamentals. Rehm HJ, Reed G, Pühler A, Stadler P, editors. New York: VCH. 155 p.

Sato K, Shikida M. 1994. An Electrostatically Actuated Gas Valve with an S-Shaped Film Element. Journal of Micromechanics and Microengineering 4(4):205-209.

Shikida M, Sato K, Tanaka S, Kawamura Y, Fujisaki Y. 1994. Electrostatically Driven Gas Valve with High-Conductance. Journal of Microelectromechanical Systems 3(2):76-80.

Shoji S, Esashi M. 1994. Microflow Devices and Systems. Journal of Micromechanics and Microengineering 4(4):157-171.

Shuler ML, Kargi F. 2002. Bioprocess engineering - basic concepts. Guerrierri P, editor. Upper Saddle River: Prentice Hall PTR. 156-175 p.

Song JW, Gu W, Futai N, Warner KA, Nor JE, Takayama S. 2005. Computer-controlled microcirculatory support system for endothelial cell culture and shearing. Analytical Chemistry 77(13):3993-3999.

Terry SC, Jerman JH, Angell JB. 1979. Gas-Chromatographic Air Analyzer Fabricated on a Silicon-Wafer. Ieee Transactions on Electron Devices 26(12):1880-1886.

Thorsen T, Maerkl SJ, Quake SR. 2002. Microfluidic large-scale integration. Science 298(5593):580-584.

Unger MA, Chou HP, Thorsen T, Scherer A, Quake SR. 2000. Monolithic microfabricated valves and pumps by multilayer soft lithography. Science 288(5463):113-116.

Urbanski JP, Thies W, Rhodes C, Amarasinghe S, Thorsen T. 2006. Digital microfluidics using soft lithography. Lab on a Chip 6(1):96-104.

van den Berg A, Bergveld P. 2006. Labs-on-a-Chip: Origin, highlights and future perspectives - On the occasion of the 10th ?TAS conference. Lab on a Chip - Miniaturisation for Chemistry and Biology 6(10):1266-1273.

van Lintel HTG, van de Pol FCM, Bouwstra S. 1988. A Piezoelectric Micropump Based on Micromachining of Silicon. Sensors and Actuators 15(2):153-167.

Verachtert H, de Mot R. 1990. Yeast: Biotechnology and Biocatalysis. McGregor WC, editor. New York: Marcel Dekker, Inc. 122-123 p.

Waits CM, Modafe A, Ghodssi R. 2003. Investigation of gray-scale technology for large area 3D silicon MEMS structures. Journal of Micromechanics and Microengineering 13(2):170-177.

Waits CM, Morgan B, Kastantin M, Ghodssi R. 2005. Microfabrication of 3D silicon MEMS structures using gray-scale lithography and deep reactive ion etching. Sensors and Actuators a-Physical 119(1):245-253.

Walther I, van der Schoot B, Boillat M, Cogoli A. 2000. Performance of a miniaturized bioreactor in space flight: microtechnology at the service of space biology. Enzyme and Microbial Technology 27(10):778-783.

Weibel DB, Whitesides GM. 2006. Applications of microfluidics in chemical biology. Current Opinion in Chemical Biology 10(6):584-591.

Whitesides GM, Ostuni E, Takayama S, Jiang XY, Ingber DE. 2001. Soft lithography in biology and biochemistry. Annual Review of Biomedical Engineering 3:335-373.

Yalkowsky SH, He Y. 2003. Handbook of aqueous solubility data. Boca Raton: CRC Press LLC.

Yang X, Grosjean C, Tai YC, Ho CM. 1998. A MEMS thermopneumatic silicone rubber membrane valve. Sensors and Actuators a-Physical 64(1):101-108.

Yuan XC, Jiang HJ, Cheong WC. 2001. Characterization of photosensitive hybrid sol-gel glass with high-energy beam-sensitive grey-scale mask in single-step fabrication of blazed gratings. Journal of Physics D-Applied Physics 34(23):L125-L128.

Zhang ZY, Boccazzi P, Choi HG, Perozziello G, Sinskey AJ, Jensen KF. 2006. Microchemostat - microbial continuous culture in a polymer-based, instrumented microbioreactor. Lab on a Chip 6(7):906-913.

Chapter 8: Conclusions and recommendations

In this chapter, some overall conclusions are drawn. These conclusions are followed by a reiteration of the conclusions per chapter. Subsequently, recommendations are given for improving the overall performance of the developed system and expanding its functionality and applicability.

8.1 Conclusions

In this thesis the development of a microbioreactor array with integrated sensors suitable for on-line screening of micro organisms is described. Therefore, an array of 2 micro bioreactors compatible with the 96-well microtiterplate format has been made and tested. The developed system was shown to be suitable for monitoring dissolved oxygen, viable biomass, pH and temperature during batch fermentations of *Candida utilis* cells using integrated electrochemical sensor arrays. No signal degradation was observed after autoclaving the sensor arrays several times. PDMS microvalves have been developed as to enable expansion of the system with fed-batch functionality and pH control.

The applicability of ISFETs for long-term measurements was investigated by studying characteristics of ISFET drift. The drift response of ISFETs shows exponential behavior in the first few hours of operation. Thereafter, the drift becomes (nearly) linear with time and very reproducible. It was observed that the long-term drift rate shows a strong correlation with solution pH, contaminations in the gate oxide and the duty cycle used to connect the ISFET to the ISFET amplifier. It was also shown that the long-term drift response of ISFETs fabricated on the same wafer is very comparable.

The above observations suggest that long-term drift can be compensated for using a predetermined constant. Drift influence can also be reduced by compensating response of an ISFET in an environment where small changes with respect to a constant pH value need to be monitored with the drift response of an ISFET placed in a constant pH environment. It was shown that the resulting drift rate can be reduced to at most a few tenths of millivolts, which is acceptable for the intended application. Another method for reducing the influence of ISFET drift is by connecting the device to the ISFET amplifier according to a <100% duty cycle. Low duty cycles, however, limit the measurement resolution and might lead to noise.

For monitoring the dissolved oxygen concentration, two different techniques were investigated. ^{E}MOSFETs show a good sensitivity towards the dissolved oxygen concentration. Corresponding transfer coefficient values were in accordance with previous studies on ^{E}MOSFETs and independent of solution pH. However, ^{E}MOSFET sensitivity was not reproducible for different devices fabricated on the same wafer and tends to decrease considerably in a time span of several hours. This might indicate the device is very sensitive to fouling or other effects taking place at the iridium oxide interface.

Amperometry is a well established technique to monitor dissolved oxygen. Drawbacks related to amperometric cells consisting of macro electrodes, such as high oxygen consumption and flow dependence, can be circumvented by applying ultra micro electrodes. Cyclic voltammograms and calibration experiments obtained in a supernatant solution show that at an electrode polarization close to the beginning of the current plateau corresponding to the reduction of oxygen (i.e. ~-0.4V vs. NHE), selectivity towards oxygen is assured in supernatant. From the experiments, it was concluded that amperometry is the preferred method to monitor dissolved oxygen.

For applicability of ISFETs and amperometric oxygen sensors, a stable reference electrode is needed. It was therefore proposed to place a single conventional glass reference electrode in a separate reservoir and connect it to the micro bio reactors using salt bridges. By filling the salt bridges with a conductive liquid not harmful to the cell culture (e.g. the culture medium), the amount of silver chloride solution leaking into the reactor can be greatly reduced. If the solution in the reservoir containing the reference electrode is buffered at culture pH, the ISFET used for differentially subtracting out the effect of ISFET drift can be placed in this reservoir as well.

Impedance measurements show that impedance spectroscopy is a feasible method for biomass determination. The measured capacitance change, as obtained by comparing the capacitance between the electrodes at both high and low frequencies, increases linearly with the biomass concentration in a range of 0-10 g DW/l. Observed noise magnitude was considerable, since the capacitance changes measured were very small. Signal-to-noise performance can be enhanced by adjusting the geometry of the conductivity sensor in such a way that the capacitance between the electrodes is increased. An alternative is to measure the spectral variation in solution resistance instead of the variation in electrochemical cell capacitance.

The characteristic frequency describing the dielectric dispersion in a S. *cerevisiae* cell suspension was observed to equal 2.8 MHz, as found using a micromachined impedance sensor consisting of planar platinum electrodes. This value corresponds well to empiric data in literature. The measured capacitance change due to dielectric dispersion shows a linear response to concentration and matches the calculations quite well for typical fermentor concentrations of yeast cells in a standard yeast buffer solution, confirming the relevance of the applied theory on microreactor scale.

The measurements with the pHEMA covered electrode pair show that the measured resistance does depend linearly on the actual electrolyte conductivity and that the measured cell capacitance is independent of the viable yeast cell concentration. This

confirms that the pHEMA membrane gets hydrated, but is impermeable to yeast cells. This makes the proposed 3-electrode configuration suitable for determining the background electrolyte conductivity independent of the viable cell concentration. This signal can thus be used for compensating the measured impedance spectrum for changes in the background electrolyte.

The optimal hydrated membrane thickness arises from the observed electric properties of the membrane and finite element modeling and is found to equal 1 micron for the electrode configuration under study. The electric and transient properties of the membrane can be further optimized by altering the physical membrane properties.

Experiments show that the conductivity of a S. *cerevisiae* cell suspension clearly increases for frequencies above 1 MHz. A calibration experiment shows the conductivity difference to scale linearly with the biomass concentration, which can be estimated with an accuracy of approximately 1 g/l. Dissolved oxygen calibration experiments in a supernatant solution shows the current through the ultra micro electrode array to scale linearly with the dissolved oxygen concentration with sensitivity close to its theoretical value. Flow dependence of the sensor was shown to be negligible compared to the flow dependence of macro electrodes. The ISFET and the temperature sensor were shown to be sufficiently sensitive in the desired range. The drift could be effectively compensated for.

The electrochemical sensor chip turned out to be robust and give reliable reading. All sensors were shown to be sufficiently accurate within the range relevant to yeast fermentations under conditions the sensor ultimately should function.

The ultra micro electrode array used for monitoring the dissolved oxygen concentration showed an accuracy of ~0.2 mg/l and negligible drift. Oxygen consumption was shown to be insignificant, even if the sensor is applied in a microreactor with a 200 µl volume. The results of the biomass sensor matched very well with dry weight measurements and showed a limit of detection of ~1 g/l. Impedance measurements suffered from significant noise levels. An important potential noise source is formed by the conventional electrochemical probes present in the fermentor and is cancelled if no other electrochemical sensors operate in parallel in the final application. Sensor performance can be further improved by better shielding of electrical wires and connections and by fitting the impedance data on more advanced electrical circuit models. pH was monitored using an ISFET with an accuracy well below 0.1 pH unit. Measurements performed during the continuous cultivation experiments show ISFET drift could effectively be compensated for using a device-specific constant factor. The platinum thin-film temperature resistor followed temperature changes with ~0.1 ^{o}C accuracy.

Examination of the sensor surface under a microscope showed no visible damage or defects caused during the performed experiments. In combination with previously reported results showing that no signal degradation is observed after autoclaving the sensor several times (Krommenhoek et al. 2007), it can be concluded that the sensor array has high potential for implementation in reusable systems.

From feasibility studies on the salt bridge comprising a Nafion hollow fiber membrane filled with medium, it can be concluded that the thus created electrical connection between the micro wells and the reservoir containing the reference electrode shows high stability in the pH range relevant to yeast fermentations.

Based on this salt bridge, a micro bioreactor array comprising two micro wells suitable for the batch fermentation and on-line monitoring of micro organisms was constructed and tested. The measurement results shown above indicate that viable biomass, dissolved oxygen, pH and temperature could successfully be monitored in multiple wells during the batch growth of *candida utilis*. When the batch phase has ended, all substrate is metabolized and the culture is expected to enter the stationary phase, where growth slows down or completely stops. pH rapidly increases due to acid consumption which corresponds to the measurements shown above.

Dispersion signals obtained during batch 1a and batch 1b decrease rapidly after the batch phase has ended. This could indicate that the cells die shortly after the batch phase has ended. However, this effect can not explain why the signal decrease obtained during batch 2a and batch 2b largely recovers. Since the results in figure 6-15 indicate that the solution resistance changes dramatically after the batch phase has finished, it may be that the impedance model used is not accurate anymore in the frequency range studied. This hypothesis could however not be confirmed by testing with other impedance models or by looking at other frequencies.

The increase in dissolved oxygen signals obtained after the batch growth of *Candida utilis* is smaller than expected from the experiments shown in chapter 5. This could indicate that the cells still show metabolic activity. However, this hypothesis does not explain the observed behavior of the biomass sensor. Another explanation for the lower-than-expected signals acquired from the dissolved oxygen sensors, is that the electrode area is reduced. This can be due to either fouling or physical degradation of the electrodes. Physical degradation of the electrodes was not observed. Moreover, only fouling can also explain the behavior of the biomass sensor: if the sensor gets fouled, the electrical field between the electrodes will be deformed and consequently does not penetrate the cell-containing

solution. Partial signal recovery obtained in batch 2, could be due to re-suspension of sedimentated species.

Similar effects did not (or less pronounced) take place in the large scale fermentations shown in chapter 5. This may be due to the positioning of the sensors; the sensors were placed in upright position in the lab-scale fermentor. In case of the microreactor experiments, however, the sensors were located on the bottom of the reactor and therefore more sensitive to substances sedimenting. Moreover, the microreactors suffer from worse mixing conditions compared to the lab-scale fermentors.

The cause of the fouling effect described above might have a biological cause. As explained in section 6-1, the composition of the cells might change significantly when the culture enters the stationary phase. Cells become less robust and a significant part of the cells might die. In that case, membrane parts and cell contents such as proteins might become subject to sedimentation thereby leading to the observed sensor response.

In order to expand the microreactor array under study with pH control and fed-batch functionality, the development of a microvalve array was proposed. A new method for fabrication of microvalves with rounded cross sections was proposed. The microvalves were tested in combination with three different actuation principles as to investigate the feasibility of both Braille display actuation and pneumatic actuation for microvalve array control.

The desired microchannel structures were isotropically etched in glass. After casting and curing PDMS, a PDMS mold containing negative relief features was formed. This mold was coated and PDMS was cast and cured as to create a PDMS substrate with the desired channel structures which could be bonded to a PDMS membrane spun on a dummy wafer. This simple fabrication method was verified to result in microchannels with rounded to semicircular cross section with accurate control of channel dimensions.

An electromagnetic actuator with rounded tip was verified to generate forces similar to those generated by the piezo-electrically activated pins of commercially available Braille displays. Experiments with both electromagnetic actuation as with Braille display actuation showed that the flowrate in the fabricated microchannels can be accurately controlled in the desired range using Braille display pins. The experiments also showed that accurate control of pin shape and pin alignment is needed to achieve satisfying reproducibility.

Valve closure could always be achieved at a sufficiently high rate of actuation. Moreover, the flow rate at zero actuation is nearly independent of tip shape and alignment, since in this case the force exerted on the membrane is negligible. This indicates that

reproducibility could be increased by operating the valves in on/off modes such that the effective flow rate is determined by the duty cycle of the applied signal. On/off measurements with the developed microvalves show that valve opening occurs considerably slower than valve closure. This limits the controllability of the effective flow rate when the microvalve is operated in pulse mode, although the effect could be compensated for analytically or by applying microvalves with smaller channels.

In case of pneumatic actuation, the effective flowrate can be controlled in the desired range in an accurate manner. The results are very reproducible, since the alignment of the control channel is fixed once it is bonded to the membrane-covered microchannel. Valve closure happens considerably faster compared to Braille display actuation. The reason for this presumably is that the total force exerted on the membrane is more equally distributed over its surface.

For further development of a microfluidic platform which enables for pH control and fed-batch functionality, the use of pneumatic actuation is recommended since this method allows for more robust and reproducible control of fluid flow. Although Braille display actuation is an attractive alternative for actuation of small microvalve arrays, pneumatic actuation seems to be favorable for the actuation of large arrays of microvalves, since use of multiplexing principles can be made.

8.2 Recommendations

The developed system was shown to be suitable for performing and monitoring batch fermentations of *Candida utilis* cells using integrated electrochemical sensor arrays. When the batch phase has ended, however, the response of the biomass and dissolved oxygen sensors is considerably lower than expected, indicating that a fouling effect took place. This behavior was not observed in the lab-scale fermentors where the sensors were placed in upright position instead on the bottom of the reactor and where mixing conditions were believed to be much better. Therefore, the observed fouling effect was believed to be caused by sedimentation of species.

The reasoning above indicates that the developed microreactor system can be further improved by improving mixing. Adequate mixing should prevent the occurrence of sedimentation. It should be further investigated whether excessive cell death takes place when the culture enters the stationary phase and if so, the origin of this effect should be found and solved. Electrochemical cleaning steps might help in further reducing fouling effects.

The measurements of dissolved oxygen and biomass suffer from considerable noise levels. It is believed that noise can be reduced by improving the shielding of the wiring. The accuracy of the biomass measurements can be further improved by fitting the impedance data on more accurate electrical equivalent circuits.

In the current setup, the time required to monitor all 4 parameters sequentially equals approximately 2 minutes. Because only a minor part of this interval is required for the measurements themselves, measurement resolution can be improved significantly by optimizing the software controlling the data communication between the measurement equipment and the computer.

The complexity of the sensor array can be reduced by the combined use of electrodes, since the sensors are operated sequentially and all electrodes not used for analysis are floating. Combined use of electrodes results in a reduced number of contacts. For instance, the secondary electrode of the biomass sensor and the counter electrode of the dissolved oxygen sensor can be combined.

The reactor array can be expanded for pH control and fed-batch functionality by incorporating microfluidics allowing for control of fluid inflows. Chapter 7 shows the development of microvalves for this purpose, but more research is required for integration in microreactor arrays and for setting up control algorithms.

In order to further expand the application field of the system under development, its feasibility for culturing and monitoring other types of micro-organisms and cells should be investigated.

Samenvatting

Het doel van het in samenwerking met de TU Delft uitgevoerde “Fed-batch on a chip”-project is het miniaturiseren en parallelliseren van micro bioreactoren die geschikt zijn voor het on-line screenen van micro-organismen zoals gist. In dit proefschrift is een ten behoeve daarvan ontwikkelde electrochemische sensor array beschreven. De sensor array bevat sensoren voor het on-line meten van pH, temperatuur, concentraties opgeloste zuurstof en concentraties biomassa.

De pH-sensor is een Ion-selectieve veldeffect transistor (ISFET). De invloed van drift kon verminderd worden door de sensor gepulseerd aan te sturen. Daarnaast werd aangetoond dat de invloed van drift verder gereduceerd kan worden door een tweede sensor in een constante pH omgeving te plaatsen en differentieel te meten. De temperatuursensor is een platina strip met een nominale weerstand van 1 kOhm. De concentratie opgeloste zuurstof wordt gemeten middels een amperometrische ultra micro electrode array (UMEA), bestaande uit electroden met een diameter van 4 micrometer. Uit experimenten blijkt dat de sensor bij een juiste polarisatie (-0.4V vs Ag/AgCl) voldoende selectief is voor zuurstof. Tevens tonen metingen aan dat de sensor overeenkomstig de theorie flow-onafhankelijk is. De concentratie biomassa wordt gemeten met behulp van impedantie spectroscopie. Omdat voor een geminiaturiseerde impedantiesensor met hoge celconstante de capaciteit tussen de electroden erg klein is, wordt in plaats daarvan de Ohmse weerstand tussen de electroden gemeten. In een gistcel suspensie blijkt de weerstand tussen de elektroden voor frequenties hoger dan 1 MHz toe te nemen; de toename is lineair evenredig met de celconcentratie. De sensoren zijn gefabriceerd met behulp van cleanroom technieken en klein genoeg om onder de well van een 96-wells microtiterplaat te passen.

Tijdens integrale tests in fermentoren met een werkvolume van 4 liter is de tijdens de batch cultivatie van *candida utilis* gistcellen verkregen respons van de sensoren vergeleken met die van conventionele methoden. Vervolgens zijn de sensoren toegepast in een array van microreactoren met een werkvolume van 100 microliter. Hiertoe werden de sensor arrays onder de wells van een 96-wells microtiterplaat geplaatst. Een enkele referentie electrode werd in een apart reservoir geplaatst en met de microreactoren verbonden middels met medium gevulde zoutbruggen op basis van Nafion holle-vezel membranen. Voor de menging van de vloeistof werd gebruik gemaakt van een

magneetroerder, gefixeerd op een asje. Met behulp van deze configuratie werden batch cultivaties van *candida utilis* gistcellen uitgevoerd en gemonitord. Na afloop van de batch groei lijkt er sprake te zijn van buitensporig veel celdood en sensor vervuiling. Het verdient aanbeveling meer onderzoek te doen naar de oorzaken en oplossingen voor dit fenomeen.

Dit proefschrift beschrijft tevens de ontwikkeling van microfluidica ten behoeve van pH-regulatie en fed-batch functionaliteit. Hiertoe werden PDMS-microvalves ontwikkeld. De kanalen met een afgeronde tot half ronde doorsnede werden gefabriceerd met behulp van een nieuw fabricageproces dat gebruik maakt van het isotrope etsprofiel dat ontstaat bij het nat etsen van glas. De klepjes werden gekarakteriseerd door ze te actueren met behulp van een electromagnetische actuator, Braille displays of pneumatische actuatie. Aangetoond werd dat met name in het geval van pneumatische actuatie de vloeistofstroming zeer nauwkeurig en reproduceerbaar te controleren is. Wanneer gebruik gemaakt wordt van een op het membraan drukkende pin is dit enkel het geval, wanneer de dimensies en uitlijning van de pin zeer nauwkeurig te controleren zijn.

List of publications

Full papers

Krommenhoek EE, Gardeniers JGE, Bomer JG, Van den Berg A, Li X, Ottens M, van der Wielen LAM, van Dedem GWK, van Leeuwen M, van Gulik WM and others. 2006. Monitoring of yeast cell concentration using a micromachined impedance sensor. Sensors and Actuators B-Chemical 115(1):384-389.

Krommenhoek EE, Gardeniers JGE, Bomer JG, Li X, Ottens M, van Dedem GWK, van Leeuwen M, van Gulik WM, van der Wielen LAM, Heijnen JJ and others. 2007. Integrated Electrochemical Sensor Array for On-Line Monitoring of Yeast Fermentations. Anal. Chem. 79(15):5567-5573.

Krommenhoek EE, van Leeuwen M, Gardeniers JGE, van Gulik WM, van den Berg A, Li X, Ottens M, van der Wielen LAM, Heijnen JJ. 2007. Lab-scale fermentation tests of micro chip with integrated electrochemical sensors for pH, temperature, dissolved oxygen and viable biomass concentration. Biotechnology & Bioengineering. *Article in press.*

Other contributions

E.E. Krommenhoek, J.G.E. Gardeniers, A. van den Berg, X. Li, M. Ottens, L.A.M. van der Wielen, G.W.K. van Dedem, M. van Leeuwen, W.M. van Gulik, J.J. Heijnen, Design of miniaturized fermentors for high thoughput optimization of industrial fermentations, oral presentation at: ACTS-IBOS work conference, Nunspeet, Netherlands, June 17, 2004

J.G.E. Gardeniers, E.E. Krommenhoek, A. van den Berg, Xiaonan Li, M. Ottens, L.A.M. van der Wielen, G.W.K. van Dedem, M. van Leeuwen, W.M. van Gulik, J.J. Heijnen, Design of miniaturized fermentors for high throughput optimization of industrial fermentations, invited oral presentation at: 5th European Symposium on Biochemical Engineering Sciences, Stuttgart, Germany, September 11, 2004.

E.E. Krommenhoek, J.G.E. Gardeniers, A. van den Berg, X. Li, M. Ottens, L.A.M. van der Wielen, G.W.K. van Dedem, M. van Leeuwen, W.M. van Gulik, J.J. Heijnen, Design of miniaturized fermentors for high thoughput optimization of industrial fermentations, poster presentation at: MESA+ Dag 2004, Enschede, Netherlands, September 30, 2004

J.G.E. Gardeniers, E.E. Krommenhoek, A. van den Berg, Xiaonan Li, M. Ottens, L.A.M. van der Wielen, G.W.K. van Dedem, M. van Leeuwen, W.M. van Gulik, J.J. Heijnen, Miniaturized biofermentors with integrated sensing elements, invited oral presentation at: Micro-Bioprocessing Engineering Symposium, Dechema, Frankfurt am Main, Germany, November 11, 2004.

E.E. Krommenhoek, J.G.E. Gardeniers, A. van den Berg, X. Li, M. Ottens, L.A.M. van der Wielen, G.W.K. van Dedem, M. van Leeuwen, W.M. van Gulik, J.J. Heijnen, Design of miniaturized fermentors for high thoughput optimization of industrial fermentations, poster presentation at: the 8th Annual European Conference on Micro & Nanoscale Technologies for the Biosciences, Montreux, Switzerland, November 16-18, 2004

E.E. Krommenhoek, J.G.E. Gardeniers, A. van den Berg, X. Li, M. Ottens, L.A.M. van der Wielen, G.W.K. van Dedem, M. van Leeuwen, W.M. van Gulik, J.J. Heijnen, Monitoring of yeast cell concentration using a micromachined impedance sensor, oral presentation at: Transducers 2005, Seoul, South Korea, June 7, 2005

E.E. Krommenhoek, J.G.E. Gardeniers, A. van den Berg, X. Li, M. Ottens, L.A.M. van der Wielen, G.W.K. van Dedem, M. van Leeuwen, W.M. van Gulik, J.J. Heijnen, Monitoring of yeast cell concentration using a micromachined impedance sensor, abstract in: *Transducers 2005* (283-286)

E.E. Krommenhoek, J.G.E. Gardeniers, A. van den Berg, X. Li, M. Ottens, L.A.M. van der Wielen, G.W.K. van Dedem, M. van Leeuwen, W.M. van Gulik, J.J. Heijnen, Keep your little cells happy in a fed-batch microreactor with integrated sensors and microfluidic, poster presentation at: MESA+ Dag 2005, Enschede, Netherlands, September 29, 2005

E.E. Krommenhoek, J.G.E. Gardeniers, A. van den Berg, Xiaonan Li, M. Ottens, L.A.M. van der Wielen, G.W.K. van Dedem, M. van Leeuwen, W.M. van Gulik, J.J. Heijnen, Development of Integrated Sensor Array for Micro Bioreactors, poster presentation at: ACTS-IBOS work conference, Nunspeet, The Netherlands, September 29-30, 2005

E.E. Krommenhoek, Rapid screening of micro-organisms in "Fed -batch on a chip, De Vonk, periodiek der E.T.S.V. Scintilla, pp. 5-8, 2005

E.E. Krommenhoek, Electrochemical Sensor Arrays for On-Line Screening of Micro-Organisms, invited oral presentation at: MESA+ Colloquium, Enschede, The Netherlands, March 14, 2006

E.E. Krommenhoek, J.G.E. Gardeniers, A. van den Berg, Xiaonan Li, M. Ottens, L.A.M. van der Wielen, G.W.K. van Dedem, M. van Leeuwen, W.M. van Gulik, J.J. Heijnen, Development of Integrated Sensor Array for Micro Bioreactors, poster presentation and demonstartion at: Sense of Contact 8, Wageningen, The Netherlands, March 28, 2006

E.E. Krommenhoek, J.G.E. Gardeniers, J.G. Bomer, A. van den Berg, X. Li, M. Ottens, L.A.M. van der Wielen, G.W.K. van Dedem, M. van Leeuwen, W.M. van Gulik, J.J. Heijnen, Integrated Electrochemical Sensor Array for On-Line Monitoring of Yeast Fermentations, poster presentation at: MESA+ day, Enschede, The Netherlands, September 28, 2006

E.E. Krommenhoek, Development and testing of an integrated sensor array for micro bio reactors, oral presentation at: ACTS-IBOS work conference, Nunspeet, The Netherlands, September 29, 2006

E.E. Krommenhoek, J.G.E. Gardeniers, A. van den Berg, Xiaonan Li, M. Ottens, L.A.M. van der Wielen, G.W.K. van Dedem, M. van Leeuwen, W.M. van Gulik, J.J. Heijnen, Integrated electrochemical sensor array for on-line monitoring of yeast fermentations, poster presentation at: Micro Total Analysis Systems, Tokyo, Japan, November 5-9, 2006

E.E. Krommenhoek, J.G.E. Gardeniers, A. van den Berg, Xiaonan Li, M. Ottens, L.A.M. van der Wielen, G.W.K. van Dedem, M. van Leeuwen, W.M. van Gulik, J.J. Heijnen, Integrated electrochemical sensor array for on-line monitoring of yeast fermentations, abstract in: *Micro Total Analysis Systems 2006*, pp. 729-731

E.E. Krommenhoek, Screening micro-organisms in Fed-batch on a Chip, The µCATtentie 2007, pp. 18-21

W. Olthuis, E. Faber, E. Krommenhoek, A. van den Berg, Sensing with FETs – once, now and future, invited oral presentation at: Dresdner Sensor Symposium 8, Dresden, Germany, December 10-12, 2007

Dankwoord

Hoewel ik –uiteraard- ontzettend veel plezier beleefd heb aan het schrijven van het voorgaande, heb ik me nog het meest verheugd op het schrijven van het dankwoord. Want dat brengt me eindelijk in de gelegenheid om officieel mijn dank uit te spreken tegenover diegenen, die ik zo veel dank verschuldigd ben.

Traditiegetrouw begin ik bij mijn promotor: Albert van den Berg. Bedankt voor het begeleiden, voor het motiveren en voor het delen van je kennis en expertise. Ik heb erg veel waardering voor hoe je in elke discussie binnen luttele seconden de vinger op de zere plek weet te leggen. Maar ook voor hoe je je inzet voor de sfeer in de groep. Ik kijk met veel plezier terug op de vele BIOS-uitjes die je organiseerde. Ook al hield ik er vaak spierpijn en vieze kleren aan over.

Ook mijn begeleider annex co-promotor Han Gardeniers ben ik heel wat dank verschuldigd. Hoe druk je ook bent, je was altijd geïnteresseerd en stond altijd voor me klaar. Nooit was je te beroerd mij te voorzien van wijze raad, van je ongezouten mening of van je droge en politiek volkomen incorrecte grapjes. Bedankt daarvoor!

Dit project kon daarnaast niet zonder de partners uit de industrie en van de TU Delft. Ik bedank daarom (op alfabetische volgorde) Annie, Arthur, Gijs, Henk, Jaap, Jan, Joep, Luuk, Marcel, Michiel, Sef, Teun, Walter en Xiaonan voor de samenwerking en de vele, vaak pittige, discussies die er gevoerd zijn. Vooral met Michiel heb ik intensief samengewerkt. We kwamen uit twee totaal verschillende werelden en hebben heel wat frustraties moeten doorstaan. Maar daar hebben we ons uitstekend doorheen geslagen. Michiel, bedankt!

Er zijn nog veel meer mensen die een directe bijdrage aan dit proefschrift hebben geleverd. Ik ben Johan zeer dankbaar voor het werk in de cleanroom. Paul wil ik graag bedanken voor het mij wegwijs maken in het “kliederen met PDMS”. Ook Ad, Ed, EdwinO, Erik, Hermine, de Jannen, Sebastiaan, de Wouters en vele anderen stonden mij regelmatig met hun wijze raad en daad terzijde. Bovendien mocht ik twee afstudeerders begeleiden; Ramon en Vélan.

Niet minder belangrijk voor het uitvoeren van een promotieonderzoek is een goede werksfeer. En wat dat betreft had ik met de BIOS groep als werkomgeving niets te klagen.

Dat is in de eerste plaats te danken aan de vele kamergenoten die ik versleet; op min of meer chronologische volgorde zijn dat Sebastiaan, EdwinO, Monica, Kevin, héél even Edwin en natuurlijk de twee buitengewoon snoezige vrouwen die mij tot de laatste snik hebben bijgestaan: Iris en Svetlana.

Het bovenstaande maakt al duidelijk dat het binnen BIOS een komen en gaan van mensen is. Aanvankelijk werd de dagelijkse lunchwandeling afgelegd met Bjorn, Doro, Ed, Erik, Jurjen, Koen en Sebastiaan. Vier jaar later waren het vooral Iris, Jan, Paul, nog steeds Erik en met een beetje geluk ook Floor, Jacob en Wouter die me vergezelden. Hoe dan ook, ik beleefde altijd veel plezier aan het wandelingetje. Maar er werd niet alleen gewandeld; Doro en Martin hebben mij zelfs aan het hardlopen gekregen, waarvoor mijn hartelijke dank. Onder meer Alexander, Ana, Chris, Egbert, Iris, Jos, Lingling en Séverine wil ik bedanken omdat zij zich ook lieten overhalen door het duo. Daarnaast bedank ik alle andere (ex-)collega's, als Daniël, Eddy, Egbert, Georgette, Henk, Langlang, Pangpang, Mathieu, Patrick, Roald, Séverine, Vincent en tegenwoordig ook de vroegere Biochippers voor de fijne tijd.

Velen lieten zich tevens buiten werktijd van hun beste kant zien. Zo heb ik heel wat gezellige avonden achter de rug, of dat nu in de BIOS koffiekamer was, in de filmzaal van de Vestingbar, op het terras van de Beiaard of op het dakterras van het Ibis in Seoul. Bedankt! Jan van Nieuwkasteele wil ik graag bedanken voor de uitstekende organisatie van de zeilweekendjes in Heeg.

Maar niet alleen op de UT had ik het naar mijn zin. Hoewel een lullig regeltje de lading niet dekt wil ik allereerst mijn familie, met voorop mijn ouders, mijn zus Anja en haar vriend Paul bedanken voor hun onvoorwaardelijke steun en interesse gedurende de afgelopen 4 jaar. En ook voor die gedurende de 24 jaar die daaraan vooraf gingen trouwens. Daarnaast bedank ik mijn schoonouders, Kors, Josien en de rest van de schoonfamilie. Met Sander en Esther, Menno en Arjen heb ik, vaak ver verwijderd van de UT, heel wat biertjes soldaat gemaakt. Met Wietse en (The) King heel wat achtbaantjes. Bedankt!

De laatste alinea van dit dankwoord is bestemd voor mijn vriendin Annet. Je had geen idee van waar ik me mee bezig hield. Had het niet iets te maken met gist? Misschien was het juist daarom zo plezierig om thuis te komen en zo makkelijk om de knop om te zetten. Annet, bedankt voor je steun, liefde en toewijding. Je hebt recht op nog veel meer gezemel, maar dat bewaren we wel voor onder vier ogen ☺

Erik